People`s Democratic Republic of Algeria

Ministry of Higher Education and Scientific Research

University of Echahid Hamma Lakhdar - El Oued

Faculty of Technology

Department of Electrical Engineering

Dissertation

ACADEMIC MASTER

Domain: Science and Technology

Division: Electrical Engineering

Specialty: Electrical Control

Presented by:

- LAIB Mohammed Lakhdar
- AMANI Aymen
- BOUALLAGA Aymen

Entitled:

Direct Torque Control of Induction Motor Drive for PV Array Water Pumping system

Dissertation Submitted in Partial Fulfillment of the Requirements for the Master Degree in MASTER ACADEMIC

Publicly defended in: 03/06/2024

Board of Examiners:

Dr. BEKAKERA Youcef	**Chairman**
Dr. KECHIDA Ridha	**Supervisor**
Dr. MAHNI Tidjani	**Examiner**

Academic Year: 2023/2024

Acknowledgments

First and foremost, I would like to thank God "Allah" the Most Gracious and the Most Merciful, for blessing me with knowledge and giving me strength, courage, patience, and serenity during all these years of study.

I would also like to express my sincere appreciation to all those who contributed to the successful completion of this work. All thanks and appreciation to my honorable supervisor: ***Dr. KECHIDA Ridha*** *for his unwavering support, guidance, and encouragement have been invaluable during the course of my project. His extensive expertise and diligent efforts have significantly enriched my academic journey.*

Last but not the least, I am profoundly thankful to my parents. Their prayers, guidance, and unwavering support have been instrumental in my education. Their inspiration and encouragement have been a beacon of light, guiding me through the challenges and triumphs of my academic pursuit.

Dedication

I dedicate this thesis to my parent "LAIB NABIL" and "DAOUDI FAIZA", who have taken the biggest part of sacrificing for my education. May Allah protect them. To my brothers and sister. To all my family.

LAIB Mohammed Lakhdar

Dedication

I dedicate this thesis to my father, I also dedicate it to my mother who has taken the biggest part of sacrificing for our education. May Allah protect them. To my brothers and sisters. To my nephews and nieces. To all my friends, in my life.

AMANI AYMEN

BOUALLAGA AYMEN

التحكم المباشر في عزم الدوران للمحرك التعريفي لنظام ضخ المياه الكهروضوئي

ملخص - حاليًا، تعاني العديد من المناطق من مشكلات في إمدادات المياه، مثل المواقع المعزولة في الصحراء. كما يُعتبر نظام ضخ المياه بالطاقة الشمسية المستقل أحد الحلول المقترحة، حيث يحتاج إلى صيانة أقل مقارنةً بأنظمة الطاقة الأخرى. يتكون هذا النظام من مولد كهروضوئي متصل برافع للجهد هذا الأخير متصل بعاكس مصدر جهد مزود بمحرك حثي مقترن بمضخة ذات طرد مركزي. يهدف هذا البحث إلى استخدام تقنية التحكم المباشر في عزم الدوران (DTC) للتحكم في المحرك اللاتزامني الذي يستمد تغذيته من النظام الكهروضوئي. ولضمان التشغيل الأمثل للطاقة لهذا النظام عند ظروف مناخية مختلفة يتم استخدام خوارزميات تتبع النقطة القصوى للطاقة (MPPT) حيث سنستخدم خوارزمية P&O و خوارزمية INC لإنشاء المرجع المناسب. نقدم بين أيديكم هذا المحتوى والذي نناقش فيه النتائج المتحصـل عليها لهذا النظام وهذا للتحقق من أداءه وجودته.

الكلمات المفتاحية: المحرك الحثي، التحكم المباشر في عزم الدوران (DTC)، تتبع النقطة القصوى للطاقة (MPPT)، الألواح الكهروضوئية، مضخة الطرد المركزي، الطاقة المتجددة.

Direct torque control (DTC) of induction motor drive for PV array water pumping system

Abstract: The limited access to electricity poses significant challenges for water security, particularly in isolated desert regions. This thesis proposes a standalone solar-powered water pumping system as a low-maintenance solution. The system comprises a photovoltaic generator connected to a DC-DC boost converter, followed by a voltage source inverter (VSI) driving an induction motor coupled to a centrifugal pump. To optimize energy extraction under varying climatic conditions, Direct Torque Control (DTC) is employed to regulate the induction motor. Additionally, Maximum Power Point Tracking (MPPT) algorithms, specifically Perturb and Observe (P&O) and Incremental Conductance (INC), are implemented to generate the appropriate reference signal for the VSI. This work presents the system design, analyzes its performance using MATLAB/SIMULINK simulations, and verifies its effectiveness in delivering reliable water pumping functionality.

Keywords: Induction Motor, Direct Torque Control (DTC), Inverter, Photovoltaic, Centrifugal Pump, Solar Energy, Maximum Power Point Tracking (MPPT).

List of figures

List of tables

List of Abbreviations

AC: Alternative Current.
DC: Direct Current.
DTC: Direct Torque Control.
IM: Induction Motor.
GPV: generator Photovoltaic.
MPP: Maximum Power Point
MPPT: Maximum PowerPoint Tracking.
P&O: Perturb and Observe.
PWM: Pulse Width Modulation.
PV: Photovoltaic.
SPWM: Sinusoidal Pulse Width Modulation.
STC: Standard Test Conditions
VSI: Voltage Source Inverter.
I_{pv}: Current of the photovoltaic panel
V_{pv}: Voltage of the photovoltaic panel
P_{pv}: Power of the photovoltaic panel
I_{cc}: Short circuit current
V_{co}: Open circuit voltage
Is: the saturation current
i_{ph}: Current delivered by the cell
vph: Voltage at the output of the cell
i_d: Current flowing through the diode
v_d: Voltage across the diode
r_s: Series resistor
r_p: Parallel resistance
a: the ideality factor of Junction $1<n<3$
K_b: Boltzmann constant (1 ,38.10-23 J/K)
T: temperature of the cell in degrees kelvin
q: Electron charge ($1{,}602.10^{-19}$)
G: The illumination
G_n: The nominal illumination
V_{sabc}: Stator voltages
V_{rabc}: Rotor voltages
I_{sabc}: Stator currents
I_{rabc}: Rotor currents
Φ_{sabc}: Stator Fluxs
Φ_{rabc}: Rotor Fluxs
L_{ss} : matrix of stator inductors
L_{rr} : matrix of rotor inductors

$R_s.R_r$: Stator and rotor resistances respectively
$L_s.L_r$: Stator and rotor inductances respectively
M_{sr} : Stator-rotor mutual inductance
m_s : Mutual inductance between stator phases.
m_r : Mutual inductance between rotor phases.
θ : Flux angle
(α , β): stator Axes
P: Number of poles pairs
T_{em}: electromagnetic torque
J: moment of inertia of the rotating masses
f: viscous friction coefficient
Ω_r: Speed of rotation of the machine
σ: Blondel's coefficient
[A] : Transition matrix.
[B] : Command matrix.
[P] : PARK transformation matrix.
φ: The water flow (m^3/s)
H: The total height (m)
ω: Rotation speed (rad/s)
a_0 , a_1, a_2: are the coefficients given by the manufacturers.
ψ: is a constant which depends on conduit diameter and on all frictional losses of the pipe network.
H_g : is the geodesic height (m)
V_s : Effective value of the voltage.
Te : Sampling period.
S_{abc} : Boolean control values of the inverter arms.
ξ : Damping Coefficient.

Table of contents

Chapter IV: Direct torque control (DTC) of induction motor

General Introduction

General Introduction

In recent decades, a symbiotic relationship has emerged between industrial development and global energy consumption. However, this ever-increasing energy demand faces a stark challenge: the depletion of non-renewable resources. Fossil fuels, including coal, hydrocarbons, and uranium, are crucial players in our current energy mix. However, their finite nature and slow natural replenishment rates raise significant concerns. The rapid consumption of these resources further exacerbates the situation, contributing to environmental issues like rising pollution levels and a changing climate.

The detrimental environmental impact of fossil fuels has spurred a global movement towards renewable energy sources. Among these, solar energy has garnered significant attention due to its numerous advantages. Its abundance, clean nature, and continuous technological advancements are propelling solar energy to become a mainstream and competitive alternative in many applications. One particularly promising area is photovoltaic (PV) water pumping systems. These systems offer a sustainable and environmentally friendly alternative to conventional diesel-powered pumping systems. By harnessing the power of the sun, PV technology eliminates the dependence on fossil fuels and associated emissions, contributing to a cleaner and more sustainable future.

There are two types of standalone PV systems. One uses a storage battery to store the excess electricity from the PV system, while the other uses a tank to store the pumped water. Using battery storage in a photovoltaic solar water pumping system may increase the PV system cost by 10–50% and affect the lifetime of the system [1-3]. As a result, the implementation of a photovoltaic solar water pumping system without a storage battery increased, especially in rural areas where grid connectivity is unavailable [4].

This thesis investigates the implementation of a solar photovoltaic (PV) water pumping system utilizing Direct Torque Control (DTC) for an induction motor driving a centrifugal pump. The system is designed to extract water from a well and store it in a tank.

In the first chapter, this chapter lays the groundwork by presenting a theoretical overview of photovoltaic pumping systems. It delves into the essential components of PV systems, exploring the various types available. Additionally, it explores the theoretical underpinnings of photovoltaic pumping strategies, introducing the system's constituent components.

The second chapter focuses on the mathematical modeling of the PV array and the boost converter, incorporating Maximum Power Point Tracking (MPPT) control. The chapter examines two prominent MPPT algorithms: Perturb and Observe (P&O) and Incremental Conductance (INC) methods.

In the third chapter, this chapter delves into the mathematical modeling of the key system components. It begins with the induction motor, followed by the application of the Park transformation for simplified analysis. Subsequently, the mathematical models of the centrifugal pump and the voltage source inverter (VSI) are presented.

The concluding chapter delves into the principles of the Direct Torque Control (DTC) strategy. Following this theoretical foundation, the chapter details the implementation of the entire system under investigation. Finally, the chapter presents and analyzes the results obtained under various operating conditions.

Chapter I.
Photovoltaic pumping systems

Chapter I.
Photovoltaic pumping systems

I.1 Introduction

Numerous global populations, particularly those residing in rural areas and isolated locations, encounter significant challenges in fulfilling their fundamental requirements due to the scarcity of electrical energy. Consequently, institutions are exploring alternative solutions to enhance living conditions in these regions.

To improve the supply of drinking water, the utilization of solar energy, particularly photovoltaic energy, for water pumping is well suited for most of these regions, due to the existence of a shallow underground hydraulic potential, less than 30 meters in the majority of Saharan desert areas, and a large solar energy potential, greater than 6 KW_h/m^2 on a surface inclined at the latitude of the place.

This chapter lays the foundation for understanding photovoltaic water pumping systems. We begin by exploring the fundamental principles of solar energy and the process of electricity generation through the photovoltaic effect. Subsequently, we will delve into the core components that comprise photovoltaic systems and provide an overview of the various system types. Finally, the chapter will conclude with a theoretical framework for photovoltaic pumping strategies. This framework will introduce the essential components of these systems and analyze the factors influencing their design parameters.

I.2 Overview of photovoltaic energy

I.2.1 History of photovoltaic energy

The very first discovery of the solar cell marked the beginning of the change in energy production. This change would be iterated over and over to make new progress in the field of solar energy by researchers and is still going on. The history of solar energy is a story of innovation that all started in the early 19th century.

❖ **Solar energy in the 1800's**

In 1839, French scientist Edmond Becquerel discovered the photovoltaic effect at the young age of 19. He realized when electrons were in an excited state in a conduction band, they could move freely through a material, thus creating a current.

But this wasn't widely recognized until Einstein wrote a paper about the power of solar for which he eventually received the Nobel prize in 1922. The first solar panel was invented by Charles Fritts in 1883 where he coated a thin layer of selenium with an extremely thin layer of gold. The resulting cells had a conversion electrical efficiency of only about 1%. This invention led to the launching of a movement for producing solar energy.

❖ **Solar energy in the 1900's**

The solar era began in 1950 when Bell Laboratory scientists focused on photovoltaic (PV) developments and began utilizing silicon to produce solar cells. This breakthrough is credited to *Daryl Chapin*, *Calvin Fuller*, and *Gerald Pearson* which produced an efficiency of 4% only. In the 1960s and 1970's the production of solar panels was made possible but the downside was it was too expensive for mainstream consumers but scientists continued to develop solar energy technology to reduce the cost. With the rise of semiconductors in 1941, *Russel. S Ohl* described a process of forming silicon ingots that led to the first P-N junction cell. Ohl cut a section from the ingot including the top, barrier, and bottom portions, and attached electrodes to the top and bottom portions, yielding the first silicon solar cell. The figure below represents the first-ever patented silicon P-N -EMF (PN junction Electromotive force) cell.[4]

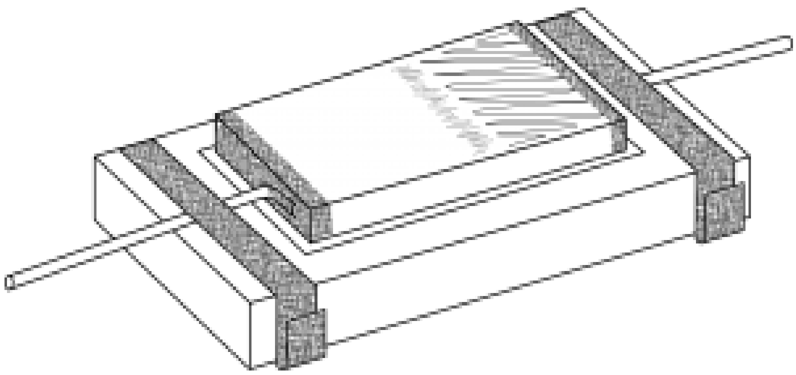

Fig I.1: silicon P-N photo-EMF cell from US patent [5].

I.2.2 Solar energy in Algeria

Algerian achievements in the field of renewable energies are very limited compared to the current evolution of the global or European renewable energy sector, which has reached very advanced stages. The use of renewable energies in Algeria has not exceeded the threshold of experimentation during five decades of independence, despite the country's strategic geographical position, which has one of the largest solar deposits in the world.

The duration of sunshine on almost the entire national territory exceeds 2000 hours per year and can reach 3900 hours on the high plateaus and the Sahara. The energy received daily on a horizontal surface of $1m^2$ is about 5 kW_h over most of the national territory, which is nearly $1700kW_h/m^2$/an at the North and 2263 kW_h/m^2/an at the South [6]. The map below illustrates the solar radiation potential in Algeria.

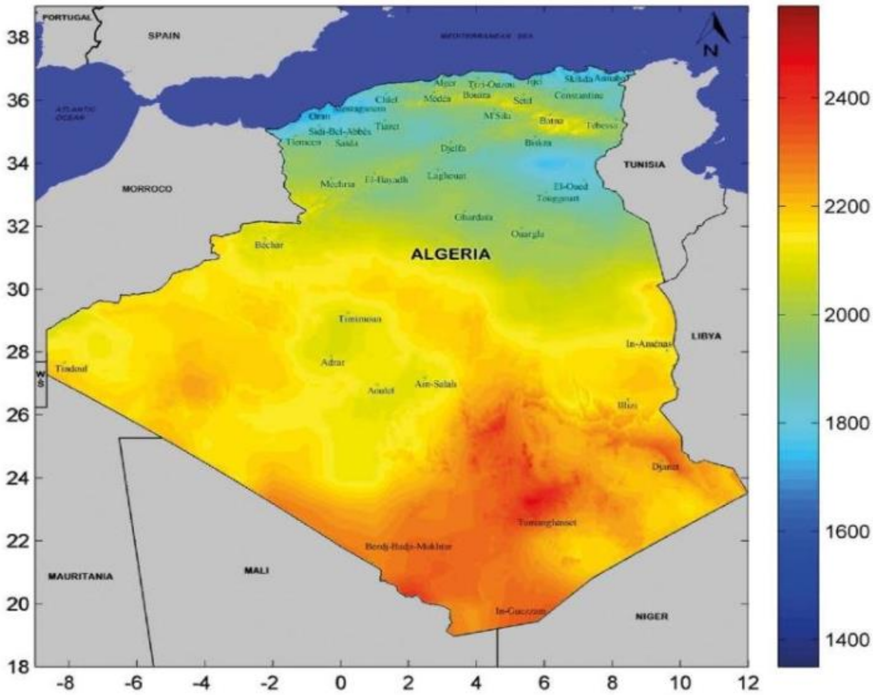

Fig I.2: Solar radiation potential in Algeria [7].

I.3 Photovoltaic solar energy

The sun produces an enormous amount of energy that leaves its surface in the form of electromagnetic radiation with a spectrum ranging from 0.2 μm (ultraviolet) to 4 μm (infrared).

Despite the considerable distance between the Earth and the sun (150.106 km), the Earth's surface receives an amount of energy of 180.106 GW. This energy received on Earth varies depending on the geographical and climatic situation of the regions. The solar radiation received at ground level depends on:

- The orientation, nature, and inclination of the Earth's surface.
- The latitude of the collection site, its degree of pollution, and its altitude.
- The time of year.
- The moment considered during the day.
- The nature of the cloud layers.

The operation of photovoltaic devices is based on the ability of certain specially treated semiconductor materials to convert solar radiation energy into electrical energy (direct current) without the need for moving mechanical parts. The most commonly used semiconductor material for this purpose is silicon. The basic component of a PV installation is the photovoltaic cell, capable of producing approximately 1.5 W of power under standard conditions, i.e., at a temperature of 25°C and subjected to a radiation power equal to 1000 W/m². Fig (I.3) shows the photovoltaic energy conversion [8] [9].

Fig I.3: The conversion of photovoltaic solar energy.

I.3.1 Photovoltaic cell

A photovoltaic cell is an energy harvesting technology, that converts solar energy into useful electricity through a process called the photovoltaic effect. There are several different types of PV cells which all use semiconductors to interact with incoming photons from the Sun in order to generate an electric current.

I.3.1.1 Photovoltaic cell working principle to generate electricity

Solar cells convert the energy in sunlight to electrical energy. Solar cells contain a material such as silicon that absorbs light energy.

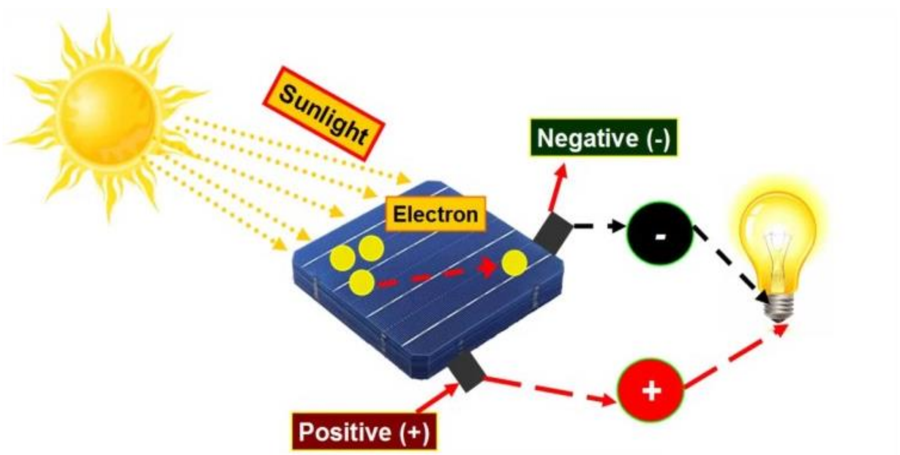

Fig I.4: Photovoltaic cell working principle to generate electricity

The energy knocks electrons loose so they can flow freely and produce a difference in electric potential energy, or voltage. The flow of electrons or negative charge creates electric current. Solar cells have positive and negative contacts, like the terminals in a Battery. If the contacts are connected with a conductive wire, current flows from the negative to positive contact. Fig (I.4) shows how a PV cell works to generate electricity [10].

I.3.1.2 Connecting of photovoltaic cells

❖ **Connecting in series**

By adding identical cells in series, the avalanche current remains the same but the voltage increases in proportion to the number of cells in series.

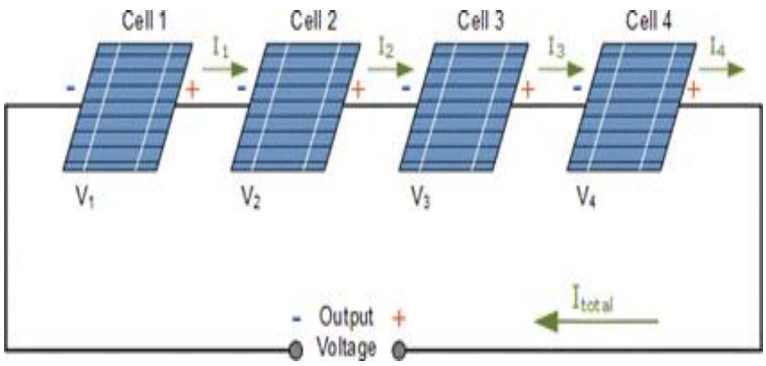

Fig I.5: Connecting of PV cells in Series.

❖ **Connecting in parallel**

The current-voltage characteristic obtained during the parallel assembly of two identical cells shows that the maximum power of the assembly is equal to twice the maximum power of a cell and the optimal voltage is the same for a single cell while the optimal current of the assembly is equal to twice the optimal current of a single cell.

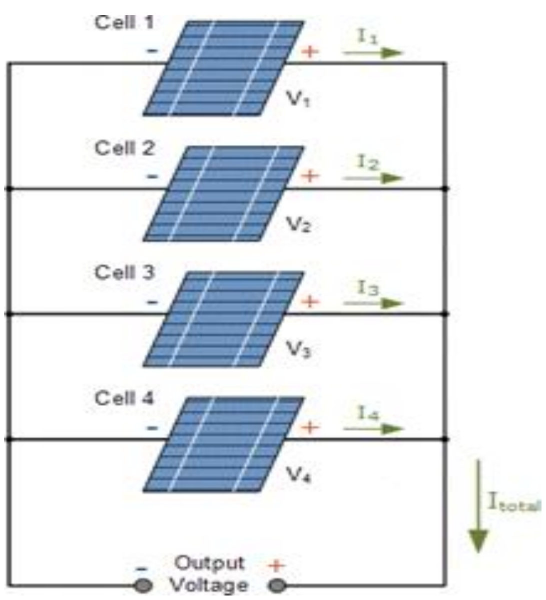

Fig I.6: Connecting of PV cells in Parallel.

I.3.2 Photovoltaic modules

A PV module consists of many PV cells wired in parallel to increase current and in series to produce a higher voltage. 36 cell modules are the industry standard for large power production. The module is encapsulated with tempered glass (or some other transparent material) on the front surface, and with a protective and waterproof material on the back surface. The edges are sealed for weatherproofing, and there is often an aluminum frame holding everything together in a mountable unit. In the back of the module there is a junction box, or wire leads, providing electrical connections.

I.3.3 Photovoltaic panels

PV panels include one or more PV modules assembled as a pre-wired, field-installable unit. The modular design of PV panels allows systems to grow as needs change. Modules of different manufacture can be intermixed without any problem, as long as all the modules have rated voltage output within 1.0 volt difference.

I.3.4 Photovoltaic array

A PV Array consists of a number of individual PV modules or panels that have been wired together in a series and/or parallel to deliver the voltage and amperage a particular system requires. An array can be as small as a single pair of modules, or large enough to cover acres [11].

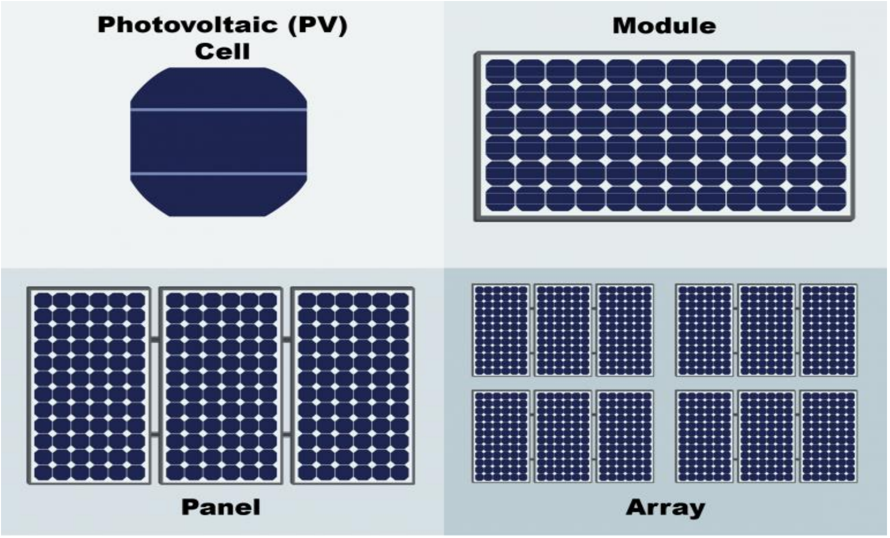

Fig I.7: PV cells, modules, panels and arrays.

I.4 Different kinds of solar photovoltaic system

There are basically three kinds of solar power systems through which electricity can be generated. These include [12]:

1. **On-grid solar**
2. **Hybrid solar**
3. **Off-grid solar**

I.4.1 On-grid photovoltaic system

In terms of energy and cost, a unit connected to the grid (or to a distribution center) is often the best solution for solar energy production. These installations consist of interconnected photovoltaic modules, one (or more) inverters. The inverter converts the direct current generated by the photovoltaic modules and generates alternating current according to the grid.

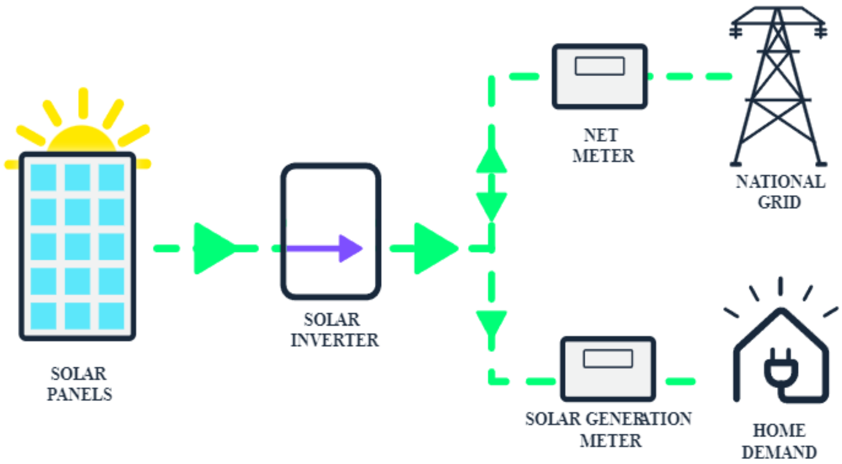

Fig I.8: On-Grid Photovoltaic System

I.4.2 Hybrid Photovoltaic System

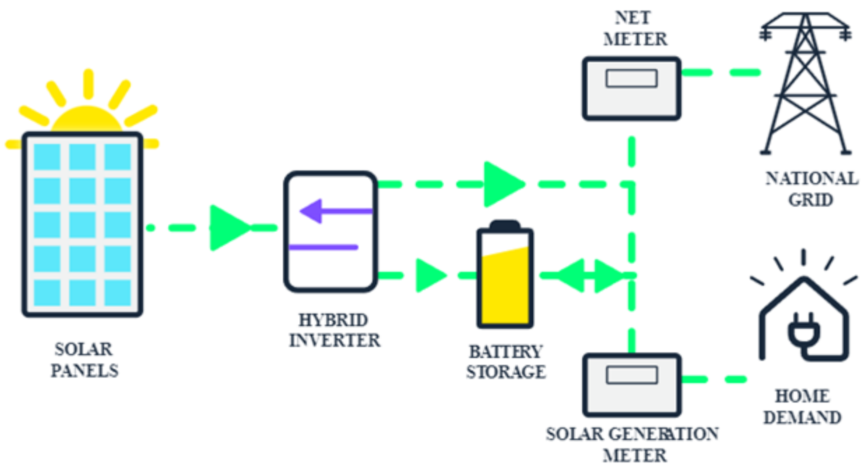

Fig I.9: Hybrid Photovoltaic System.

Hybrid systems are generally photovoltaic systems in which solar panels are combined with other energy sources, such as hybrid independent power plants combined with photovoltaic fields, wind turbines and diesel generators (group backup generators), the combination of which makes it a Consume renewable natural resources at production sites to ensure security of supply and minimize environmental disturbances regardless of atmospheric conditions.

I.4.3 Off-grid photovoltaic system

These systems are installed to ensure autonomous operation without resorting to other energy sources. Often these systems are used in areas far from the grid and, depending on the use, they can be installed either without power supply or on batteries to ensure adequate power supply during long cloudy days [13].

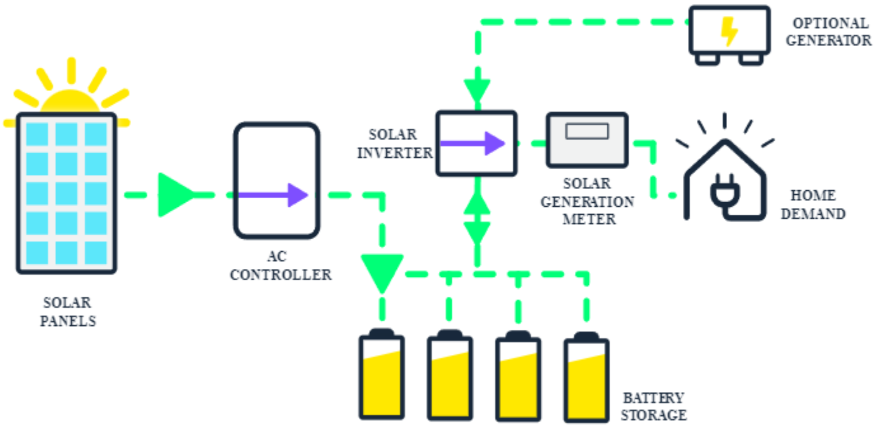

Fig I.10: Off-grid photovoltaic system.

I.5 Systems of photovoltaic pumping

Many populations in rural areas of developing countries face major problems due to the lack of water. These problems are especially accentuated in desert areas. The water deficit in arid zones is a vital issue for populations. The improvement of living conditions in these areas is linked to the search for adequate solutions to this problem. Photovoltaic pumping represents the ideal solution for water supply wherever the electricity grid is absent [14].

Currently, two photovoltaic pumping systems are used, with and without batteries. The technology without batteries has some disadvantages, its main flaw is to have a water flow that depends on the sunshine during the day.

I.5.1 Pumping without batteries

The storage is done hydraulically, the water being pumped when there is enough sunlight, into a tank above the ground. It is then distributed by gravity as needed. Pumping over the sun makes it possible to have a simpler photovoltaic system, as shown in Fig (I.11) [15]:

The operating principle of such an installation remains relatively simplified with photovoltaic panels supplying a pump (surface or submerged) assisted by a regulator controller (which can be integrated into the pump depending on the manufacturer) which supply the water when the panels are exposed to the sun. The over-the-sun pumping uses a tank to store the water until the moment of its use.

This solution is less expensive, but these pumps do not have a constant flow rate and do not operate below a certain level of illumination (beginning and end of the day), their efficiency being lower outside the nominal operating power.

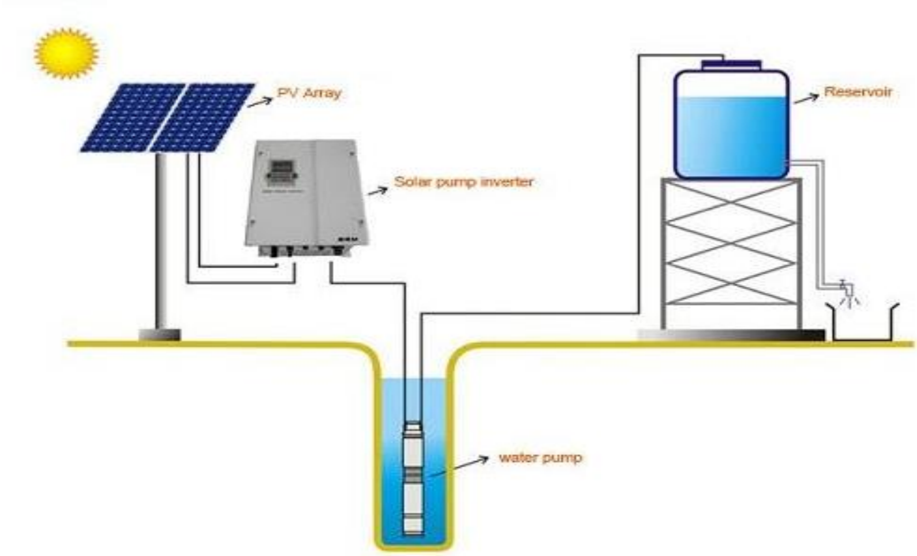

Fig I.11: Pumping without batteries.

I.5.2 Pumping with electrochemical storage (batteries)

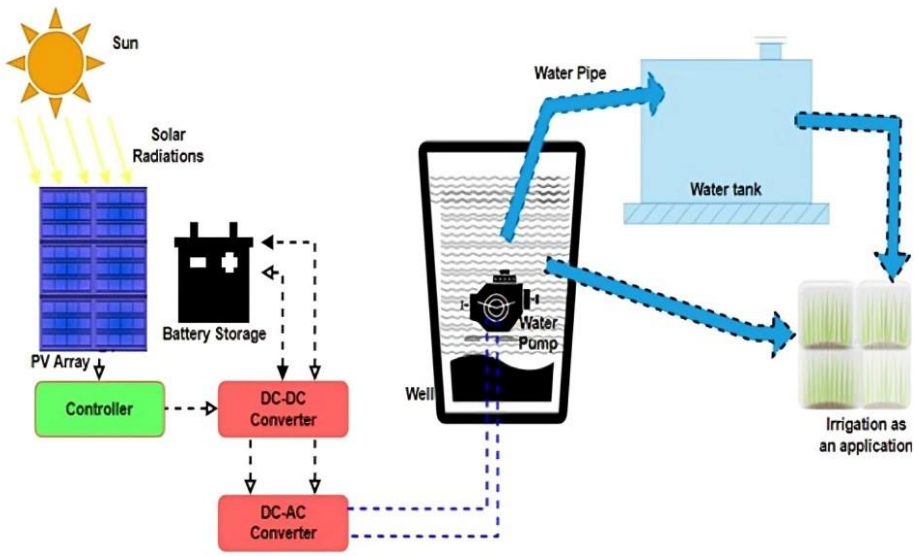

Fig I.12: Pumping with electrochemical storage.

Very often, photovoltaic pumping does not correspond to the hours of sunshine where a regular intensity is required, which implies storage. Photovoltaic pumping with battery makes it possible to ensure energy autonomy, and a constant flow rate according to demand [16].

The batteries make it possible to store electricity in order to restore it in a timely manner. A regulator is then essential to protect the batteries against overloads or deep discharges harmful to its service life.

I.6 Components of a photovoltaic water pumping system

The PV water pumping system is generally composed of:

- PV generator.
- DC/DC Converter (boost)
- DC/AC Converter (inverter).
- Motor-pump unit.

The effectiveness of a solar water pumping system relies on both site-specific characteristics (such as sunshine, temperature, and geographical location) and equipment-related factors (including efficiency and service life). In our study, the photovoltaic pumping system comprises the components illustrated in Fig I.13.

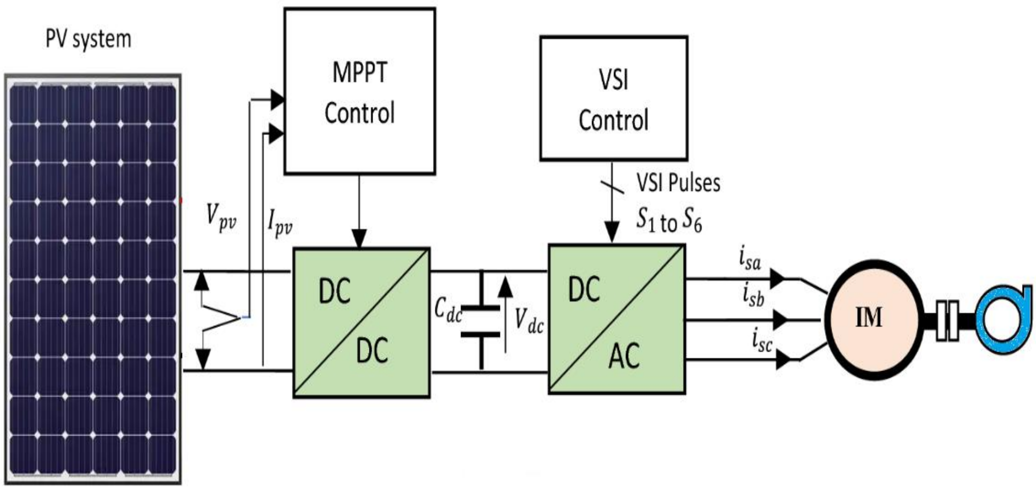

Fig I.13: PV array water pumping system design.

Photovoltaic solar panels that convert solar radiation into electrical energy, electrically interconnected to constitute a direct current production unit.

A power control and monitoring unit, consisting of a converter (boost) and a converter (inverter), capable of providing voltages with adjustable amplitudes and frequencies depending on the available power of the solar generator. A submerged electric pump unit, consisting of an asynchronous motor and a centrifugal pump.

An electrical wiring, through which the energy passes from the generator to the engine, and the information relating to the safety controls. A hydraulic infrastructure that leads the water from the well to the distribution points.

I.6.1 PV generator

A photovoltaic generator consists of a number of modules formed by a number of photovoltaic cells, connected together in series and in parallel to provide the necessary current and voltage. The performance of the generator depends on the variability of the modules that the generator comprises and the cells comprised by the modules.

The output voltage of the photovoltaic generator depends on the number of modules in series while the output current depends on the number of modules in parallel. The integrated set of photovoltaic modules is defined as a photovoltaic array, shown by Fig (I.7), [17].

I.6.2 DC/DC converter

The DC / DC converters have the function of providing a variable DC voltage from a fixed DC voltage. This energy conversion is carried out thanks to a high-frequency "cutting" characterized by a high efficiency [18]. There are different types of DC/DC converters [19]:

I.6.2.1 Buck converter

A buck converter reduces voltage and the output voltage is lower than the input voltage. See Fig (I.14).

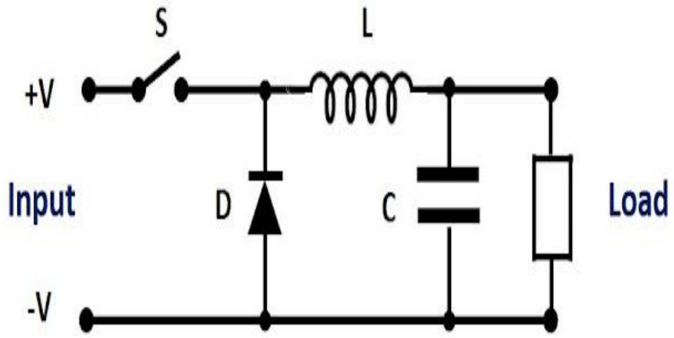

Fig I.14: Buck converter.

When transistor S is turned on, energy is stored in inductor L as the current flows to the load and capacitor C is charged. When S is off, the energy stored in L is released and current flows into the load and circulates via diode D. Capacitor C also provides energy to the load. This is repeated at a high frequency, greater than 100,000 times a second. The length of the time S is turned on defines the output voltage.

I.6.2.2 Boost converter

A boost converter increases voltage and the output voltage is higher than the input voltage. See Fig (I.15).

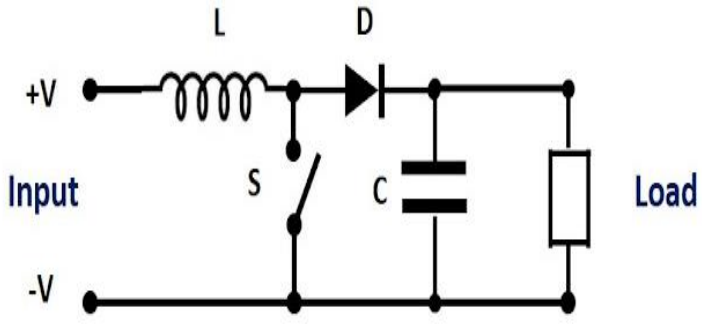

Fig I.15: Boost converter.

When transistor S is turned on, current flows through inductor L, through transistor S back to the input. During this period energy is stored in the inductor. When transistor S is off, the inductor acts a voltage source in series with the input voltage. The inductor's stored energy is circulated through diode D to the load. This charges capacitor C to a higher level than the input voltage. Again, the length of the time S is turned on defines the output voltage.

I.6.2.3 Buck-boost converter

A buck-boost converter is a combination of a buck and boost converter. The output voltage can be higher or lower than the input voltage. See Fig (I.16). As you can see the circuit is more complicated and has more components. S_2, L, and D_2 is the boost converter (S_1 being on) and S_1, L and D_1 the buck section (S_2 being off).

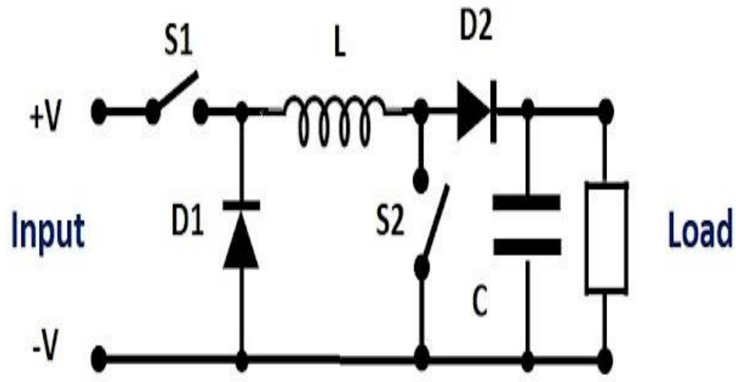

Fig I.16: Buck-boost converter.

I.6.3 DC/AC Converter (inverter)

The function of the inverter is to transform the direct current produced by the photovoltaic generator, into single-phase or three-phase alternating current. Inverters are bridge structures most often consisting of electronic switches such as IGBTs (power transistors) [20].

I.6.4 Motor-pump unit

I.6.4.1 Motors

The motor of a Motor-pump unit converts electrical energy into mechanical energy. It can be direct current or alternating current. In the latter case, an electronic converter or an inverter is necessary to convert the direct current coming from a photovoltaic generator into alternating current [21-22].

❖ **DC motor**

These motors are powered by direct voltages. The main advantage of direct current machines lies in their simple adaptation to the means making it possible to adjust or vary their speed, their torque and their direction of rotation.

❖ **AC motor**

The Induction motors are well-suited for solar panel systems due to their inherent characteristic of operating without a rotor power supply. This eliminates the need for complex brushes or slip rings, enhancing the system's autonomy and reliability. Additionally, the use of an inverter (DC/AC converter) to power the induction motor allows for optimization of the generated power output [18].

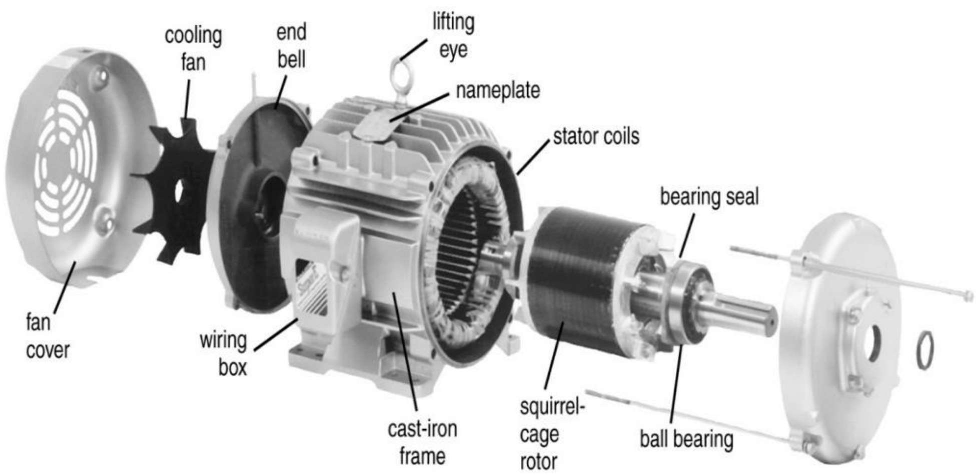

Fig I.17: Induction motor.

I.6.4.2 Pumps

A pump is a hydraulic machine that sucks and delivers a liquid (water, oil, gasoline, food liquids etc ....) from a point to a desired place. The pump is intended to raise the load of the pumped liquid. Pumps conveying liquids are divided into two main categories: **positive displacement** and **centrifugal pumps** [23].

❖ **Positive displacement pump**

These pumps operate by trapping a fixed amount of fluid and then forcing it into the discharge pipe. They create flow by physically displacing the fluid using reciprocating, rotary, or diaphragm mechanisms. These pumps provide a relatively constant flow rate regardless of changes in system pressure. They are suitable for applications requiring a steady flow or handling viscous fluids [24].

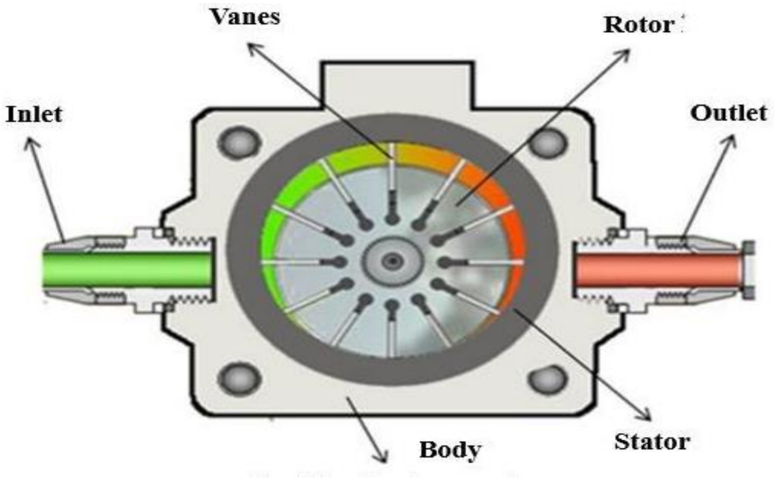

Fig I.18: Positive displacement pump.

❖ **Centrifugal pump**

These pumps operate by converting rotational energy into kinetic energy. They use a rotating impeller to increase the fluid's velocity and create a centrifugal force that moves the fluid from the center to the periphery of the impeller. The flow rate of centrifugal pumps varies with changes in system pressure. Their flow rate increases as the discharge pressure decreases. They are better suited for applications with higher flow rates and low to medium viscosity fluids. [24]

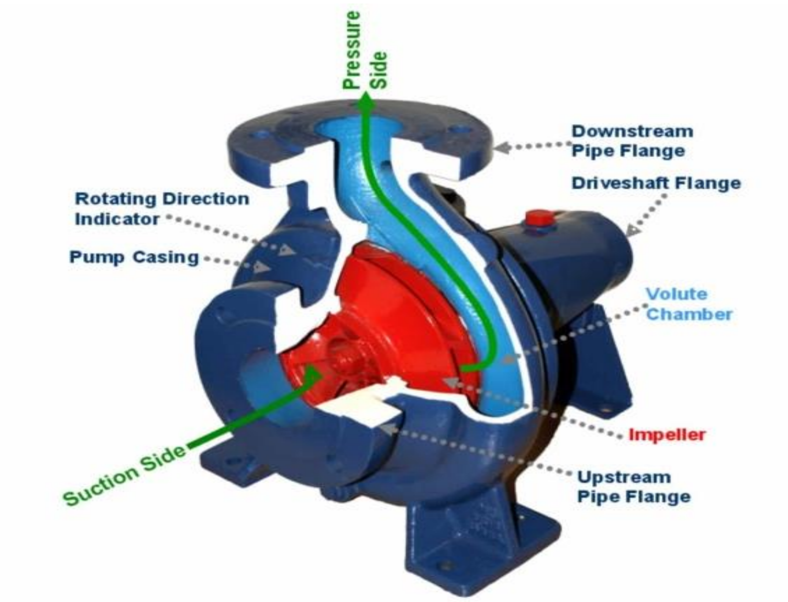

Fig I.19: Centrifugal pump.

❖ **Comparison between the centrifugal pump and the positive displacement pump** [25]

Below is a quick comparison table that highlights the main performance differences between centrifugal (rotodynamic) pumps and positive displacement pumps.

Factor	Centrifugal	Positive Displacement
Mechanics	Impellers pass on velocity from the motor to the liquid which helps move the fluid to the discharge port (produces flow by creating pressure).	Traps confined amounts of liquid and forces it from the suction to the discharge port (produces pressure by creating flow).
Performance	Flow rate varies with a change in pressure.	Flow rate remains constant with a change in pressure.
Viscosity	Flow rate rapidly decreases with increasing viscosity, even any moderate thickness, due to frictional losses inside the pump.	Due to the internal clearances high viscosities are handled easily and flow rate increases with increasing viscosity.
Efficiency	Efficiency peaks at a specific pressure; any variations decrease efficiency dramatically. Does not operate well when run off the middle of the curve; can cause damage and cavitation.	Efficiency is less affected by pressure, but if anything tends to increase as pressure increases. Can be run at any point on their curve without damage or efficiency loss.
Suction Lift	Standard models cannot create suction lift, although self-priming designs are available and manometric suction lift is possible through a non return valve on the suction line.	Create a vacuum on the inlet side, making them capable of creating suction lift.
Shearing	High speed motor leads to shearing of liquids. Not good for shear sensitive mediums.	Low internal velocity means little shear is applied to the pumped medium. Ideal for shear sensitive fluids.

Table I.1: Comparison between centrifugal pumps and positive displacement pumps.

I.7 Advantages and disadvantages of photovoltaic systems

I.7.1 The advantages

- First of all, high reliability. The installation does not have any moving parts, which make it particularly suitable for isolated regions. This is the reason for its use on spacecraft.
- the modular nature of the photovoltaic panels allows a simple assembly and adaptable to various energy needs. The systems can be dimensioned for power applications ranging from milli Watt to Mega Watt.
- The operating cost is very low considering the reduced maintenance and it does not require fuel, nor its transport, nor highly specialized personnel.
- Photovoltaic technology has qualities from an ecological point of view because the finished product is non-polluting, silent and does not cause any disturbance to the environment, except by occupying space for large-scale installations [26].

I.7.2 The disadvantages

- The manufacture of the photovoltaic module is high-tech and requires high-cost investments.
- The real conversion efficiency of a module is low, of the order of 10-15% (between 10 and 15 MW/ km^2 per year for the BENELUX) with a theoretical limit for a cell of 28%.
- Photovoltaic generators are not competitive with diesel generators only for low energy demands in isolated regions.
- Dependent on weather conditions
- When the storage of electrical energy in chemical form (battery) is necessary, the cost of the generator is increased [26].

I.8 Conclusion

This chapter has comprehensively explored the fundamental concepts that constitute a photovoltaic water pumping system. We have delved into the operation of each essential element, providing a clear understanding of their individual functionalities. This in-depth exploration lays the groundwork for the subsequent chapter, which will focus on the modeling and analysis of these integrated systems.

Chapter II.

Modeling of the PV array and the boost converter

Chapter II.
Modeling of the PV array and the boost converter

II.1 Introduction

Photovoltaic (PV) systems have emerged as a promising solution for clean and sustainable energy generation. These systems convert sunlight directly into electricity through the photovoltaic effect. However, to maximize their efficiency and performance, accurate modeling of both the PV panel itself and the DC-DC converters used within the system is crucial.

Mathematical modeling serves as a critical preliminary step for any photovoltaic pumping system. It lays the groundwork for subsequent stages, including system dimensioning, optimization, and simulation. The system under investigation here is a photovoltaic pumping system, primarily comprised of a photovoltaic generator, static converters, and a motor-pump unit.

This chapter focuses on the mathematical modeling of a solar panel and boost converter system, incorporating a Maximum Power Point Tracking (MPPT) control strategy. The primary objective is to optimize the efficiency of the photovoltaic (PV) system by employing MPPT algorithms, specifically the Perturb and Observe (P&O) and Incremental Conductance (INC) methods, to locate the Maximum Power Point (MPP) under varying temperature and illumination conditions.

II.2 Modeling of photovoltaic cells

II.2.1 Ideal PV cell

A photovoltaic cell can be described in a simple way in figure (II.1) as an ideal current source which produces a current i_{ph} proportional to the incident light power, in parallel with a diode which corresponds to the transition area p-n of the PV cell. If a resistive load is connected to the terminals of the photovoltaic cell, the latter delivers a current i_{pv} there [27].

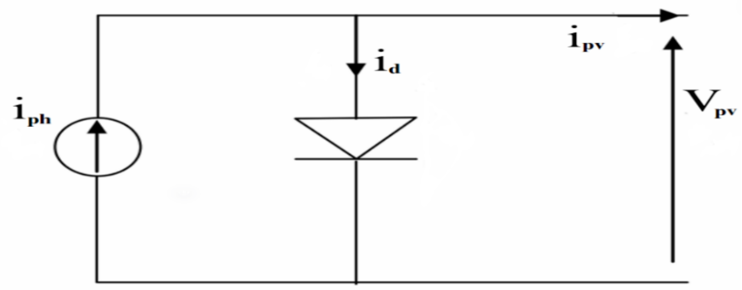

Fig II.1: Diagram of an ideal photovoltaic cell.

If the photocell is under irradiance, The current expression will be:

$$i_{pv} = i_{ph} - i_d = i_{ph} - I_s[\exp\left(\frac{q\,V_{pv}}{a\,k_b\,T}\right) - 1] \quad \text{(II-1)}$$

with:

Is: the saturation current

a: the ideality factor of Junction 1<n <3

k_b: Boltzmann constant (1 ,38.10-23 J/K)

T: temperature of the cell in degrees kelvin

q: Electron charge ($1,602.10^{-19}$)

II.2.2 Real PV cell

The previous photovoltaic model does not take into account all the phenomena present during the conversion of light energy. Indeed, in the real case, a loss of output voltage is observed as well as leakage currents. This voltage loss is therefore modeled by a series resistor R_s and the leakage currents by a parallel resistor R_p.

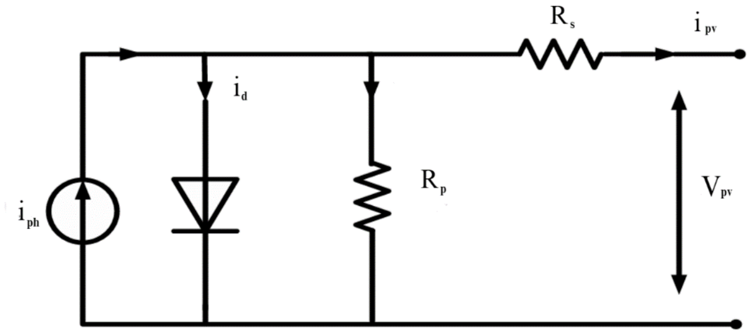

Fig II.2: Diagram of a real photovoltaic cell.

So, the expression of the cell current can have the following form:

$$i_{pv} = i_{ph} - i_d - \frac{V_{pv}}{R_p} = i_{ph} - I_s\left[\exp\left(\frac{q(V_{pv} + R_s i_{ph})}{ak_b T}\right) - 1\right] - \frac{V_{pv} + R_s i_{ph}}{R_p} \quad \text{(II-2)}$$

II.3 Modeling of a photovoltaic panel

The electric model of the PV is shown in Fig (II.3).

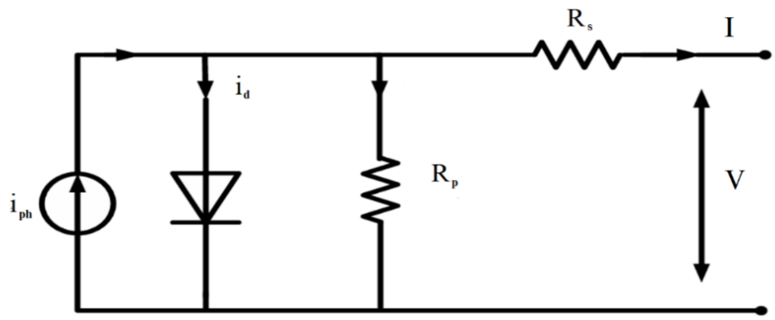

Fig II.3: The electric model of a Cell.

In this model, the photovoltaic cell is represented by a current source which generates a current I_{ph} proportional to the sunshine G. The current I supplied by the cell is modeled by the following equation:

$$I = I_{ph} - I_s\left[\exp\left(\frac{V+R_sI}{V_ta}\right)\right] - \left(\frac{V+R_sI}{R_p}\right) \quad \text{(II-3)}$$

with:

Vt: the thermodynamic potential;

a: the ideality factor of Junction 1<n <3

I_{ph}: the photocurrent (current created by the cell).

I_s: the saturation current.

R_s: series resistance (Ω).

R_p: parallel resistance (Ω).

I_{ph} is the photocurrent:

$$I_{ph} = \left(I_{pv,n} + k_I(T_n\text{-}T)\right)\frac{G}{G_n} \quad \text{(II-4)}$$

where:

$I_{pv,n}$: the current generated by the solar irradiance under the nominal conditions.

$T_n\text{-}T$: are respectively the actual and nominal temperatures (K).

G and G_n : are respectively the irradiance and the nominal irradiance (W/m^2).

k_I : the short-circuit current/temperature coefficient.

I_s is the saturation current:

$$I_s = \frac{I_{sc} + k_I \cdot \Delta t}{\exp\left(\frac{V_{oc} + K_v \cdot \Delta t}{V_t \cdot a}\right) - 1} \quad \text{(II-5)}$$

K_v : the open circuit voltage/temperature coefficient.

where V_t is the array thermal voltage given by:

$$V_t = \frac{N_s \cdot k_b \cdot T}{q} \quad \text{(II-6)}$$

II.4 Characteristic of a photovoltaic panel

In this investigation, a T5-SER-235P solar cell manufactured by *SunPower* will be examined. The module exhibits the following specifications under standard test conditions (STC) with an irradiance of 1000 W/m² and a temperature of 25°C.

Table II.1: **T5-SER-235P** module from SunPower.

Parameters of the PV cell	
Maximum power (P_{mpp})[W]	**235**
Maximum current (I_{mpp})[A]	**7.99**
Maximum voltage (V_{mpp})[V]	**29.42**
Open circuit voltage (V_{oc})[V]	**36.96**
Short circuit current (I_{cc})[A]	**8.48**

II.4.1 Current-Voltage and Power-Voltage characteristic

The characteristic of the photovoltaic module in the form of Fig (II.4) and Fig (II.5).

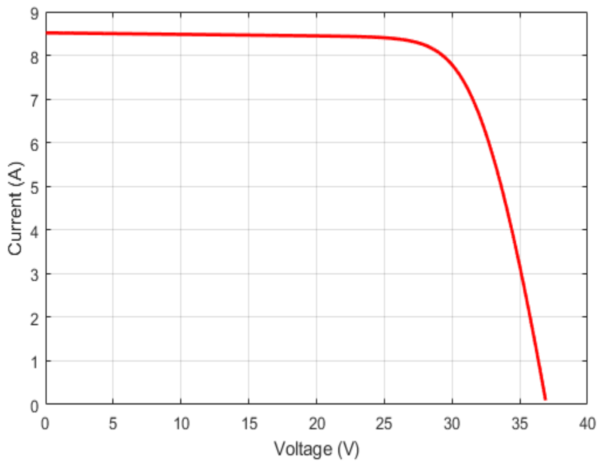

Fig II.4: Current-voltage characteristic of PV

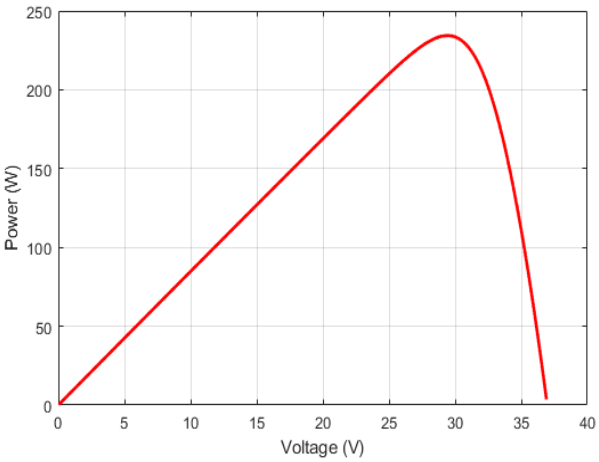

Fig II.5: Power-voltage characteristic of PV

II.4.2 Influence of irradiance

The Fig (II.6) represent the Current-voltage and Power-voltage characteristics of PV modules at constant temperature (T=25°C.) and variable irradiance (400 W/m²; 600 W/m²; 800 W/m²; 1000W/m²; and 1200 W/m²). It was observed that the value of the short-circuit current was proportional to the intensity of the radiation (luminous flux).

On the other hand, the open circuit voltage does not change in the same proportion, but remains almost constant even in low irradiance. So, it means:

- The optimal power P_{ppm} is in fact proportional to the irradiance.

- The voltage at the maximum power point is approximately the same.

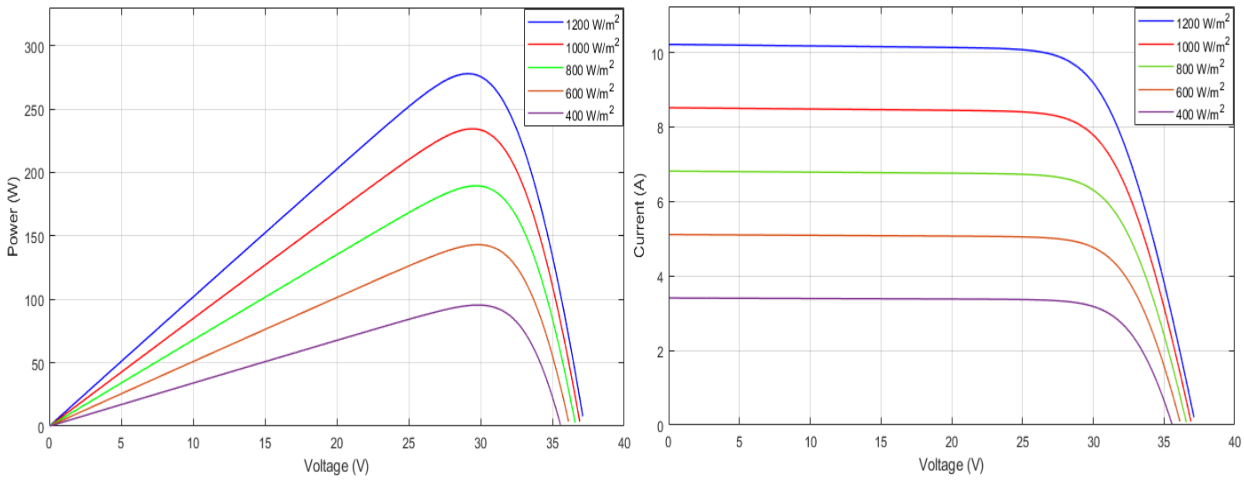

Fig II.6: influence of irradiance on the characteristics P(V) and I(V).

II.4.3 Influence of temperature

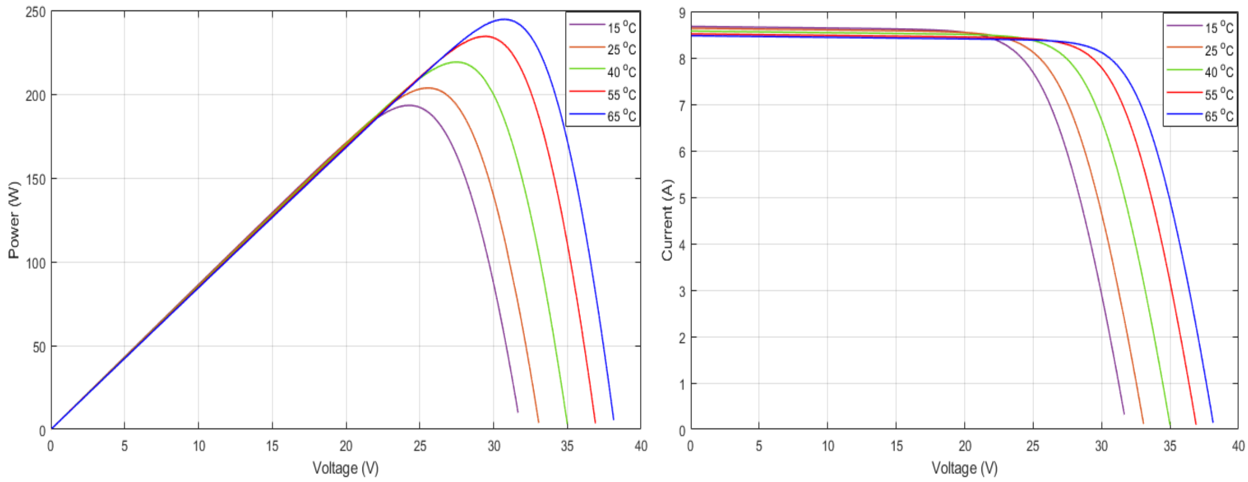

Fig II.7: influence of temperature on the characteristics P(V) and I(V).

Fig (II.7) shows the Current-voltage and Power-voltage characteristics at a constant irradiance of 1000 W_c/h for different operating temperatures of the PV module (15, 25, 40, 55 and 65° C). It is obvious that the effect of the temperature on the value of the short-circuit current is negligible. On the other hand, when the temperature increases, the open circuit voltage decreases quite strongly. For each temperature increase of 25 °C, the maximum power of the PV modules decreases by about 0.85%.

II.5 Modeling of Boost converter

Boost converter or step-up converter is a DC-to-DC converter that increases voltage. The diagram of Fig (II.8) shows the electrical circuit of the Boost.

At the first time (αT), the transistor (K) is closed, the current in the inductor gradually increases, and gradually, it stores energy, until the end of the first period. Then, the transistor (K) opens and the inductor (L) opposing the current decrease (I_L), generates a voltage which is added to the source voltage, which is applied to the load (R) through the diode (D).

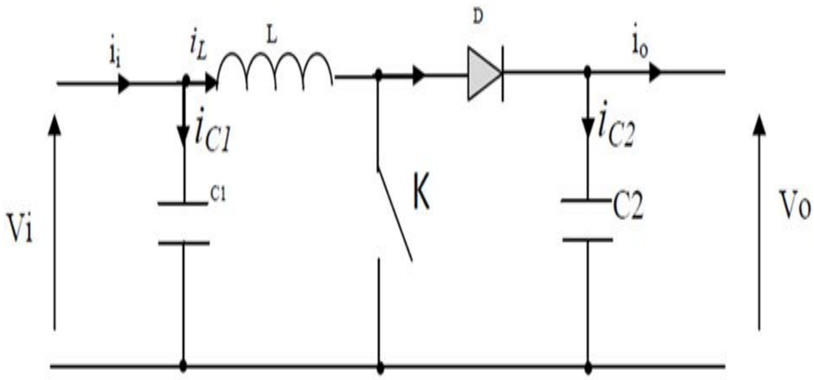

Fig II.8: Circuit diagram of Boost Converter.

II.5.1 Equivalent mathematical model

The following figures (Fig II.9) and (Fig II.10) represent the modeling of the closed and open Boost converters.

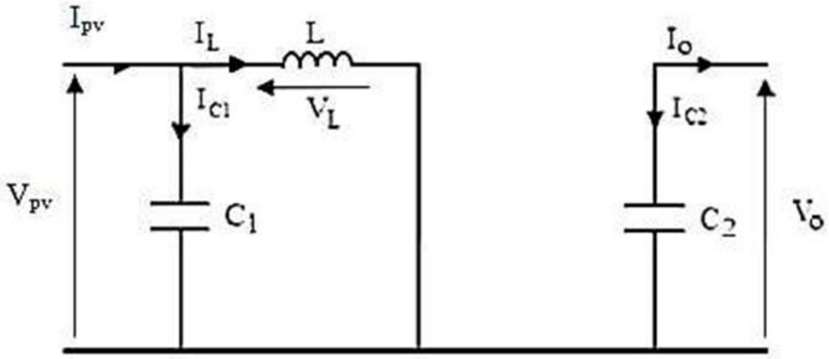

Fig II.9: Schematic diagram of a closed Boost converter.

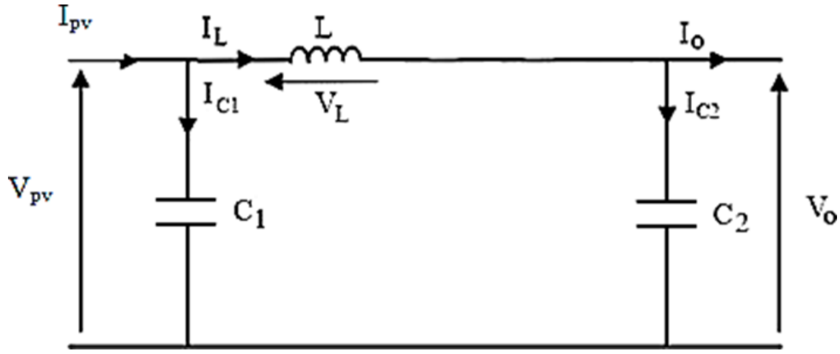

Fig II.10: Schematic diagram of an open Boost converter.

Phase 1 : $T_{On} = \alpha T\mu$

$$I_{C_1} = C_1\left(\frac{dv_{pv}}{dt}\right) = I_{pv} - I_L \tag{II-7}$$

$$I_{C_2} = C_2\left(\frac{dv_0}{dt}\right) = -I_0 \tag{II-8}$$

$$V_L = L\left(\frac{dI_L}{dt}\right) = V_{pv} \tag{II-9}$$

Phase 2: $T_{Off} = (\alpha\text{-}1)T$

$$I_{C_1} = C_1\left(\frac{dv_{pv}}{dt}\right) = I_{pv} - I_L \tag{II-10}$$

$$I_{C_2} = C_2\left(\frac{dv_0}{dt}\right) = I_L - I_0 \tag{II-11}$$

$$V_L = L\left(\frac{dI_L}{dt}\right) = V_{pv} - V_0 \tag{II-12}$$

II.6 The MPPT control

The characteristics of a PV system vary with temperature and irradiation, (Fig II.6 and Fig II.7). So, the MPPT algorithm is also obliged to keep track of the new modified maximum power point in its corresponding curve whenever temperature or irradiation variation occurs.

II.6.1 Principle of the MPPT control

By definition, an MPPT command, associated with an intermediate adaptation stage, makes it possible to operate a GPV so as to continuously produce the maximum of its power. Thus, regardless of the weather conditions (temperature and irradiation), the control of the converter places the system at the maximum operating point (V_{PPM} and I_{PPM}).

The photovoltaic conversion chain will be optimized through a Boost converter controlled by an MPPT. It can be represented by the diagram of Fig (II.11) [28-29].

The MPPT control varies the duty cycle of the Boost converter, using an appropriate electrical signal, to extract the maximum power that the GPV can provide. The MPPT algorithm can be more or less complicated to search for PPM. In general, it is based on the variation of the duty cycle of the CS as a function of the evolution of the input parameters of the latter (I and V and consequently of the power of the GPV) until it is placed on the PPM [30].

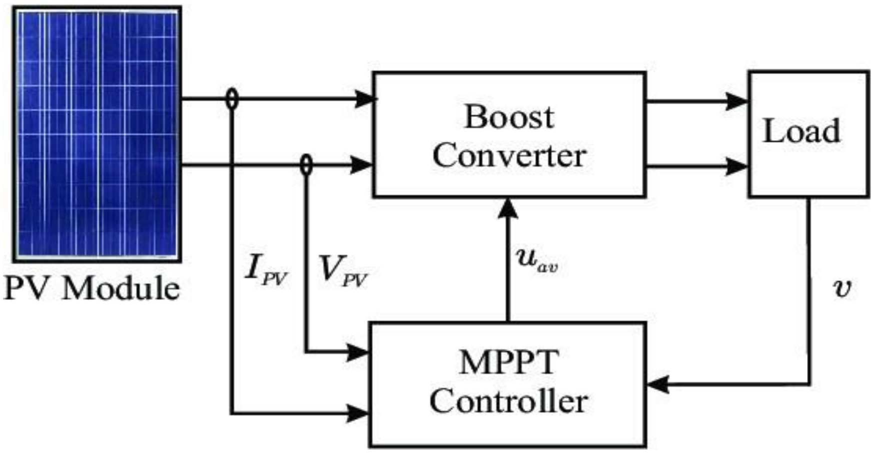

Fig II.11: Solar energy conversion chain.

II.7 MPPT Algorithms

To date, numerous maximum power point tracking algorithms have been proposed, with various trade-offs between performance (tracking speed, accuracy) and complexity (need for sensors, mathematical modeling, computation burden, etc.).

Perturb and Observe (P&O) and Incremental conductance (INC) methods are commonly used because of the ease of implementation and simplicity.

II.7.1 Perturb and Observe (P&O) method

The Perturb and Observe method is a widely used approach in the research of MPPT because it is simple and requires only voltage and current measurements of the photovoltaic panel V_{pv} and I_{pv} respectively. It can deduce the maximum power point even during variations in irradiance and temperature.

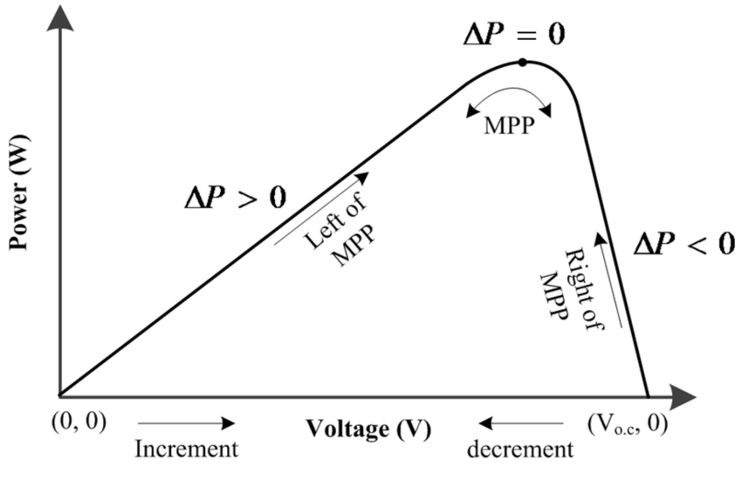

Fig II.12: Graph of Power-voltage of P&O algorithm.

Among other possible algorithms, the Perturb and Observe (P&O) tracking algorithm actively varies the current set-point and observes the corresponding impact on the output power.

Depending on whether that perturbation tends to increase or decrease the output power, the current setpoint is respectively increased or decreased accordingly.

When the maximum power point is reached, V_{pv} oscillates around the optimal value this then causes a power loss which increases with the incrementation step of the disturbance. If this incrementation step is large, the MPPT algorithm responds quickly to sudden changes in operating conditions [31].

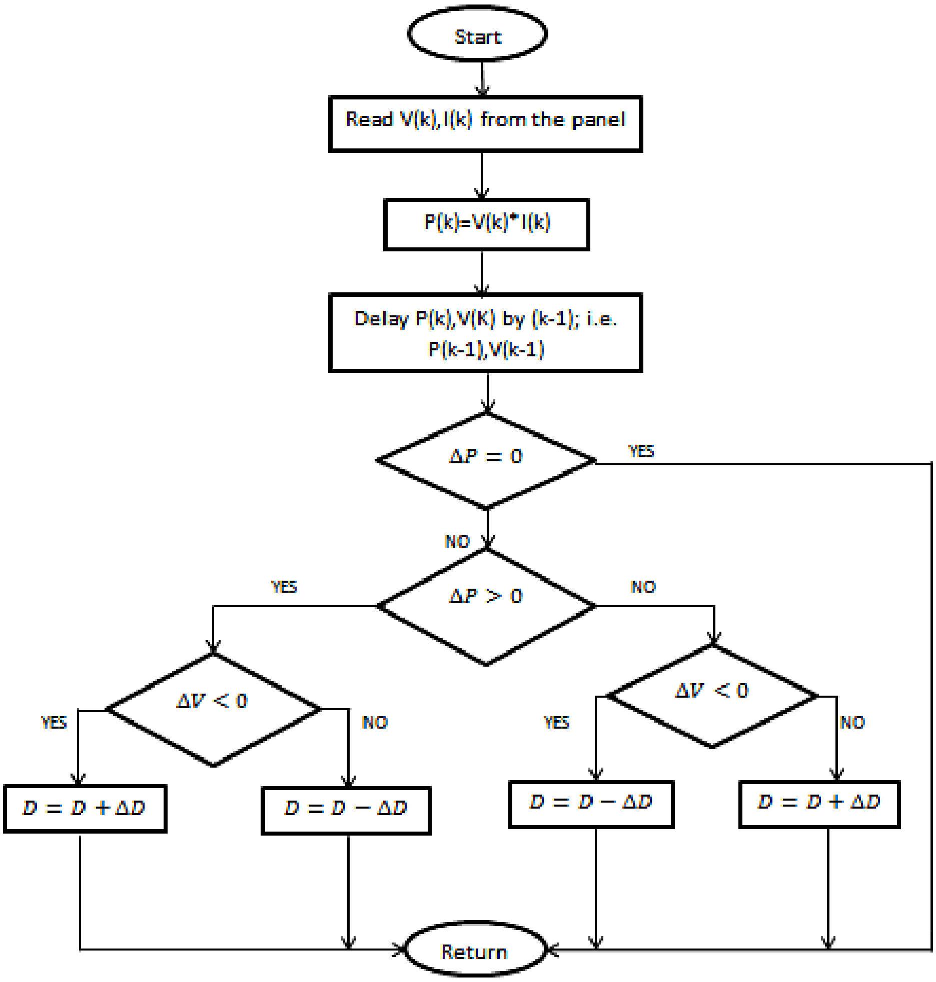

Fig II.13: Flowchart of Perturb and Observe (P&O) algorithm.

II.7.2 Incremental Conductance (INC) method

Under fast varying atmospheric condition, the problem associated with P&O method is overcome by Incremental Conductance (INC) method. The Incremental Conductance method can determine that the MPPT has reached the MPP and stop perturbing the operating point. If this condition is not met, the direction in which the MPPT operating point must be perturbed can be calculated using the relationship between dI/dV and – I/V.

This relationship is derived from the truth that dP/dV is negative when the MPPT is to the right-side curve of the MPP and positive when it is to the left side curve of the MPP.

This algorithm determines when the MPPT has reached the MPP, whereas P&O oscillates around the MPP. The incremental conductance method tracks the maximum power point accurately by comparing the incremental conductance and instantaneous conductance of a PV array [32]. Incremental conductance method can track rapidly increasing and decreasing irradiance conditions with higher accuracy than perturb and observe method [33]. The disadvantage of this algorithm is that it is more complex when compared to P&O.

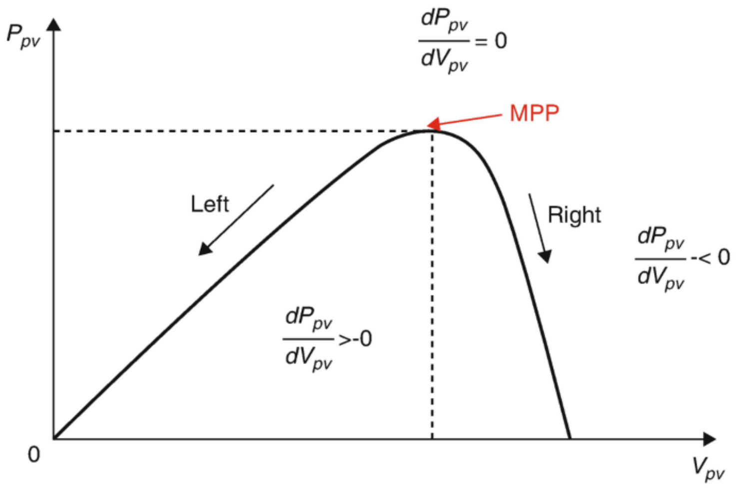

Fig II.14: Graph of power/voltage of INC algorithm.

The algorithm can be easily understood by the following flow chart which is shown in Fig (II.15).

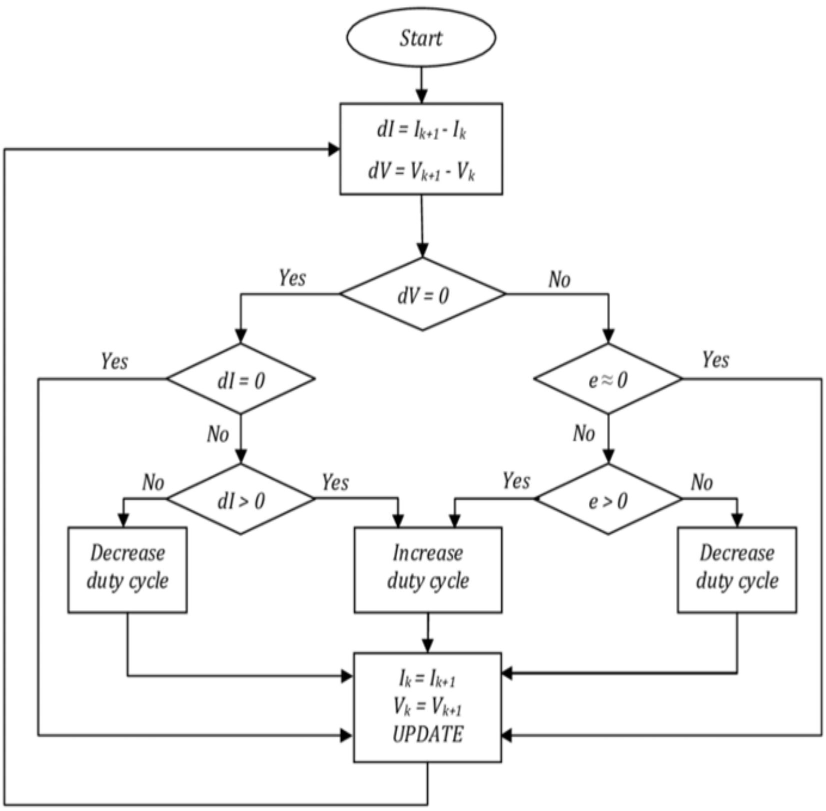

Fig II.15: Flowchart of Incremental Conductance (INC) method algorithm.

II.8 Simulation of the PV system with MPPT control

- The system is simulated under standard conditions (G=1000W/m2, T=25C) to extract the optimal power from our system.
- The electrical characteristics of the Boost converter and the Parameters of The PV cell used in this work are given in the Appendix.

II.8.1 Simulation diagram

Fig (II.16) shows the block diagram of simulation using the MATLAB/SIMULINK software of the photovoltaic system using Perturb and Observe and Incremental Conductance Methods.

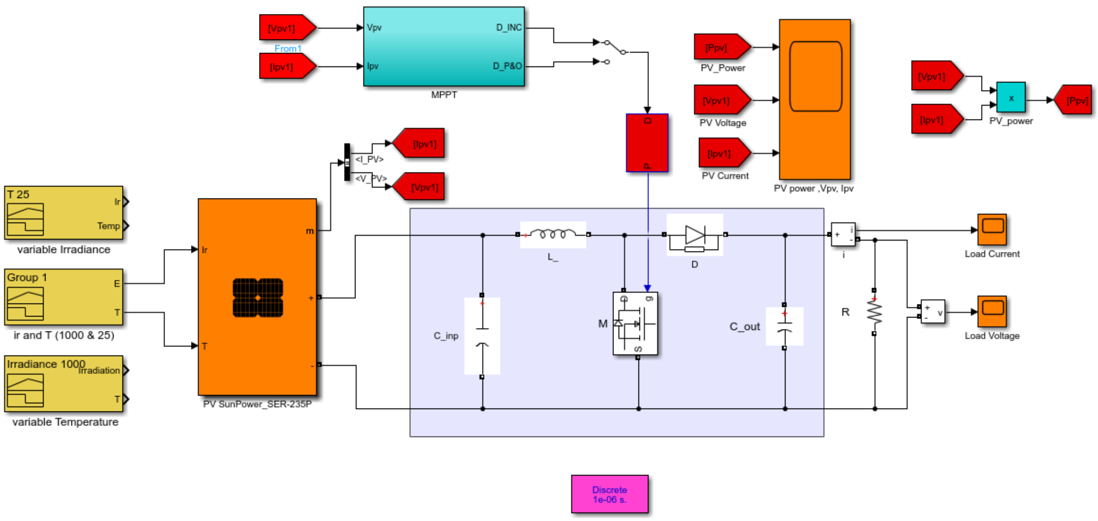

Fig II.16: Matlab/Simulink diagram of the photovoltaic system with P&O and INC Methods

II.8.2 Simulation results with P&O Algorithm

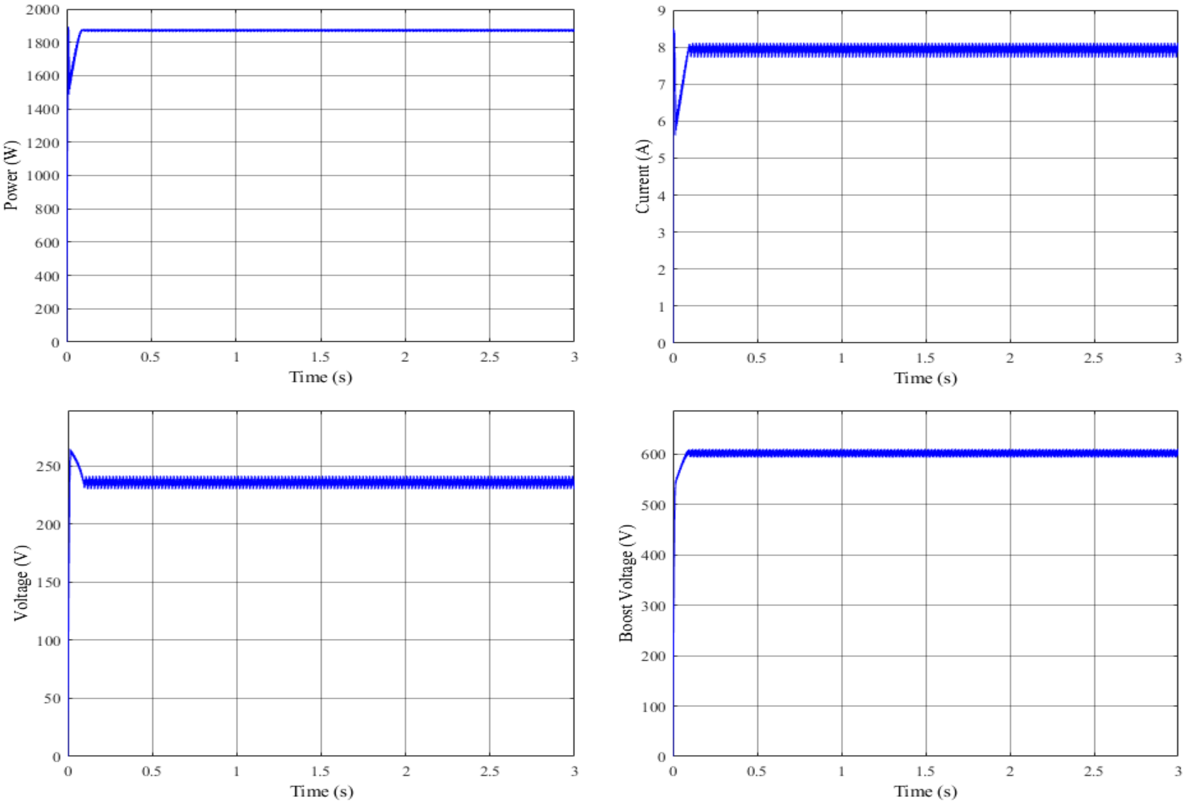

Fig II.17: PV simulation results at (T=25°C, I=1000W/m^2) with (P&O).

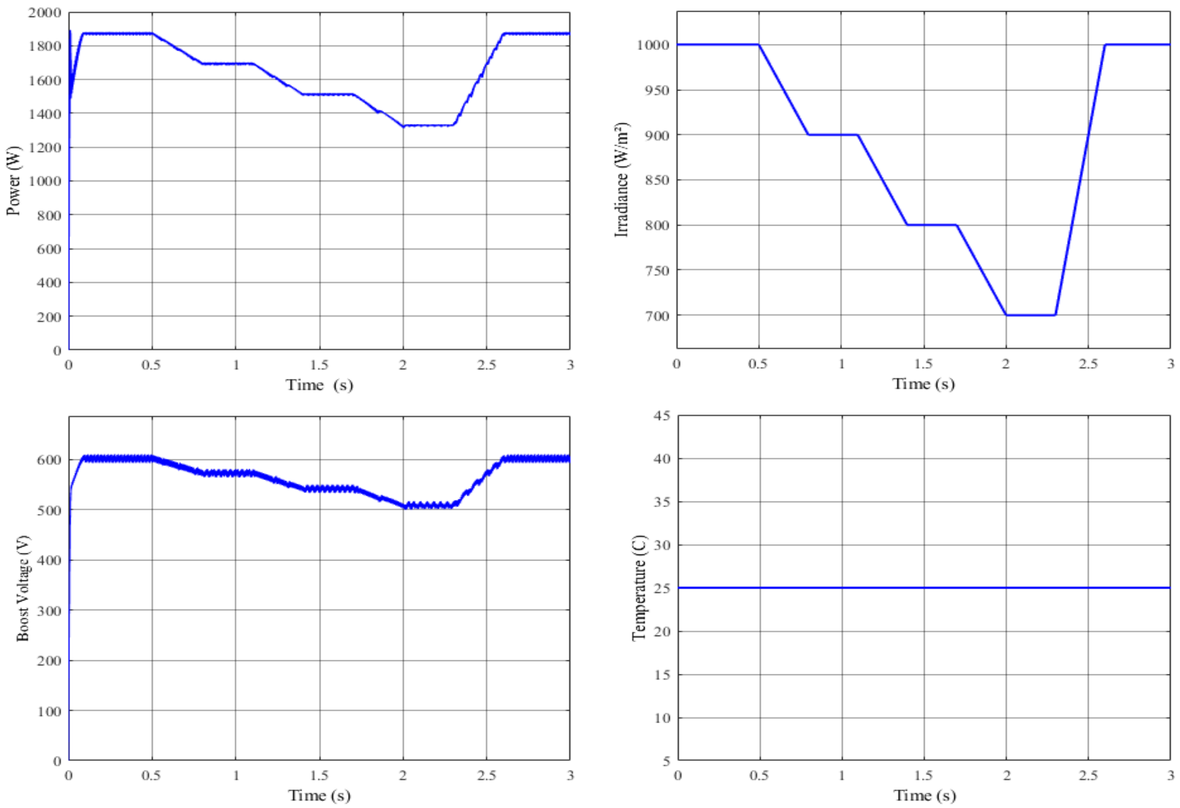

Fig II.18: PV simulation results at variable Irradiance with (P&O).

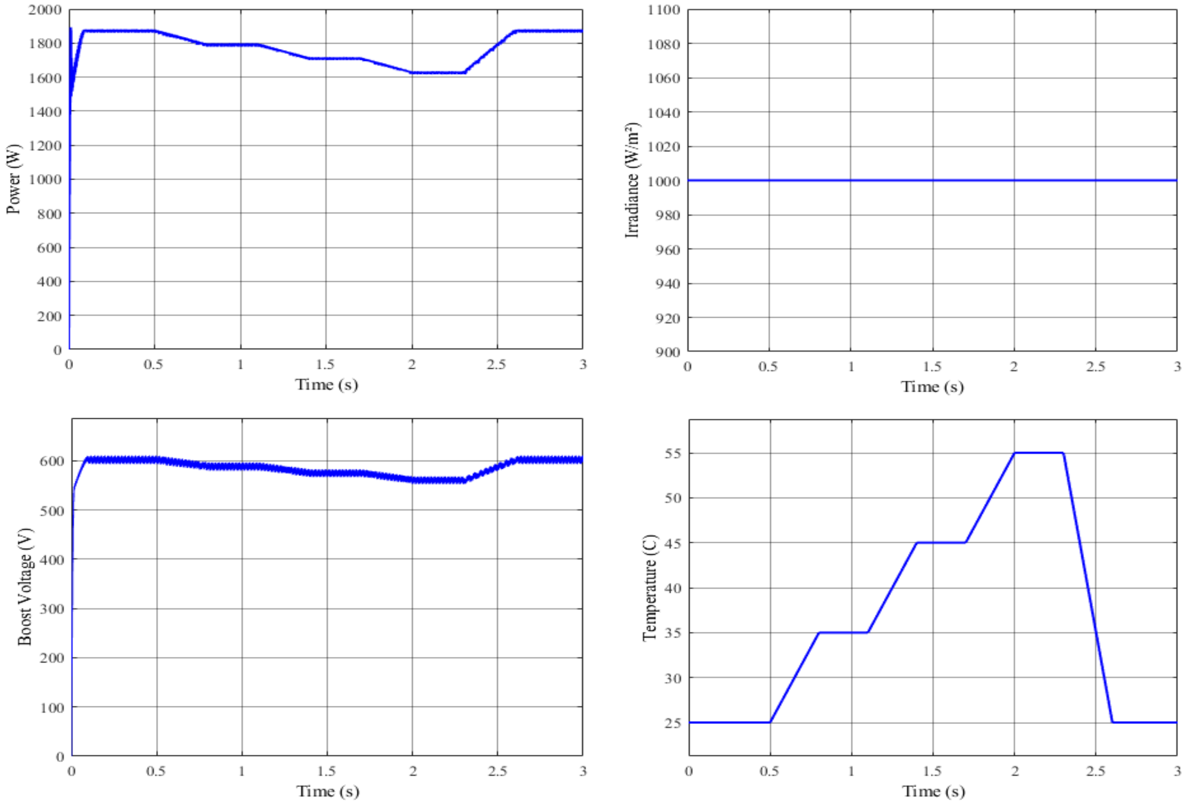

Fig II.19: PV simulation results at variable temperatures with P&O.

II.8.3 Simulation results with INC Algorithm

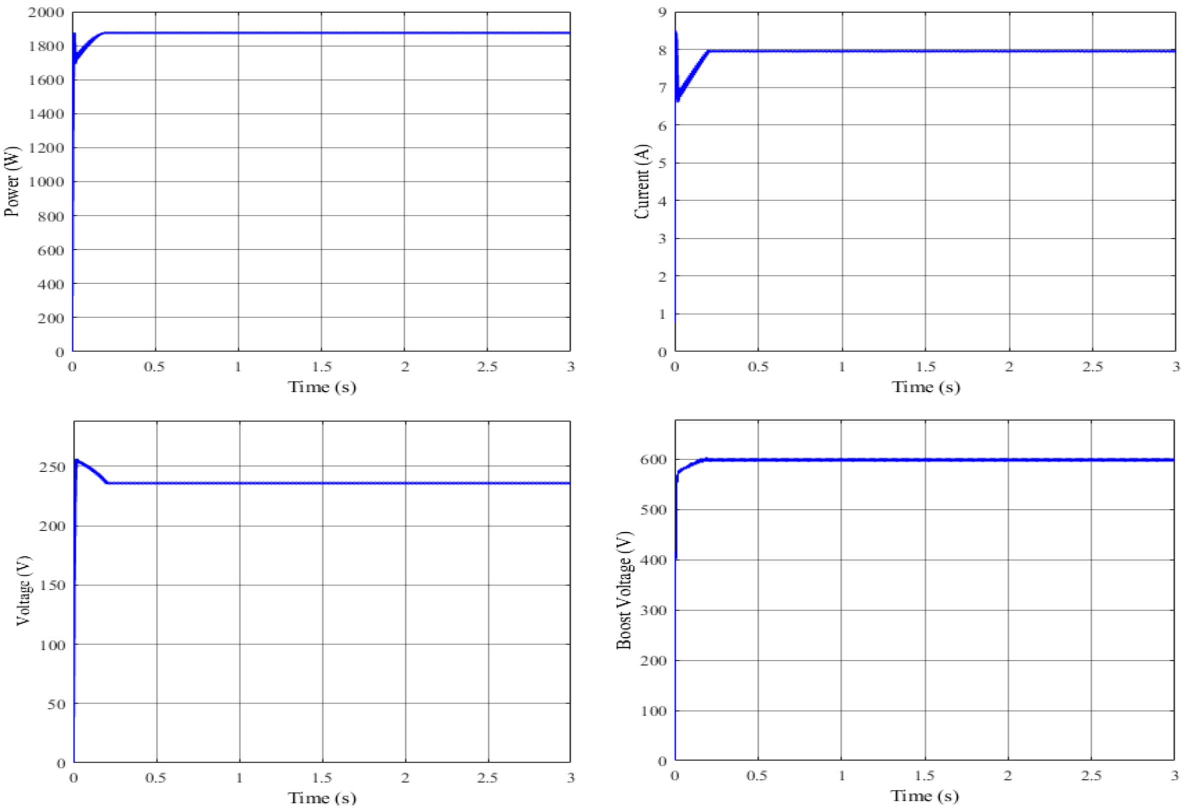

Fig II.20: PV simulation results at (T=25°C, I=1000W/m^2) with (INC).

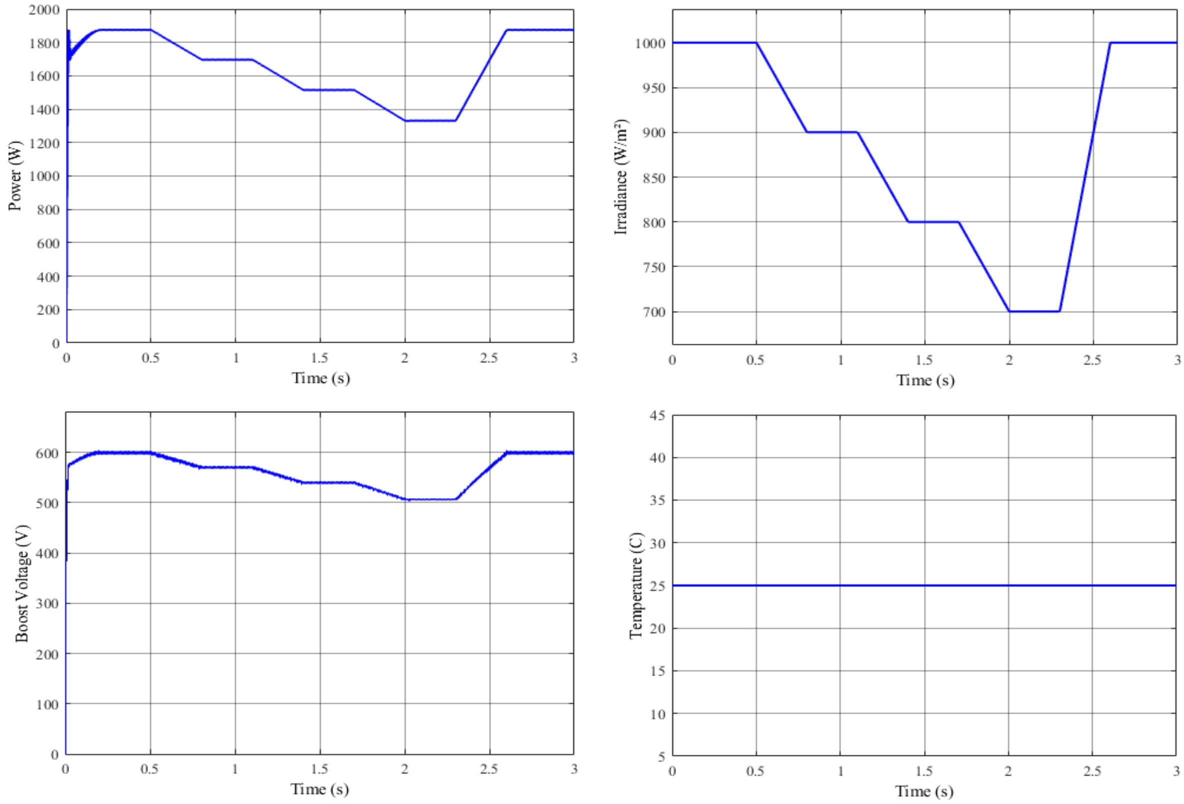

Fig II.21: PV simulation results at variable Irradiance with (INC).

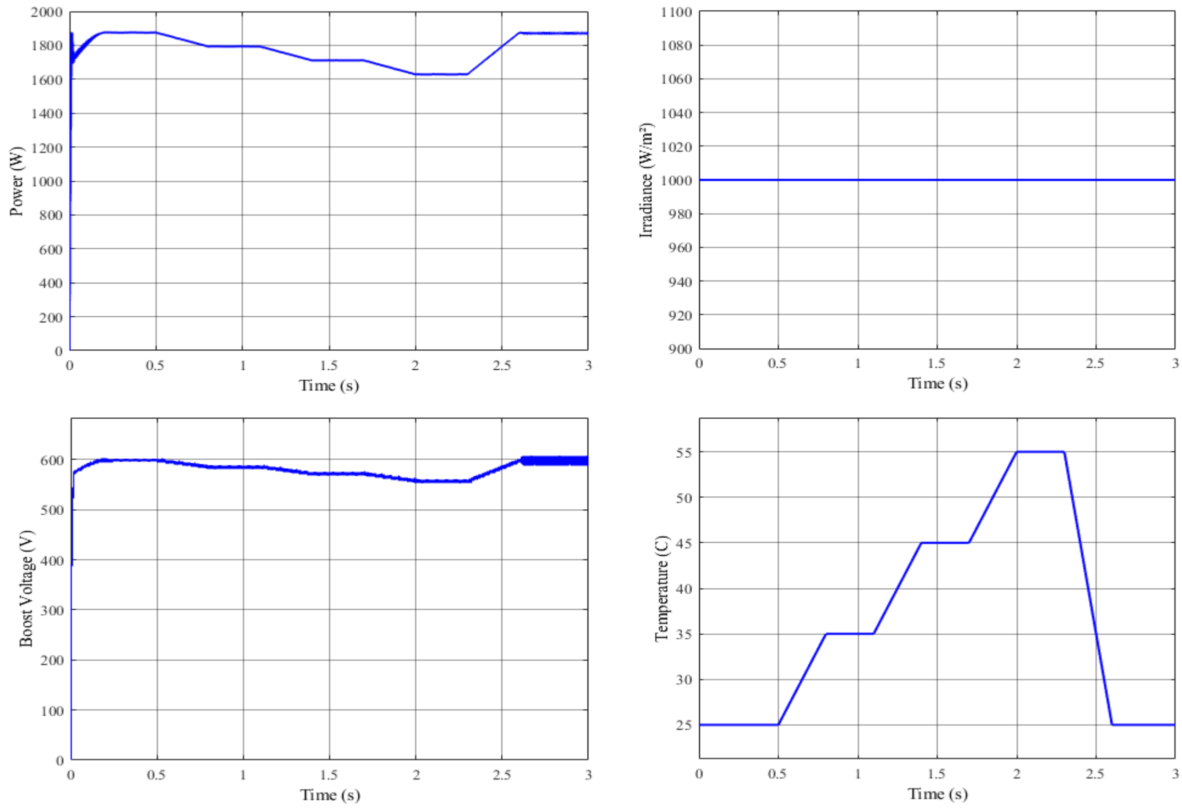

Fig II.22: PV simulation results at variable temperatures with (INC).

II.8.4 Interpretation of MPPT algorithm performance

- The P&O method: the simulation results reveal that while the P&O method is indeed straightforward to implement, its inherent perturbation nature can lead to oscillations around the Maximum Power Point (MPP). These oscillations can potentially decrease MPPT efficiency and introduce instability to the system.

- In contrast, the INC approach leverages the derivative of power to determine the direction towards the MPP. Based on the simulation findings, this algorithm demonstrates superior accuracy in tracking the MPP compared to the P&O method. However, continuous monitoring is necessary to ensure peak performance, as the INC method may also exhibit oscillatory behavior.

II.9 Conclusion

This chapter focused on the mathematical modeling of the solar panel and boost converter within a photovoltaic water pumping system. The solar panel model was developed using established equations that describe its electrical behavior, such as the one-diode model. Similarly, the boost converter was modeled mathematically using equations that represent the power converter's functionality.

Furthermore, the chapter explored various Maximum Power Point Tracking (MPPT) techniques, including Perturb and Observe (P&O) and Incremental Conductance (INC). These algorithms play a crucial role in dynamically adjusting system parameters to ensure the solar panel operates at its Maximum Power Point (MPP) under varying environmental conditions, such as fluctuating light levels and temperature.

Chapter III.

Modeling of an induction motor, centrifugal pump and inverter

Chapter III.
Modeling the induction motor, centrifugal pump and inverter

III.1 Introduction

The efficient operation of a solar photovoltaic water pumping system hinges on the intricate interplay between its key components. This chapter delves into the mathematical modeling of these essential elements: the induction motor, centrifugal pump, and inverter. By establishing a robust mathematical framework, we gain a deeper understanding of their individual characteristics and how they interact within the broader system.

III.2 Modeling of the Induction Motor

The Induction Motor is currently the most widely used electric motor in industry. Its main advantage lies in the absence of sliding electrical contacts, which leads to a simple, robust and easy to build structure, its stator is connected directly to the industrial network at constant voltage and frequency, it rotates at a speed lower than the synchronism speed; it is it that is used for the realization of almost all drives at constant speed. It also allows the realization of variable speed drives and the place it occupies in this field is constantly growing*.*

III.2.1 Simplifying assumptions

An induction machine, with its windings distribution and geometry, is so complex that it cannot be analyzed, taking into account its exact configuration. Then, it is necessary to adopt simplifying assumptions [34, 35]:

- The magnetic fields are supposed unsaturated.
- The skin effect does not exist.
- The machine has a constant air gap, which made the slotting effect is not taken account.
- The MMFs created by the different circuits of stator and rotor are spread to have sinusoidal repartitions.

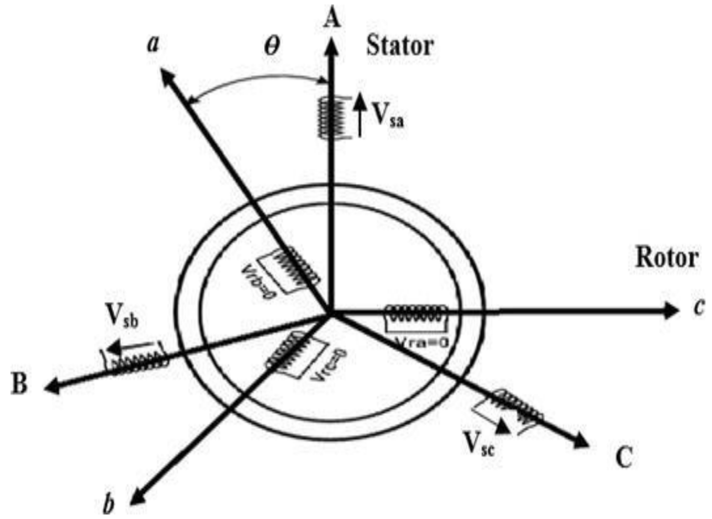

Fig III.1: Representation of the induction machine.

III.2.2 equations of the induction motor

The behavior of the induction motor is entirely defined by three types of equations:

- The electrical equations.
- The magnetic equations.
- The mechanical equations

III.2.2.1 electrical equations

By applying the generalized ohm's law for each phase:

$$\begin{cases} V_{sabc} = [R_s]\cdot[i_{sabc}] + (d/dt)\cdot[\Phi_{sabc}] \\ V_{rabc} = [R_r]\cdot[i_{rabc}] + (d/dt)\cdot[\Phi_{rabc}] \end{cases} \quad \text{(III-1)}$$

with:

$$[R_s] = \begin{bmatrix} R_s & 0 & 0 \\ 0 & R_s & 0 \\ 0 & 0 & R_s \end{bmatrix} \quad ; \quad [R_r] = \begin{bmatrix} R_r & 0 & 0 \\ 0 & R_r & 0 \\ 0 & 0 & R_r \end{bmatrix} \quad \text{(III-2)}$$

$$[V_{sabc}] = \begin{bmatrix} V_{sa} \\ V_{sb} \\ V_{sc} \end{bmatrix} \quad ; \quad [V_{rabc}] = \begin{bmatrix} V_{ra} \\ V_{rb} \\ V_{rc} \end{bmatrix} \quad \text{(III-3)}$$

$$[\Phi_{sabc}] = \begin{bmatrix} \Phi_{sa} \\ \Phi_{sb} \\ \Phi_{sc} \end{bmatrix} \quad ; \quad [\Phi_{rabc}] = \begin{bmatrix} \Phi_{ra} \\ \Phi_{rb} \\ \Phi_{rc} \end{bmatrix} \quad \text{(III-4)}$$

$$[i_{sabc}] = \begin{bmatrix} i_{sa} \\ i_{sb} \\ i_{sc} \end{bmatrix} \quad ; \quad [i_{rabc}] = \begin{bmatrix} i_{ra} \\ i_{rb} \\ i_{rc} \end{bmatrix} \quad \text{(III-5)}$$

III.2.2.2 magnetic equations

The relationship between the totalized fluxes on the windings and the currents can be described by the following matrix equation:

$$\begin{bmatrix} \Phi_{sabc} \\ \Phi_{rabc} \end{bmatrix} = \begin{bmatrix} [L_{ss}] & [M_{sr}] \\ [M_{rs}] & [L_{rr}] \end{bmatrix} . \begin{bmatrix} i_{sabc} \\ i_{rabc} \end{bmatrix} \tag{III-6}$$

So:

$$[\Phi_{sabc}]=[L_{ss}]\cdot[i_{sabc}]+[M_{sr}]\cdot[i_{rabc}] \tag{III-7}$$

$$[\Phi_{rabc}]=[L_{rr}]\cdot[i_{rabc}]+[M_{rs}]\cdot[i_{sabc}] \tag{III-8}$$

With: Φ_s : stator flux ; Φ_r : rotor flux

$$[L_{ss}] = \begin{bmatrix} l_s & M_s & M_s \\ M_s & l_s & M_s \\ M_s & M_s & l_s \end{bmatrix}; \qquad [L_{rr}] = \begin{bmatrix} l_r & M_r & M_r \\ M_r & l_r & M_r \\ M_r & M_r & l_r \end{bmatrix} \tag{III-9}$$

$$[M_{sr}] = [M_{rs}]^t = M'_{sr} \begin{bmatrix} \cos(\alpha) & \cos(\alpha+2\pi/3) & \cos(\alpha-2\pi/3) \\ \cos(\alpha-2\pi/3) & \cos(\alpha) & \cos(\alpha+2\pi/3) \\ \cos(\alpha+2\pi/3) & \cos(\alpha-2\pi/3) & \cos(\alpha) \end{bmatrix} \tag{III-10}$$

Finally, there exists:

$$\begin{cases} [V_{sabc}] = [R_s][i_{sabc}] + (d/dt)\cdot([L_{ss}]\cdot[i_{sabc}] + [M_{sr}]\cdot[i_{rabc}]) \\ [V_{rabc}] = [R_r][i_{rabc}] + (d/dt)\cdot([L_{rr}]\cdot[i_{rabc}] + [M_{rs}]\cdot[i_{sabc}]) \end{cases} \tag{III-11}$$

III.2.2.3 mechanical equations

To study electromechanical transient phenomena with a variable rotor speed (for example starting, braking, variation of the load on the shaft, etc ....), it is necessary to add the equation of motion to the system of differential equations.

$$J.\frac{d\Omega_r}{dt} = T_{em} - T_r - f.\Omega_r \tag{III-12}$$

with :

T_{em}: electromagnetic torque.

T_r: resistant torque that can be a function of speed.

J: moment of inertia of the rotating masses.

f: viscous friction coefficient.

Ω_r : Speed of rotation of the machine.

III.3 Park's transformation

To obtain a system of equations with constant coefficients, the stator and rotor windings are transformed into equivalent orthogonal windings. The representation of the three-phase machine balanced by an equivalent two-phase representation characterized by two axes (d, q) as shown in Fig (III.2).

In the context of electrical machines, the d-q reference frame simplifies modeling. By using the Park transformation, we can express the behavior of the machine in terms of two inductors (d and q) instead of three fixed real inductors. This approach streamlines the analysis while making certain assumptions about the system.

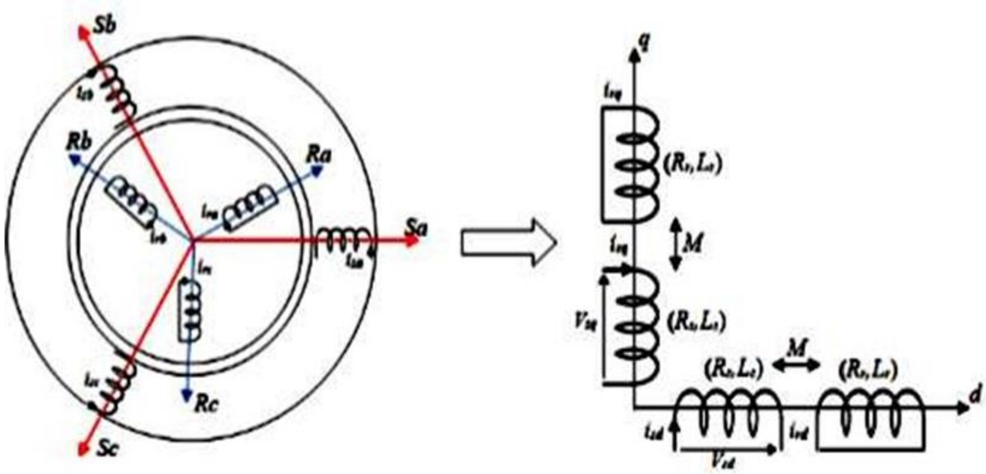

Fig III.2: Principle of Park's Transformation (Three-phase to Two-phase).

The Park transformation's representation, in general, is given as:

$$\left[P(\theta)\right]=\sqrt{\frac{2}{3}}\cdot\begin{bmatrix}\cos(\theta) & \cos\left(\theta-\frac{2\pi}{3}\right) & \cos\left(\theta-\frac{4\pi}{3}\right)\\ -\sin(\theta) & -\sin\left(\theta-\frac{2\pi}{3}\right) & -\sin\left(\theta-\frac{4\pi}{3}\right)\\ \frac{1}{\sqrt{2}} & \frac{1}{\sqrt{2}} & \frac{1}{\sqrt{2}}\end{bmatrix} \quad \text{(III-13)}$$

$$\begin{bmatrix}x_d\\ x_q\\ x_0\end{bmatrix}=P(\theta)\cdot\begin{bmatrix}x_a\\ x_b\\ x_c\end{bmatrix} \quad \text{(III-14)}$$

III.3.1 Application of the Park transformation

The expressions of the machine (III-1) can be expressed using the passage matrix is that considering that the system is balanced:

III.3.1.1 electrical equations

$$\begin{cases} V_{sd} = R_s i_{sd} + \frac{d}{dt}\Phi_{sd} - \omega_a \Phi_{sq} \\ V_{sq} = R_s i_{sq} + \frac{d}{dt}\Phi_{sq} + \omega_a \Phi_{sd} \\ V_{rd} = 0 = R_r i_{rd} + \frac{d}{dt}\Phi_{rd} - (\omega_a - \omega_r)\Phi_{rq} \\ V_{rq} = 0 = R_r i_{rq} + \frac{d}{dt}\Phi_{rq} + (\omega_a - \omega_r)\Phi_{rd} \end{cases} \quad \text{(III-15)}$$

III.3.1.2 magnetic equations

$$\begin{cases} \Phi_{sd} = L_s \cdot i_{sd} + M \cdot i_{rd} \\ \Phi_{sq} = L_s \cdot i_{sq} + M \cdot i_{rq} \\ \Phi_{rd} = L_r \cdot i_{rd} + M \cdot i_{sd} \\ \Phi_{rq} = L_r \cdot i_{rq} + M \cdot i_{sq} \end{cases} \quad \text{(III-16)}$$

$L_s = l_s - m_s$: the cyclic inductance of the stator

$L_r = l_r - m_r$: the cyclic inductance of the rotor.

$M = \frac{3}{2} M_{sr}$: the mutual cyclic inductance between stator and rotor.

III.3.1.3 mechanical equations

The application of the Park transformation for the mechanical equation gives:

$$T_{em} = p\left(\Phi_{rd} i_{sq} - \Phi_{rq} i_{sd}\right) \quad \text{(III-17)}$$

The equation of motion of the machine is then written:

$$J.\frac{d\Omega_r}{dt} = T_{em} - T_r - f.\Omega_r \quad \text{(III-18)}$$

III.4 Model of the induction motor

In a three-phase induction motor powered by a voltage source, the stator voltages (V_{alpha_s} and V_{bata_s}) and the rotating field speed (ω_r) serve as the primary control variables. Conversely, the resistance torque (T_r) acts as an external disturbance that can disrupt the system's behavior.

To express the machine model as an equation of state, the equations need modification to represent them as a function of the state vector variables X_u. Following simplification and rearrangement, the resulting expression is:

$$\dot{X_u} = A_u \cdot X_u + B_u U \qquad \text{(III-19)}$$

With:

$$A=\begin{bmatrix} 0 & \omega_{dq} & -R_s & 0 \\ -\omega_{dq} & 0 & 0 & -R_s \\ \frac{1}{\sigma LsT_r} & \frac{1}{\sigma L_s}\omega_r & -\frac{1}{\sigma T_s}-\frac{1}{\sigma T_r} & \omega_{dq}-\omega_r \\ -\frac{1}{\sigma L_s}\omega_r & \frac{1}{\sigma L_s T_r} & -(\omega_{dq}-\omega_r) & -\frac{1}{\sigma T_s}-\frac{1}{\sigma T_r} \end{bmatrix} \; ; \; B=\begin{bmatrix} 1 & 0 \\ 0 & 1 \\ \frac{1}{\sigma L_s} & 0 \\ 0 & \frac{1}{\sigma L_s} \end{bmatrix} \quad U=\begin{bmatrix} V_{ds} \\ V_{qs} \end{bmatrix}$$

and: $T_r=\frac{L_r}{R_r}$; $\delta=1-\frac{M^2}{\delta L_s L_r}$; $T_s=\frac{L_s}{R_s}$

III.5 Simulation of the induction motor

Figure III.4 presents the block diagram of the induction motor simulation developed using MATLAB/Simulink software. This simulation depicts the motor directly connected to a three-phase network with a line voltage of 220/380 V and a frequency of 50 Hz. The specific parameters employed for the induction motor model are detailed in the Appendix.

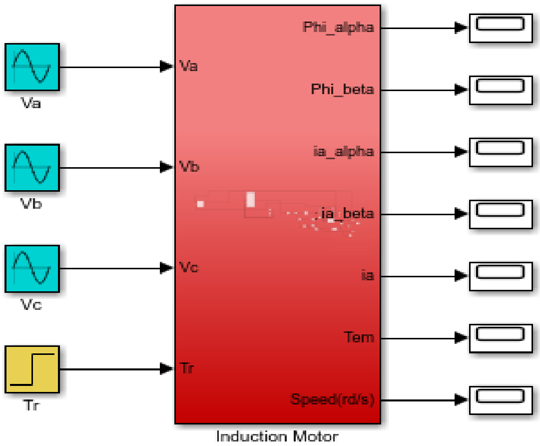

Fig III.3: Block diagram of induction motor simulation.

III.5.1 Simulation results

The simulation results represent the electrical and electromagnetic characteristics of the induction motor.

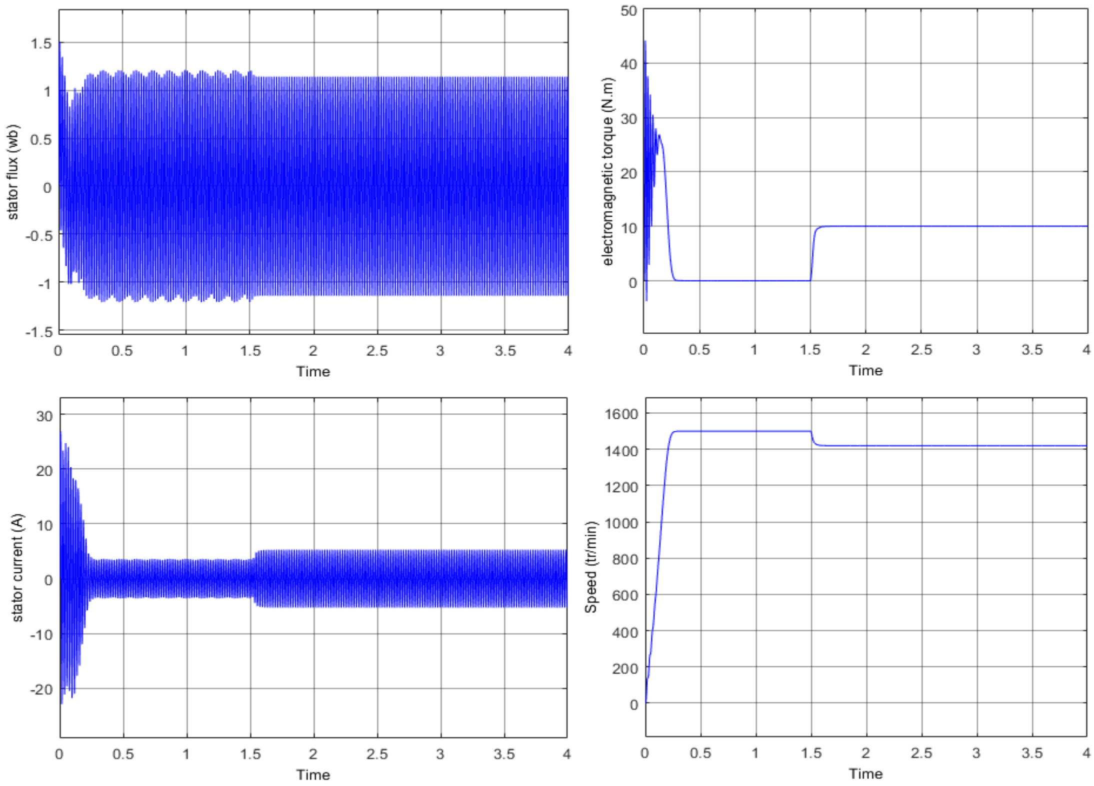

Fig III.4: Simulation of the induction motor for (T_r=10 Nm, t = 1.5 s)

III.5.2 Interpretations of the results

- The motor speed exhibits oscillatory behavior during the initial start-up phase, followed by an almost linear increase until it stabilizes at the nominal value. Applying a load at 1.5 seconds introduces a slight decrease in speed, as expected.
- The electromagnetic torque initially displays strong pulsations due to the motor's moment of inertia. It then reaches a value of approximately 45 N.m before settling towards the no-load operating regime. The application of the load at 1.5 seconds results in a torque increase that corresponds to the applied load value.
- Similar to the speed, the stator flux experiences small oscillations at the start-up. It then stabilizes at the nominal value. Interestingly, a decrease in flux is observed upon load application.
- The stator current as a function of time, we recognize the classic inrush current at startup which is equal to about 9 times the nominal current. At start-up, the stator current is

excessive, since it is of short duration, the machine could withstand it without risking dangerous heating. This current value due to the transient regime disappears after a few half-cycles in order to obtain a sinusoidal shape of constant amplitude. At the instant t=1.5s, it can be seen that the stator current increases because of the increase in the resistant torque

III.6 Modeling of the centrifugal pump

The flow-head characteristic of a centrifugal pump can be approximated by quadratic form using *Pfleider–Peterman* model, in which the rotor speed x is a parameter:

$$H = a_0\omega^2 + a_1\omega\varphi + a_2\varphi^2 \quad \text{(III-23)}$$

With:

φ: The water flow (m³/s)

H: The total height (m)

ω: Rotation speed (rad/s)

a_0, a_1, a_2: are the coefficients given by the manufacturers.

The Q–H characteristic of the pipe network can be expressed by :

$$H = H_g + \psi\ \varphi^2 \quad \text{(III-24)}$$

ψ: is a constant which depends on conduit diameter and on all frictional losses of the pipe network.

H_g : is the geodesic height (m).

The centrifugal pump imposes a load torque proportional to the square of the speed of rotation of the motor which can be described by :

$$T = k_{pump} \cdot \omega^2 \quad \text{(III-25)}$$

k_{pump} : denotes the proportionality coefficient.

Knowing the performances of a centrifugal pump for the speed ω, the similarity laws make it possible to determine the performances for a speed ω' using the following relation:

$$\varphi' = \varphi \frac{\omega'}{\omega} \quad \text{(III-26)}$$

III.7 Modeling the voltage source inverter (VSI)

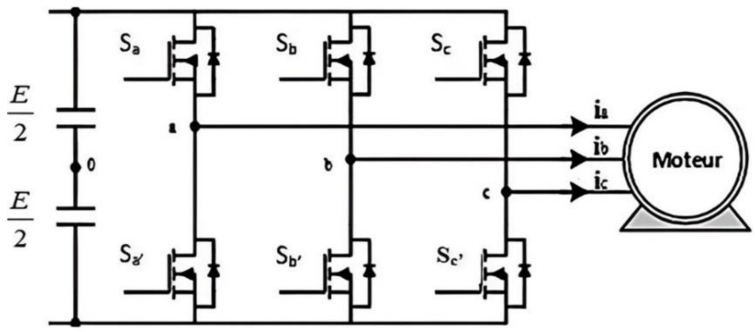

Fig III.5: Three-phase VSI fed star-connected induction machine.

The state of the switches, assumed to be perfect, can be defined by three boolean control S_i, with: i = a, b, c.

- If the upper transistor is conducting, the variables $S_i = 1$;

- If the lower transistor is conducting, the variables $S_i = 0$;

The simple voltages applied to the three stator phases are obtained from the following relationships taking into account the fictitious point "o".[36]

$$\begin{cases} V_{an} = V_{ao} + V_{on} \\ V_{bn} = V_{bo} + V_{on} \\ V_{cn} = V_{co} + V_{on} \end{cases} \quad \text{(III-27)}$$

By addition on a:

$$V_{an} + V_{bn} + V_{cn} = V_{ao} + V_{bo} + V_{co} + 3V_{on} \quad \text{(III-28)}$$

The system of the three-phase stator voltage is symmetrical there for:

$$V_{ao} + V_{bo} + V_{co} + 3V_{on} = 0 \quad \text{(III-29)}$$

Consequently, the following result emerges:

$$V_{on} = \frac{1}{3}(V_{ao} + V_{bo} + V_{co}) \quad \text{(III-30)}$$

By substituting equation (III-30) into the system of equation (III-27), the following result is obtained:

$$\begin{cases} V_{an} = \frac{1}{3}(2V_{ao} - V_{bo} - V_{co}) \\ V_{bn} = \frac{1}{3}(-V_{ao} + 2V_{bo} - V_{co}) \\ V_{cn} = \frac{1}{3}(-V_{ao} - V_{bo} + 2V_{co}) \end{cases} \quad \text{(III-31)}$$

After arranging the equations of the two systems, the following matrix system is obtained :

$$\begin{bmatrix} V_{an} \\ V_{bn} \\ V_{cn} \end{bmatrix} = \frac{1}{3} \cdot \begin{bmatrix} 2 & -1 & -1 \\ -1 & 2 & -1 \\ -1 & -1 & 2 \end{bmatrix} \cdot \begin{bmatrix} V_{ao} \\ V_{bo} \\ V_{co} \end{bmatrix} \quad \text{(III-32)}$$

with:

$$\begin{aligned} V_{ao} &= E.S_a \\ V_{bo} &= E.S_b \\ V_{co} &= E.S_c \end{aligned} \quad \text{(III-33)}$$

Finally, there exists:

$$\begin{bmatrix} V_{an} \\ V_{bn} \\ V_{cn} \end{bmatrix} = \frac{E}{3} \cdot \begin{bmatrix} 2 & -1 & -1 \\ -1 & 2 & -1 \\ -1 & -1 & 2 \end{bmatrix} \cdot \begin{bmatrix} S_a \\ S_b \\ S_c \end{bmatrix} \quad \text{(III-34)}$$

III.7.1 Sinusoidal PWM control strategy

To determine the closing and opening times of the switches, the PWM technique is used (PWM: pulse width modulation). The principle of the sinusoidal PWM control consists in comparing three reference voltages called modulating voltages to a high-frequency triangular signal called carrier (modulation wave). The reference signals are given by the following equation [37]:

$$\begin{cases} V_{sa_{ref}}(t) = r \cdot \frac{v_{dc}}{2} \sin(\omega_r t) \\ V_{sb_{ref}}(t) = r \cdot \frac{v_{dc}}{2} \sin(\omega_r t - \frac{2\pi}{3}) \\ V_{sc_{ref}}(t) = r \cdot \frac{v_{dc}}{2} \sin(\omega_r t + \frac{2\pi}{3}) \end{cases} \quad \text{(III-35)}$$

with: $\omega_r = 2\pi f_r$

Our simulation diagram of the sinusoidal PWM control is illustrated by figure (II.6)

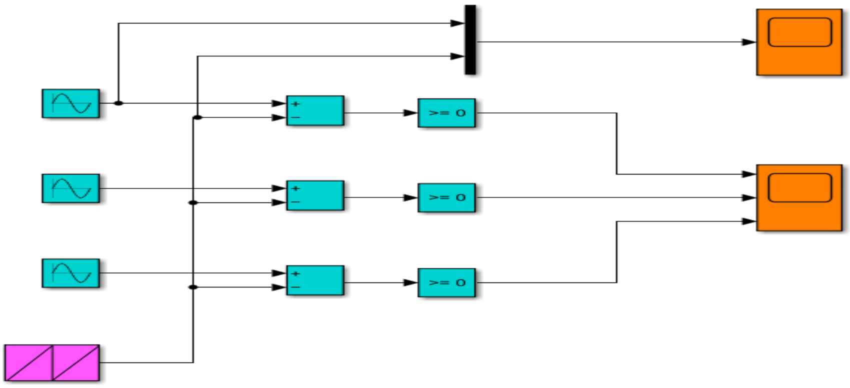

Fig III.6: Simulation diagram of the sinusoidal PWM control

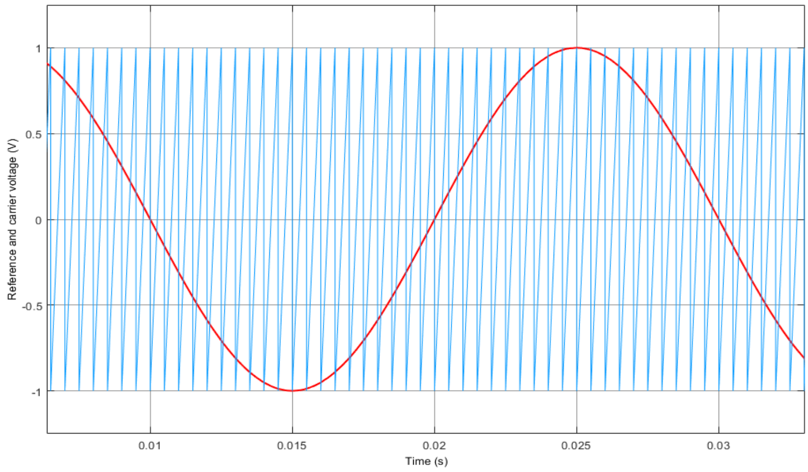

Fig III.7: Representation of the carrier and the modulator.

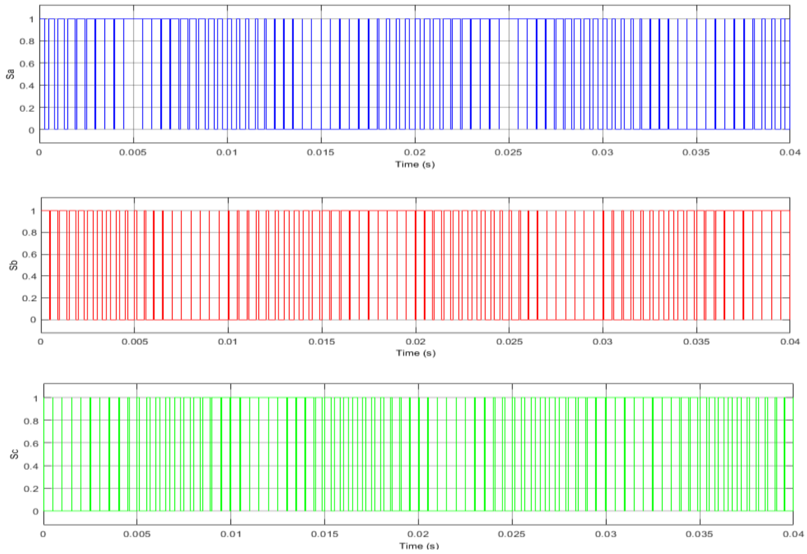

Fig III.8: simulation Results of control signals.

Two parameters characterize the command:

The modulation index "m" equal to the ratio of the frequency of the carrier to the frequency of the reference:

$$m = \frac{f_p}{f_{ref}} \qquad \text{(III-36)}$$

The voltage adjustment coefficient "r" equal to the ratio of the amplitude of the reference voltage to the peak value of the carrier:

$$r = \frac{V_{ref}}{V_p} \qquad \text{(III-37)}$$

III.8 Conclusion

This chapter delved into the mathematical modeling of the essential components within a solar photovoltaic water pumping system: the induction motor (IM), centrifugal pump, and inverter.

The d-q reference frame transformation served as the foundation for modeling the IM's mathematical behavior. A mathematical model was also established to represent the relationship between the centrifugal pumps hydraulic characteristics (flow rate and pressure head) and its operating parameters (rotational speed and motor torque).

The chapter then presented the mathematical modeling of the inverter, focusing on its function of converting the DC output from the photovoltaic system and boost converter into the AC voltage and frequency required to drive the IM.

Chapter IV.

Direct torque control (DTC) of induction motor

Chapter IV.

Direct torque control (DTC) of induction motor

IV.1 Introduction

Achieving precise control of torque and speed in AC machines is crucial for various industrial applications. Traditionally, vector control has been the dominant approach. However, in the mid-1980s, a new contender emerged: direct torque control (DTC). Proposed by *Takahashi* and *Depenbrock* as an alternative [38,40], DTC offers a distinct approach to AC machine control.

This chapter delves into the principles of DTC, offering a clear understanding of its core functionalities. We'll explore the fundamental concept of directly selecting switching states for the voltage source inverter (VSI) using a predefined switching table. DTC focuses on two key controlled variables: stator flux and electromagnetic torque. To ensure precise control, hysteresis regulators play a vital role. We'll examine how these regulators determine the optimal inverter voltage vector applied at each switching instance, ultimately dictating motor behavior. Beyond the theoretical framework, this chapter ventures into practical application. By leveraging the power of *MATLAB/SIMULINK*, we'll explore simulation results showcasing the effectiveness of DTC in controlling a pumping system.

IV.2 Basic Concept and Principle of DTC

The Direct Torque Control (DTC) method, developed by German and Japanese researchers [41], allows direct and independent electromagnetic torque and flux control, selecting an optimal switching vector, making possible fast torque response, low inverter switching frequency and low harmonic losses. Fig (IV.1) shows the block diagram of a DTC controller.

The DTC of alternating current machines is based on the "direct" determination of the control sequence applied to the switches of a voltage inverter. This choice is generally based on the use of hysteresis regulators whose function is to control the state of the system, here to know the amplitude of the stator flux and the electromagnetic torque. This type of control is classified in the category of amplitude controls, as opposed to the more conventional duration control laws which are based on an adjustment of the average value of the voltage vector by pulse width modulation (PWM).

Originally, DTC commands were strongly based on the "physical sense" and on a relatively empirical approach to the variation of states (torque, flux) over a very short time interval (interval between two switching's). This reasoning has been clearly refined and is now based on increasingly solid mathematical foundations [36].

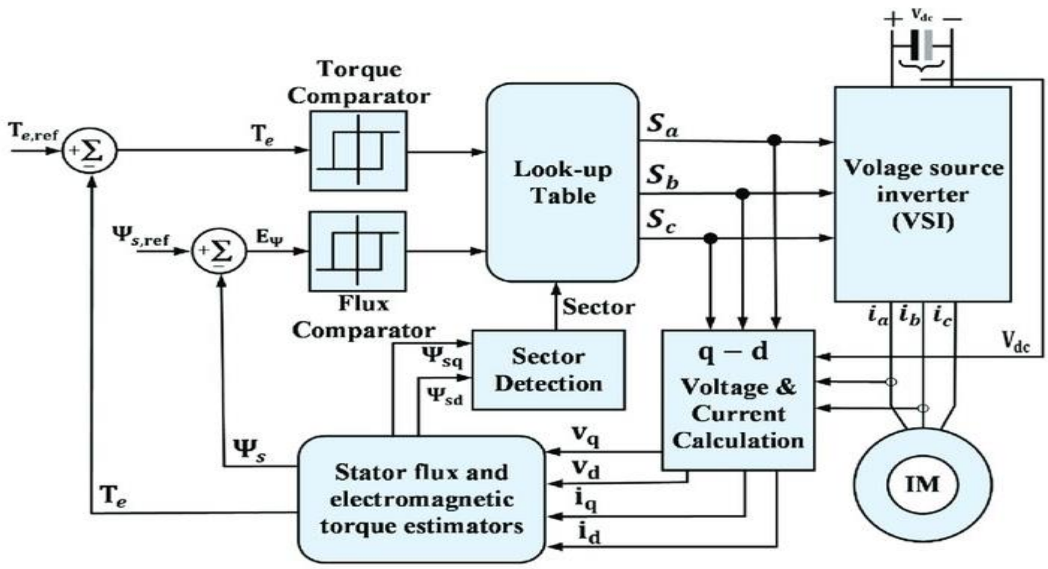

Fig IV.1: Block diagram of a basic DTC control system.

IV.3 Flux and torque control

For an effective control of the torque of the induction motor, it is first of all imperative to set the flux correctly. In DTC type control, the stator flux is adjusted, firstly because it has a faster dynamic than that of the rotor flux (the rotor time constant is greater than that of the stator, so the variation in rotor flux is negligible compared to that of the stator flux).

IV.3.1 Flux control

The Direct Torque Control (DTC) is based on the orientation of the stator flux. The expression of the stator flux in the reference frame linked to the stator of the machine is obtained by the following equation [40],[42]:

$$\Phi_s(t)=\int_0^t (V_s-R_sI_s)dt+\Phi_{s0} \quad \text{(IV-1)}$$

In the case where a non-zero voltage vector is applied during a time interval [0, T_e], the relationship becomes: $V_s \gg R_s.I_s$. Therefore (IV.1) can be written:

$$\Delta\Phi_s = \Phi_s - \Phi_s(0) = V_sT_e \quad \text{(IV-2)}$$

The equation (IV-2) implies that the end of the stator flux vector Φ_s (t) moves on a straight line whose direction is given by the applied voltage vector V_s, as illustrated by figure (IV.2).

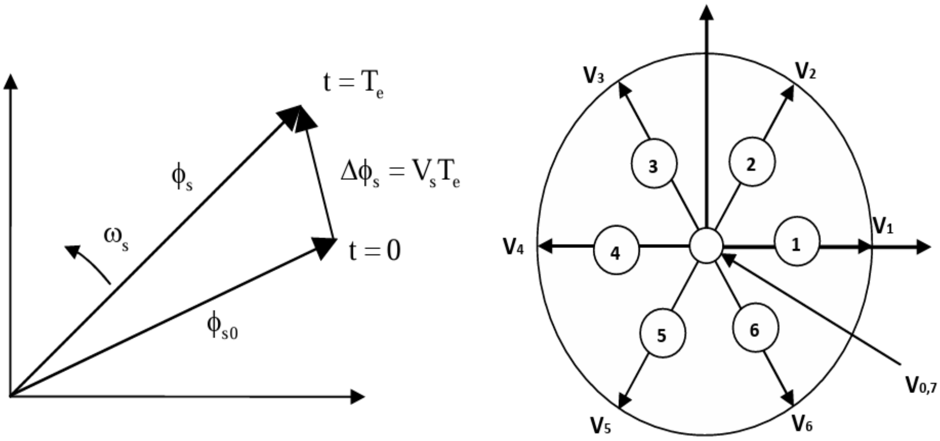

Fig IV.2: Stator and rotor flux space vector.

The "flux component" of the voltage vector (radial component) varies the amplitude of Φ_s and its "torque component" (tangential component) varies the position Φ_s.

By choosing an appropriate sequence of the vectors $V_{s,}$ over the control periods T_e, it is therefore possible to operate with a practically constant flux module Φ_s, by making an almost circular trajectory follow at the end of Φ_s, if the period T_e is very short compared to the rotation period of the stator flux.

When the selected voltage vector V_s is non-zero, the direction of displacement of the end of Φ_s is given by its derivative ($d\Phi_s/dt$), Thus the "speed" of displacement of the end of Φ_s.

When the term $R_s.I_s$ is neglected, is given by $V = d\Phi_s/dt$. The speed of rotation of Φ_s strongly depends on the choice of V_s, it is maximum for a vector V_s perpendicular to the direction of Φ_s, and zero if a zero vector is applied. It can also be negative.

IV.3.2 Torque control

Among the various forms used to represent the asynchronous machine, the one that uses the flux and the stator current, and the speed of rotation, as a state variable; its presentation in the stator reference frame (α,β), is generally the one that is chosen to implement the DTC. This model is given by the following system of equations [42]:

$$\begin{cases} \overline{V_s} = R_s \overline{I_s} + \dfrac{d\overline{\Phi_s}}{dt} \\ \overline{V_r} = \bar{0} = R_r \overline{I_r} + \dfrac{d\overline{\Phi_r}}{dt} - j\omega\overline{\Phi_r} \end{cases} \tag{IV-3}$$

$$\begin{cases} \overline{\Phi_s} = L_s \overline{I_s} + M\overline{I_r} \\ \overline{\Phi_r} = L_r \overline{I_r} + M\overline{I_s} \end{cases} \tag{IV-4}$$

Based on the expressions of the flux, one can write:

$$\overline{I_r}=\frac{1}{\sigma}\left(\frac{\overline{\Phi_r}}{L_r}-\frac{M}{L_rL_s}\overline{\Phi_s}\right) \quad \text{(IV-5)}$$

With: $\sigma=1-\frac{M^2}{L_rL_s}$ being the dispersion coefficient, from which (IV-3) deviates

$$\begin{cases}\overline{V_s}=R_s\overline{I_s}+\frac{d\overline{\Phi_s}}{dt}\\ \frac{d\overline{\Phi_r}}{dt}+\left(\frac{1}{\sigma T_r}-j\omega\right)\overline{\Phi_r}=\frac{M}{L_s}\frac{1}{\sigma T_r}\overline{\Phi_s}\end{cases} \quad \text{(IV-6)}$$

These Relations Show That:

- The vector Φ_s can be controlled from the vector V_s, to within the voltage drops $R_s\overline{I_s}$,
- The flux Φ_r follows the variations of Φ_s with a time constant σTr. The rotor acts as a time constant filter σTr between the flux Φ_s and Φ_r. This reflects the action of a low-pass filter that exists between the two streams. This time constant also determines the rapidity of variation of the angle θ_{sr} between the two stator and rotor flux. Φ_r is expressed by:

$$\overline{\Phi_r}=\frac{M}{L_s}\frac{\overline{\Phi_s}}{1+j\omega\sigma T_r} \quad \text{(IV-7)}$$

Referring to the expression of the electromagnetic torque, by setting the angle $\theta_{sr}=\left(\overline{\Phi_s}\overline{\Phi_r}\right)$, the torque is expressed by:

$$T_{em}=K\left(\Phi_s*\Phi_r\right)=K\|\Phi_s\|*\|\Phi_r\|\sin\theta_{sr} \quad \text{(IV-8)}$$

With:

$$K=\frac{pM}{L_rL_s}=p\left(\frac{1-\sigma}{\sigma M}\right) \quad \text{(IV-9)}$$

$\|\Phi_s\|$: module of the stator flux vector,

$\|\Phi_r\|$: module of the rotor flux vector,

θ_{sr}: The angle between the stator flux and rotor flux vectors.

The torque therefore depends on the amplitude of the two vectors $\overline{\Phi_s}$ and $\overline{\Phi_r}$ and on their relative position, if we manage to perfectly control the flux $\overline{\Phi_s}$ (from $\overline{V_s}$) in module and in position, we can therefore control the amplitude and the relative position of $\overline{\Phi_s}$ and $\overline{\Phi_r}$, therefore the torque. This is of course possible if the control period T_e of the voltage $\overline{V_s}$ is such that $T_e<<\sigma.T_r$ [40].

IV.4 Stator flux and electromagnetic torque estimation

The challenge of direct torque and flux control consists in obtaining a reliable estimate of the instantaneous value of the torque, the flux as well as the angle of the stator flux. The performance of the control system depends on the accuracy in the estimation of these quantities [43].

IV.4.1 Stator flux estimation

The amplitude of the stator flux is estimated from its two-phase components $\Phi_{s\alpha}$ and $\Phi_{s\beta}$. Either:

$$\overline{\Phi_s} = \Phi_{s\alpha} + j\Phi_{s\beta} \quad \text{(IV-10)}$$

In the (α-β) plane, the components of the stator flux are determined by:

$$\begin{cases} \Phi_{s\alpha} = \int_0^t \left(V_{s\alpha} - R_s I_{s\alpha}\right) dt \\ \Phi_{s\beta} = \int_0^t \left(V_{s\beta} - R_s I_{s\beta}\right) dt \end{cases} \quad \text{(IV-11)}$$

$$\Phi_s = \sqrt{\Phi^2_{s\alpha} + \Phi^2_{s\beta}} \quad \text{(IV-12)}$$

To calculate the components $i_{s\alpha}$, $i_{s\beta}$ of the stator current vector, the Concordia transformation is employed, based on the measured currents (i_{sa}, i_{sb}, i_{sc}), that is:

$$I_s = I_{s\alpha} + jI_{s\beta} \quad \text{(IV-13)}$$

$$\begin{cases} I_{s\alpha} = \sqrt{\frac{2}{3}} i_{sa} \\ I_{s\beta} = \frac{1}{\sqrt{2}}\left(i_{sb} - i_{sc}\right) \end{cases} \quad \text{(IV-14)}$$

Thus, $V_{s\alpha}$ and $V_{s\beta}$ are obtained from the input voltage of the inverter U_0 and the control states (S_a, S_b, S_c), as follows:

$$\begin{cases} V_{s\alpha} = \sqrt{\frac{2}{3}} U_0 \left(S_a - \frac{1}{2}\left(S_b + S_c\right)\right) \\ V_{s\beta} = \frac{1}{\sqrt{2}} U_0 \left(S_b - S_c\right) \end{cases} \quad \text{(IV-15)}$$

IV.4.2 Electromagnetic torque estimation

The electromechanical torque can be estimated from the estimated fluxes, and the measured currents, using the equation:

$$T_{em} = p\left(\Phi_{s\alpha} i_{s\beta} - \Phi_{s\beta} i_{s\alpha}\right) \quad \text{(IV-16)}$$

IV.5 Flux and torque correctors

IV.5.1 Flux corrector

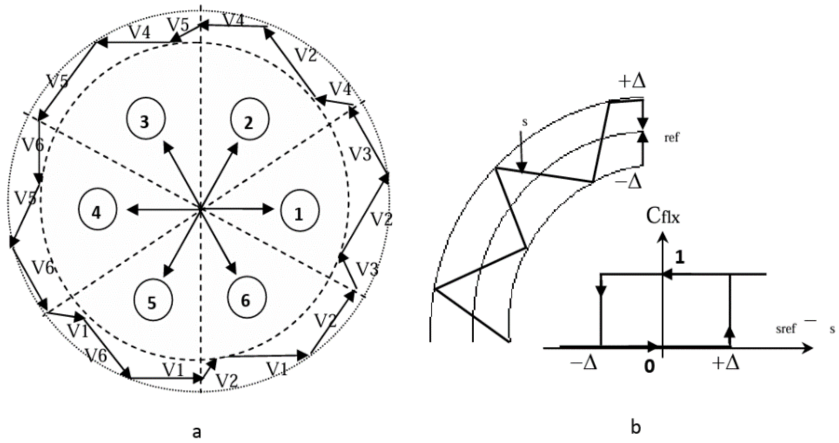

Fig IV.3: Hysteresis flux corrector and selection of the corresponding voltage vectors

With this type of controller, it is easy to control and trap the end of the flux vector in a circular ring, as shown in Fig (IV.3). The output of the corrector, represented by a boolean variable (C_{flx}), directly indicates whether the amplitude of the flux should be increased (C_{flx}=1) or decreased (C_{flx}=0) so as to maintain [42] :

$$\left|\Phi_{ref_s} - \Phi_s\right| \leq \Delta\Phi_s \qquad \text{(IV-17)}$$

With:

Φ_{ref_s} : The reference flux.

$\Delta\Phi_s$: the hysteresis width of the corrector.

Subsequently, the expression can be formulated as follows:

$$\begin{cases} \text{si} \;\; \Delta\phi_s > \varepsilon_\phi & & \text{So} \;\; C_{flx} = 1 \\ \text{si} \; 0 \leq \Delta\phi_s \leq \varepsilon_\phi & \text{and} \;\; d\Delta\phi_s / dt > 0 & \text{So} \;\; C_{flx} = 0 \\ \text{si} \; 0 \leq \Delta\phi_s \leq \varepsilon_\phi & \;\; d\Delta\phi_s / dt < 0 & \text{So} \;\; C_{flx} = 1 \\ \text{si} \;\; \Delta\phi_s < -\varepsilon_\phi & & \text{So} \;\; C_{flx} = 0 \end{cases} \qquad \text{(IV-18)}$$

Indeed, if the difference $\Delta\phi_s$ between the reference flux ϕ_{ref} and the estimated flux ϕ_s is introduced into a two-level hysteresis comparator Fig. (II.3.b), this generates at its output the value C_{flx}=+1 to increase the flux (C_{flx}=0 to reduce it); this also makes it possible to obtain a very good dynamic performance of the flux.

Thus, only the vector V_{i+1} or V_{i+2} can be selected to change the stator flux vector ϕ_s. On the other hand, this corrector does not allow the reversal of the direction of rotation of the flux vector ϕ_s. Thus, to go in reverse, it is necessary to cross an arm of the converter [44].

IV.5.2 Torque corrector

The error on the torque denoted ζ_{Tem} is defined as the difference between the reference torque and its estimated value [43],[45].

$$\zeta_{Tem} = \left| T_{ref} - T_{em} \right| \tag{IV-19}$$

The purpose of the torque corrector is to maintain the torque within the permissible limits defined as follows:

$$\left| T_{ref} - T_{em} \right| \leq \Delta T_{em} \tag{IV-20}$$

With:

T_{ref} : The reference torque,

ΔT_{em} : The hysteresis band of the corrector.

IV.5.3 Three levels comparators

The comparator allows the motor control in the two directions of rotation, either for positive or negative torque Fig (IV.4). It indicates directly if the torque amplitude must be increased in absolute value (C_{trq} = 1), for a positive order and (C_{trq} = -1), for a negative order, or decrease (C_{trq}= 0).

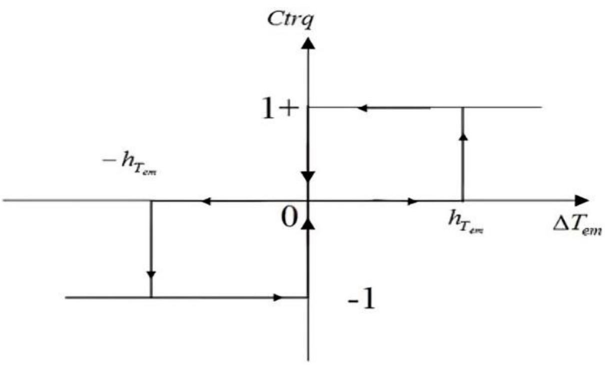

Fig IV.4: Three levels torque comparators.

IV.6 Elaboration of the switching table

The switching table of the control structure is elaborated, as a function of the outputs of the controllers C_{flx}, C_{trq} and the position zones N, such that:

$$\gamma = \arctan\left(\frac{\Phi_{s\beta}}{\Phi_{s\alpha}}\right) \tag{IV-21}$$

The evolution space $\overline{\Phi_s}$ in the frame of reference considered is broken down into six zones N(i) (i=1,...,6) and such that :

$$-\frac{\pi}{6} + (i-1)\frac{\pi}{3} \leq N(i) \leq \frac{\pi}{6} + (i-1)\frac{\pi}{3} \tag{IV-22}$$

We find clearly with the truth table (Table 1), the formulation for selecting the voltage vectors V_{i+1}, V_{i-1}, V_{i+2}, V_{i-2} corresponding to a zone (N=i) and this for a two-level or three-level hysteresis comparator.

N		1	2	3	4	5	6	COMPARATOR
$C_{flx}=1$	$C_{trq}=1$	V_2	V_3	V_4	V_5	V_6	V_1	2 LEVELS
	$C_{trq}=0$	V_7	V_0	V_7	V_0	V_7	V_0	
	$C_{trq}=-1$	V_6	V_1	V_2	V_3	V_4	V_5	3 LEVELS
$C_{flx}=0$	$C_{trq}=1$	V_3	V_4	V_5	V_6	V_1	V_2	2 LEVELS
	$C_{trq}=0$	V_0	V_7	V_0	V_7	V_0	V_7	
	$C_{trq}=-1$	V_5	V_6	V_1	V_2	V_3	V_4	3 LEVELS

Table IV.1: Switching Table of inverter voltage vector.

By selecting one of the two zero vectors V_0 or V_7, the rotation of the flux Φ_s is stopped and leads to a decrease in the torque T_{em} value. Alternatively, V_0 or V_7 is chosen so as to minimize the number of switching operations on the inverter.

IV.7 General structure of DTC

Figure (IV.5) represents the direct torque control strategy of an induction motor. The judicious choice of the bandwidths of the hysteresis of the flux comparators and of the torque remains the essential for achieving the performances of the DTC.

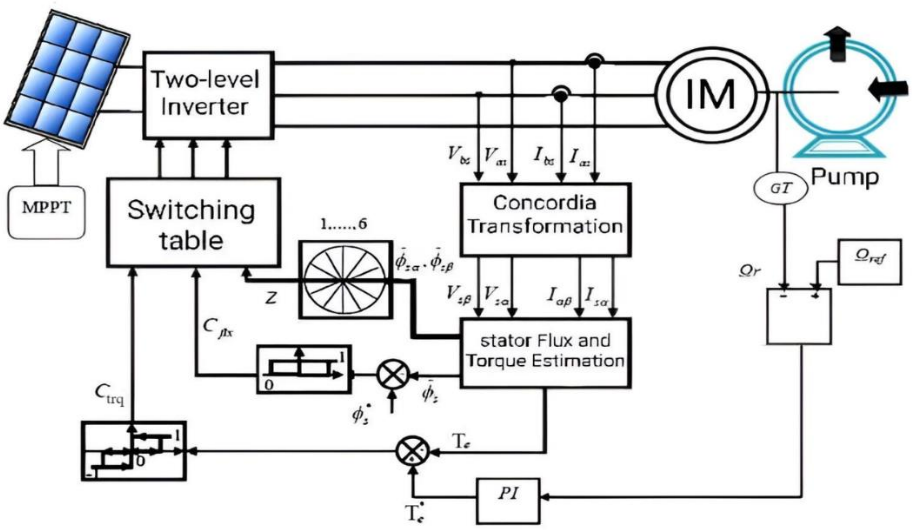

Fig IV.5: Structure of the direct torque control of the water pumping system.

IV.8 Advantages and disadvantages of DTC [46]

IV.8.1 Advantages

- Fast Torque and Flux Response: DTC allows rapid changes in torque and flux by adjusting the references efficiently.
- Low Switching Losses: Transistors are switched only when necessary to keep torque and flux within their hysteresis bands, minimizing switching losses.
- No Overshoot in Step Response: Unlike some other control methods, DTC ensures a step response without overshoot.
- Stationary Coordinate System Calculations: All calculations occur in the stationary coordinate system, eliminating the need for dynamic coordinate transforms.
- No PI Current Controllers: DTC avoids the need for tuning proportional-integral (PI) current controllers.
- Automatic Compensation for DC Voltage Variation: DTC accounts for variations in the intermediate DC circuit voltage.
- Straightforward Synchronization: Due to fast control, synchronizing to a rotating machine is straightforward.

IV.8.2 Disadvantages

- Low-Speed Torque and Flux Control Difficulty: DTC faces challenges in controlling torque and flux at very low speeds.
- High Current and Torque Ripple: Despite its benefits, DTC exhibits some torque and current ripple.
- Variable Switching Frequency Behavior: The switching frequency of transistors is not constant, affecting performance.
- Higher Sampling Rate Requirement: DTC demands a higher sampling rate (up to 40 kHz) compared to other methods, leading to increased inverter switching losses.
- Complex Motor Model: Implementing DTC requires a more complex motor model. [46]

IV.9 Simulation diagram

Fig (IV.5) shows the block diagram of Direct Torque Control simulation using the MATLAB/ SIMULINK software of the induction motor.

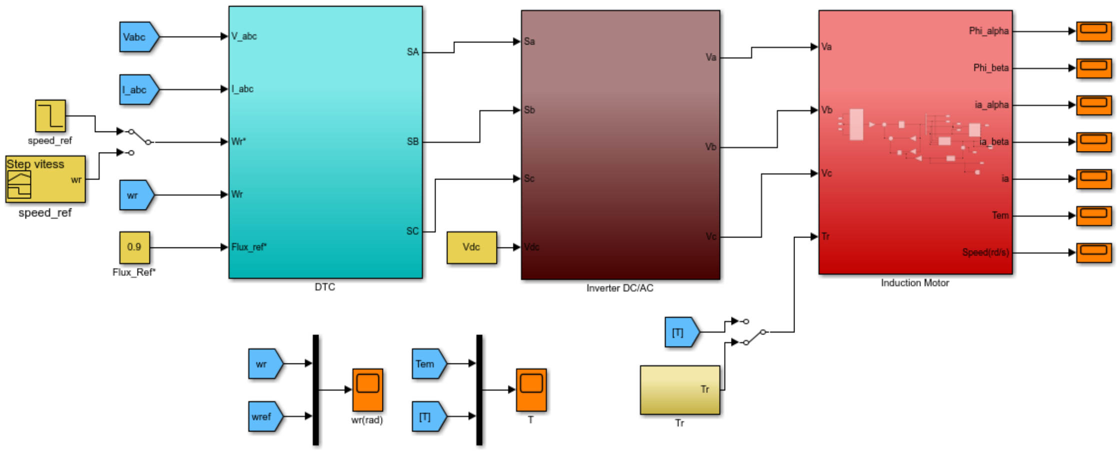

Fig IV.6: Block diagram Simulink of DTC.

IV.10 Simulation results

The DTC control algorithms have been simulated by MATLAB/Simulink software. The simulation has been conducted for a three-phase induction motor 1.5 kW with characteristics given in the appendix. The starting up and the steady states of the controlled motor with load introduction are presented.

IV.10.1 Simulation results at the steady states

Figure IV.7 presents the simulation results obtained for the control system's response to a steady-state operating condition. The simulated load torque applied to the motor shaft is 5 Nm, and the reference speed set to 148 rad/s.

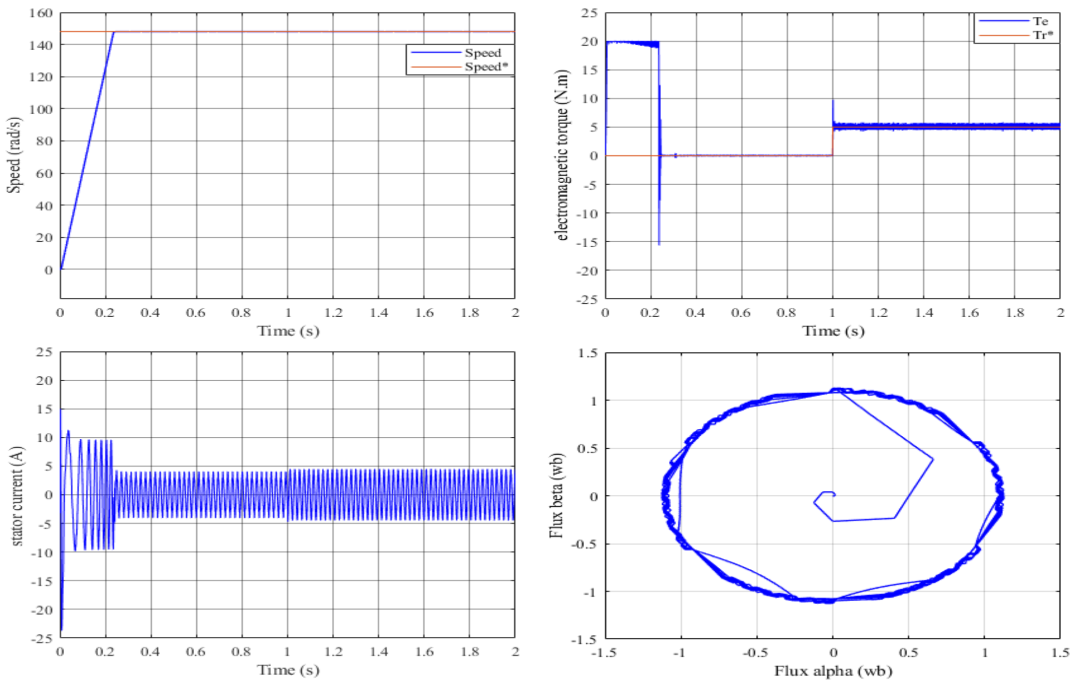

Fig IV.7: Simulation results of DTC.

IV.10.2 Simulation results for a speed reversal

To evaluate the robustness of the DTC scheme, figure IV.8 presents simulation results for the control system response to a load torque reversal and a reference speed reversal. The simulated load torque applied to the motor shaft transitions between (5 Nm and -5 Nm). The reference speed command undergoes a reversal, changing from 100 rad/s to -100 rad/s.

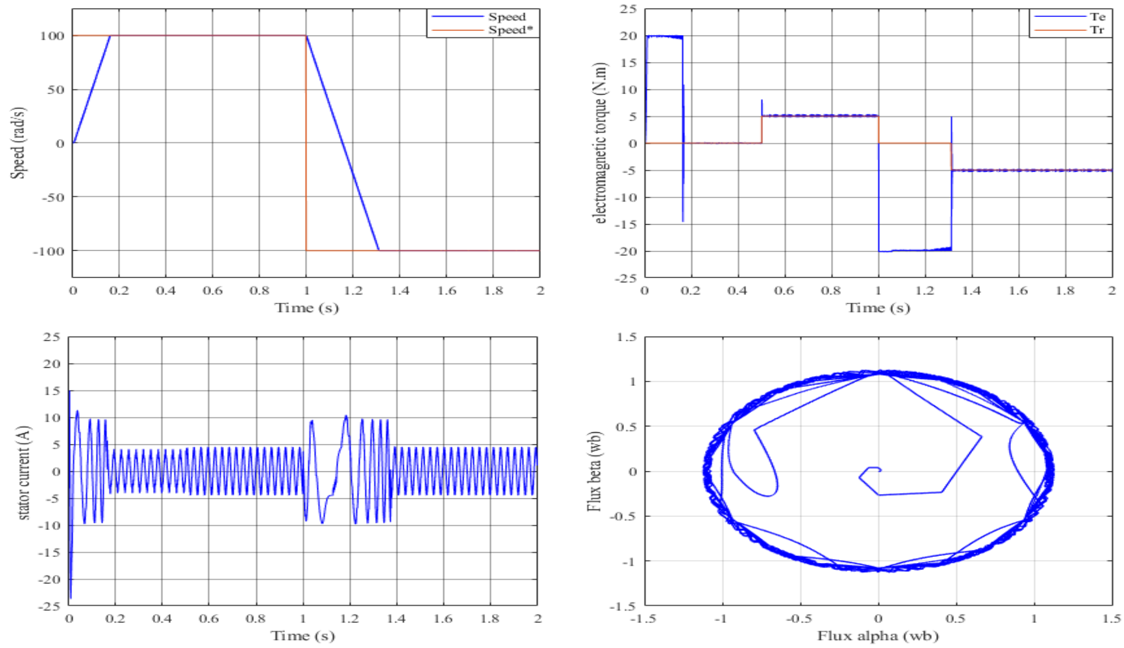

Fig IV.8: Simulation results of the DTC for a speed reversal.

IV.10.3 Simulation results at low speed

In order to test the direct torque control more. The simulations in figure (IV.9) presents the test of operating at low and reversing speed response of the studied system.

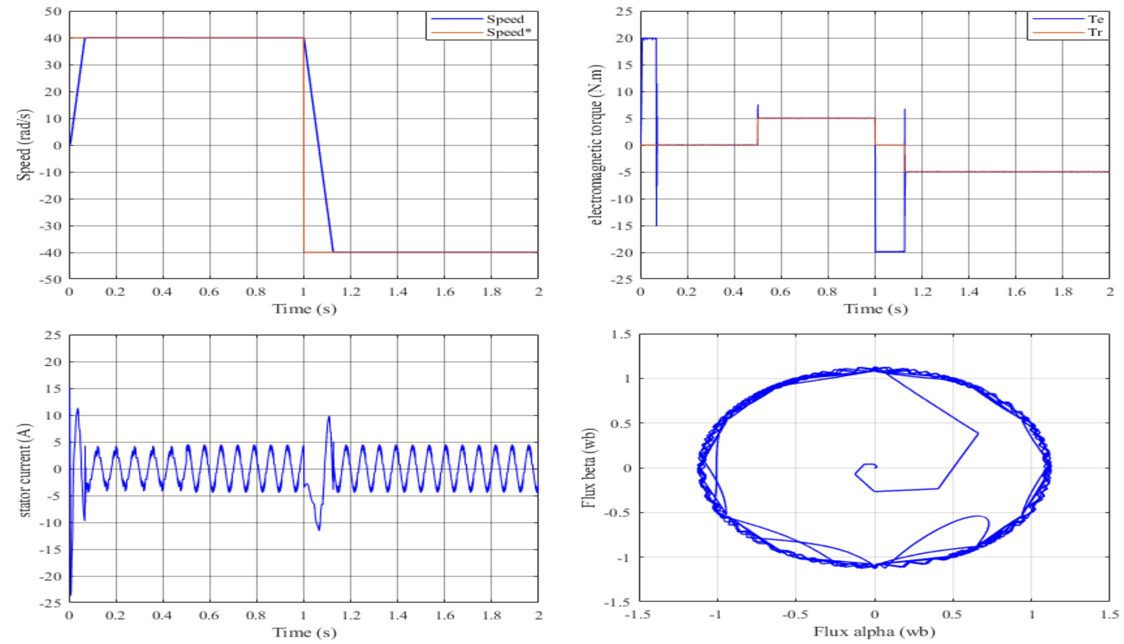

Fig IV.9: Simulation results of the DTC at low speed.

IV.10.4 Speed test at variable reference

To further evaluate the dynamic response of the DTC system, we employ a variable speed reference as the input. This allows us to assess the system's ability to track rapidly changing speed commands and its overall robustness to reference variations.

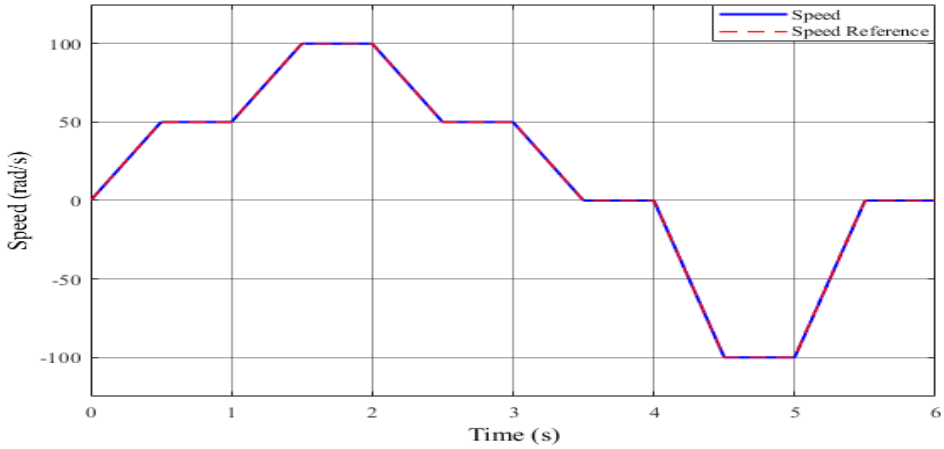

Fig IV.10: Simulation result at variable speed reference.

IV.10.5 Interpretation of the results

- The Figure (IV.7) shows the response of the control system to the application of a load of 5 Nm, and a reference speed of 148 rad/s. The torque and the speed follow their references well with a very fast dynamics with some oscillations at the level of electromagnetic torque. The stator current reach the peak value at start-up and then it tends to sinusoid of a constant amplitude. The trajectory of the stator flux is practically circular with some ripples.
- In Figure (IV.8), we note that at the speed reversal the speed pursuit is carried out but with an overtaking, the same applies to the torque which also undergoes an overtaking before stabilizing. The stator current has undulations which reach the peak value at start-up and when the speed is reversed. The trajectory of the stator flux is practically circular with some ripples.
- Figure (IV.9) presents the test of operating at low and reversing speed response of the studied system, it can be noticed that the torque and the speed follow their references well with a very fast dynamic.
- Figure (IV.10) presents the test of the Speed at selected different values. It can be noticed easily that the speed of the motor presents a good fast response.

IV.11 simulation the PV pumping system

IV.11.1 Structure of the PV water pumping system

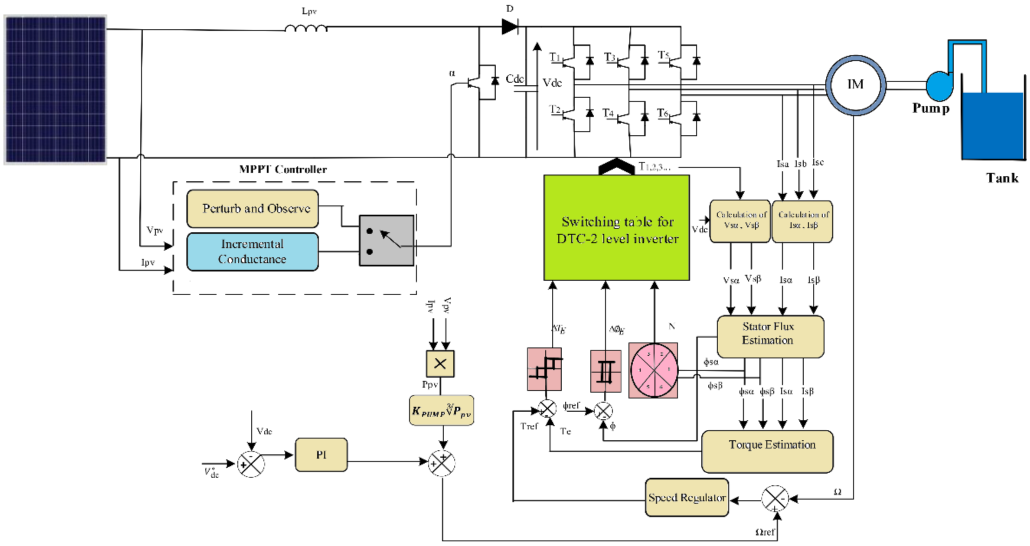

Fig IV.11: Structure of the PV water pump system for DTC-IM

IV.11.2 Simulation diagram in MATLAB/SIMULINK

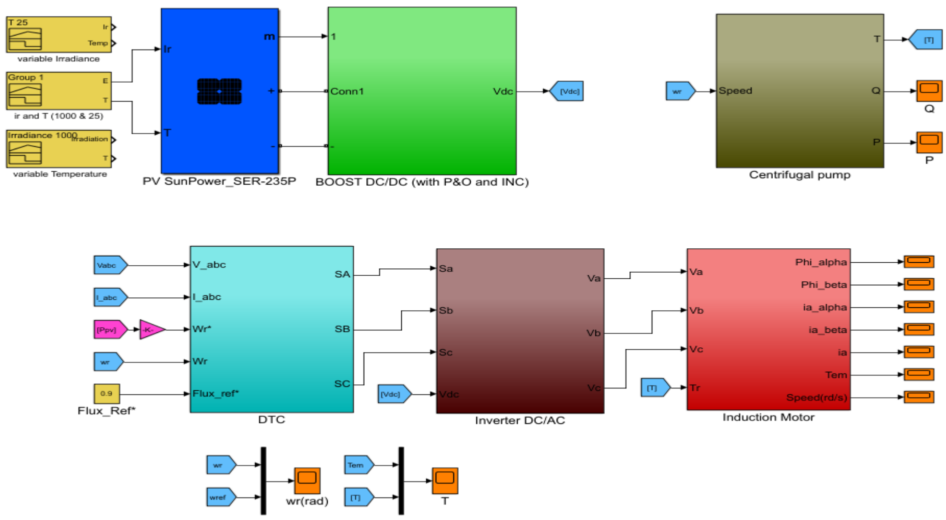

Fig IV.12: Simulation design of the photovoltaic water pumping system.

The variable references of irradiance and temperature used in this study are presented in figure IV.13.

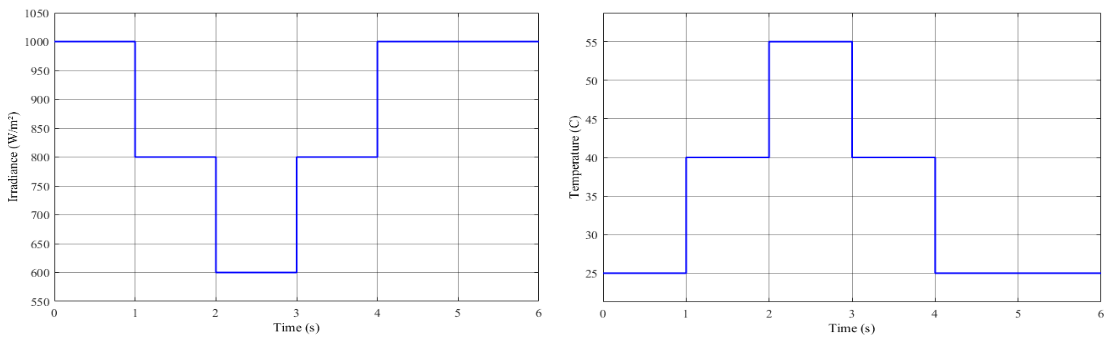

Fig IV.13: The variable references of the irradiance and the temperatures.

IV.11.3 Simulation results at standard test conditions (STC)

IV.11.3.1 P&O method

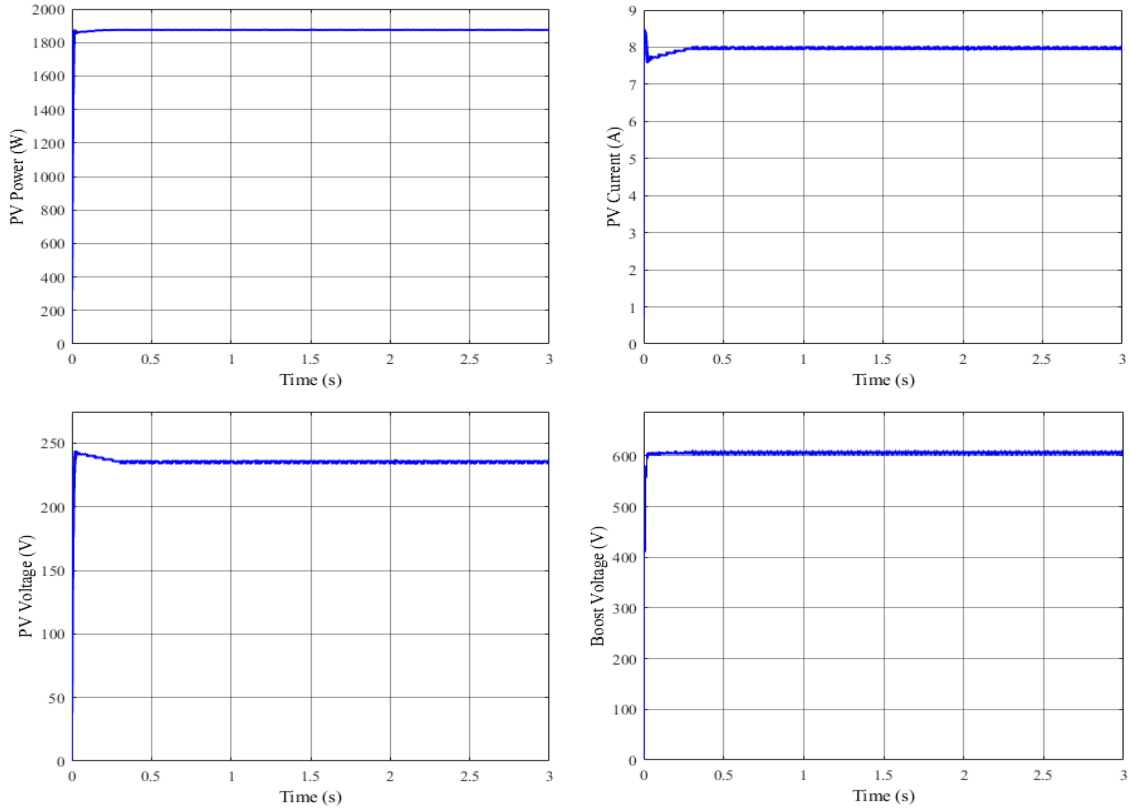

Fig IV.14: PV and Boost characteristics at (T=25°C, I=1000W/m^2).

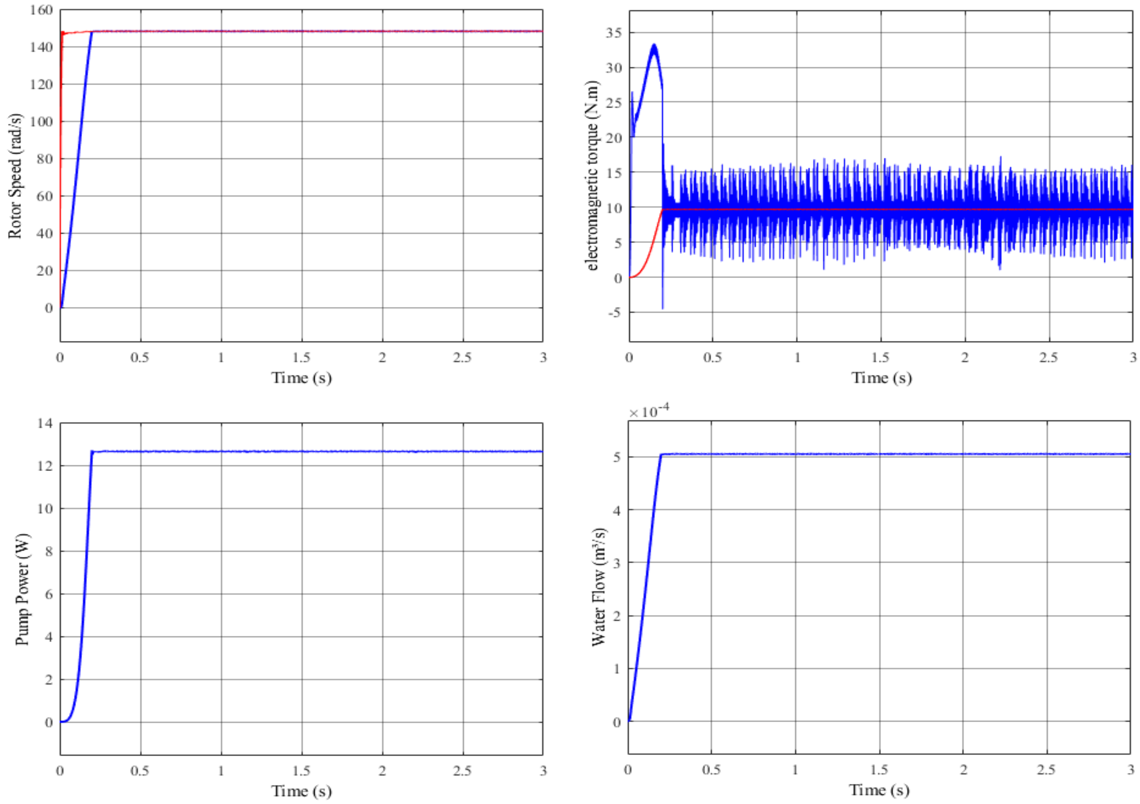

Fig IV.15: Motor-pump characteristics at (T=25°C, I=1000W/m^2).

IV.11.3.2 INC method

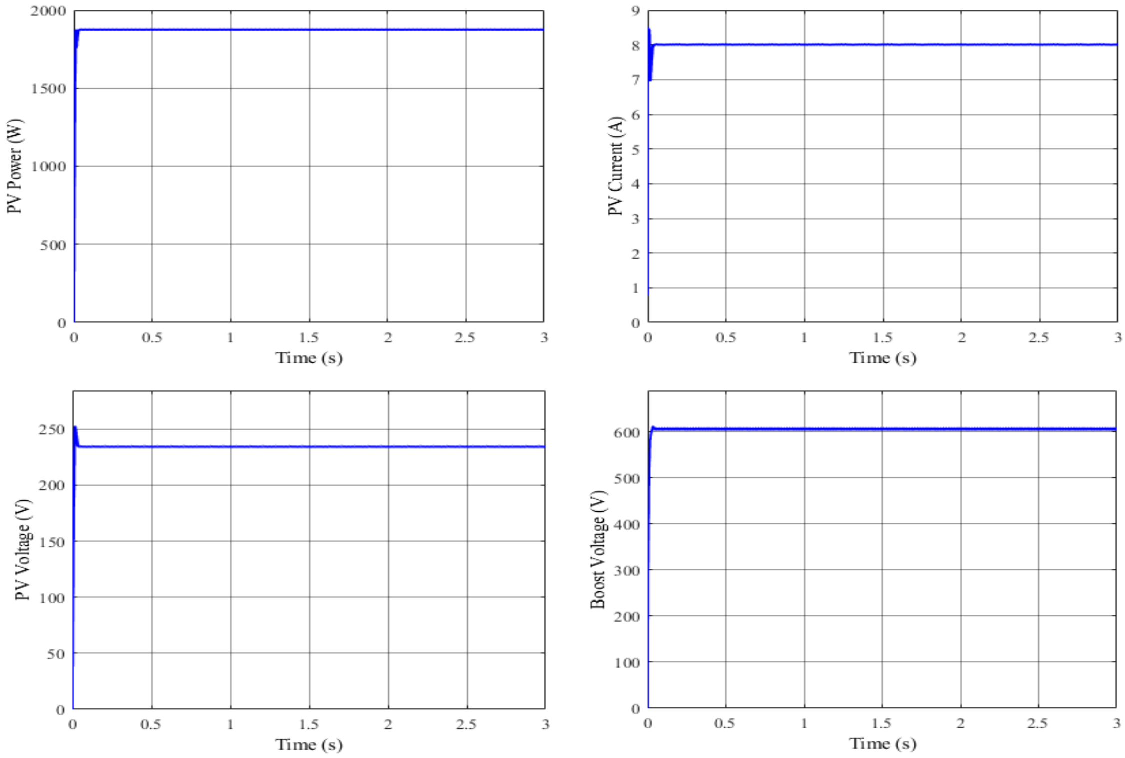

Fig IV.16: PV and Boost characteristics at (T=25°C, I=1000W/m²).

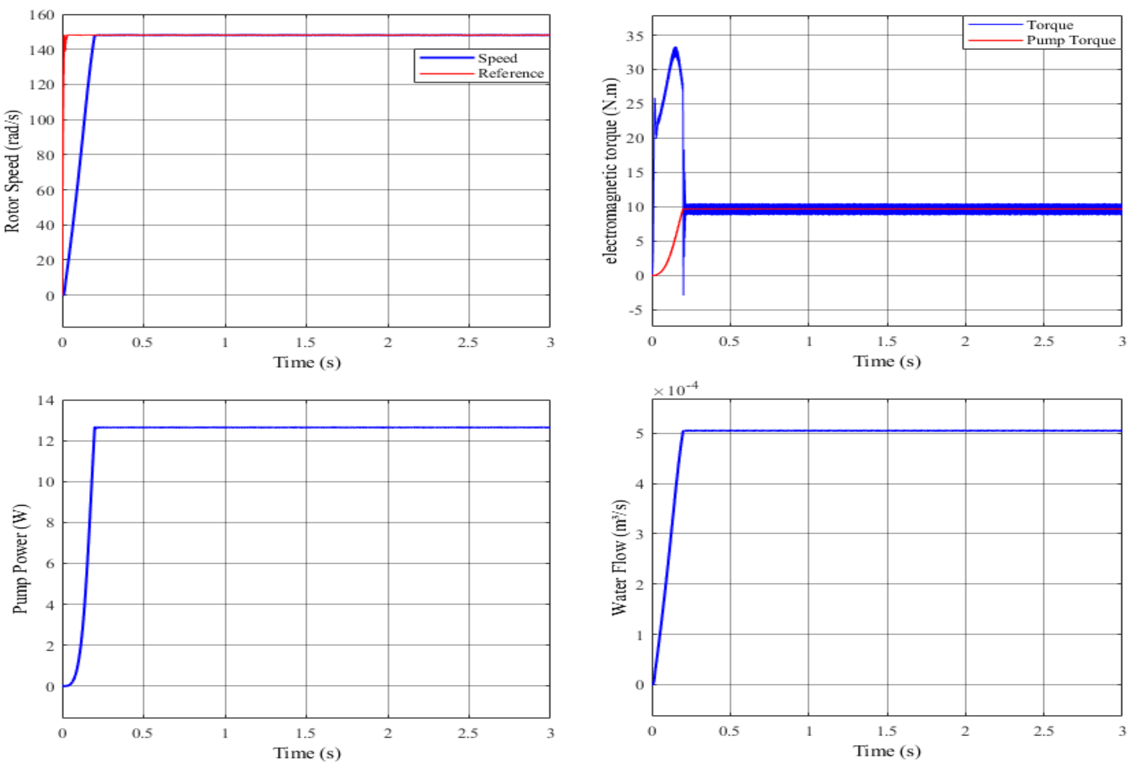

Fig IV.17: Motor-pump characteristics at (T=25°C, I=1000W/m²).

IV.11.4 Simulation results at variable Irradiance

IV.11.4.1 P&O method

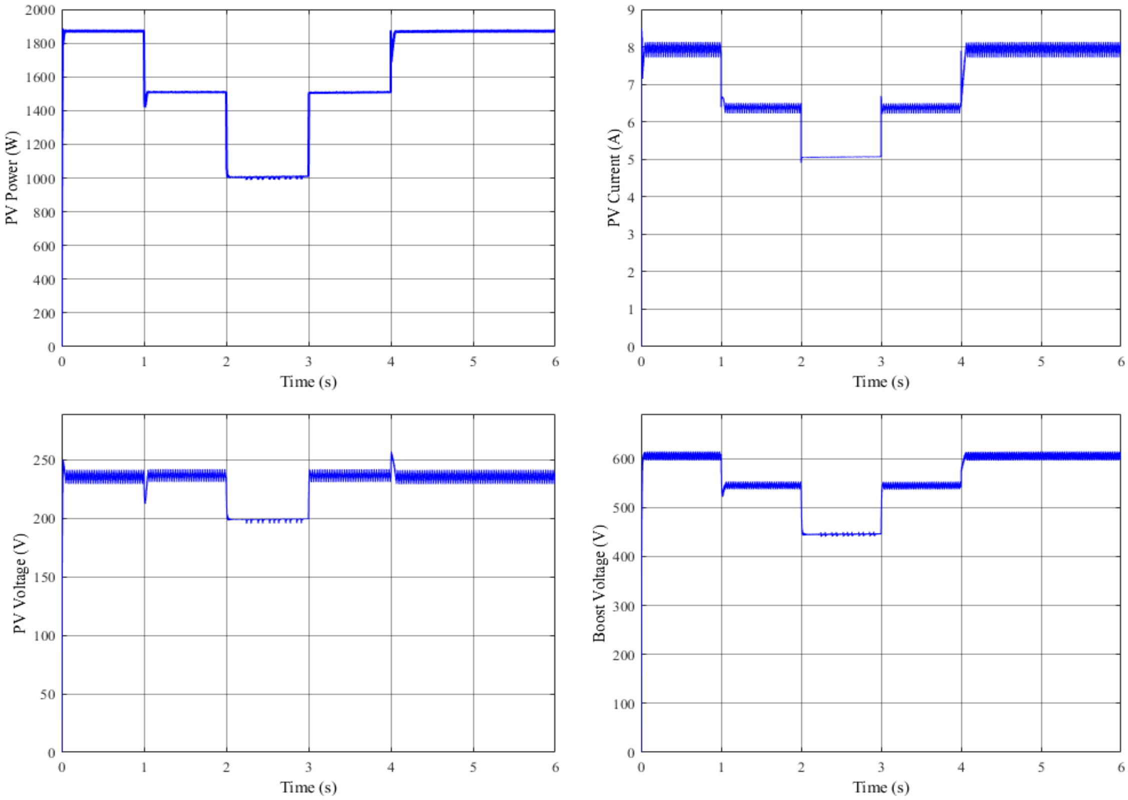

Fig IV.18: PV and Boost characteristics at variable Irradiance.

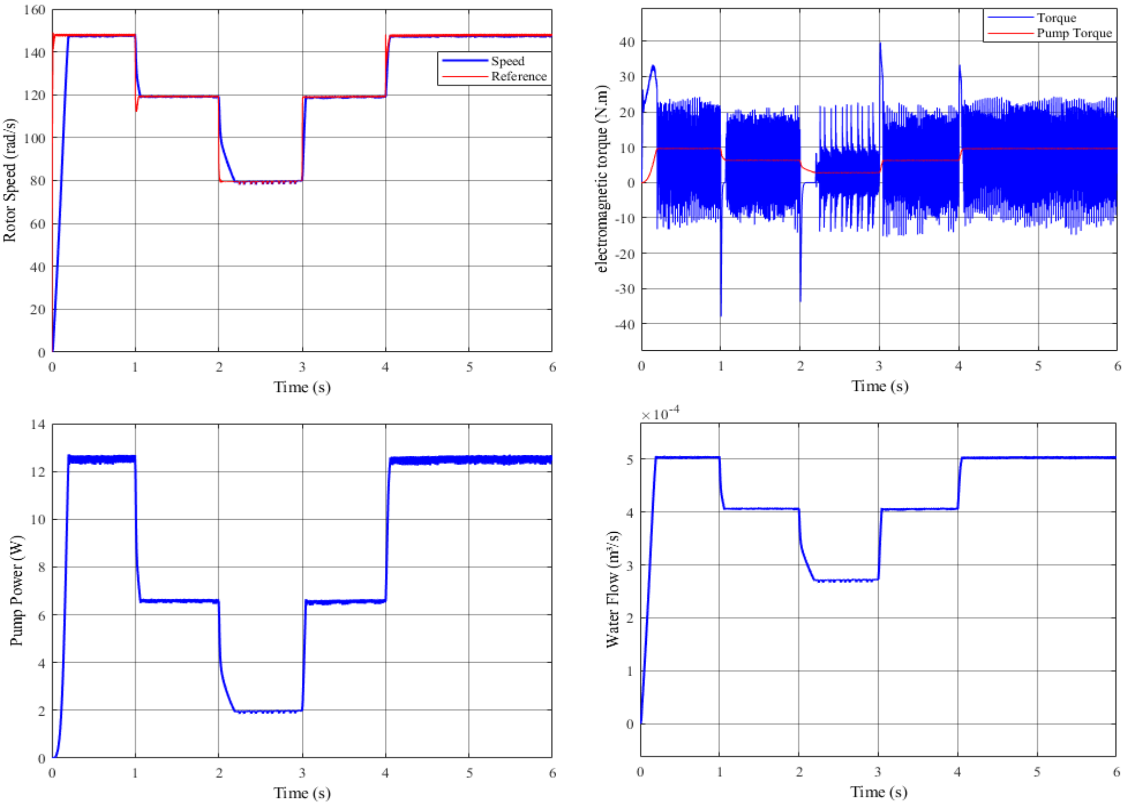

Fig IV.19: Motor-pump characteristics at variable Irradiance.

IV.11.4.2 INC method

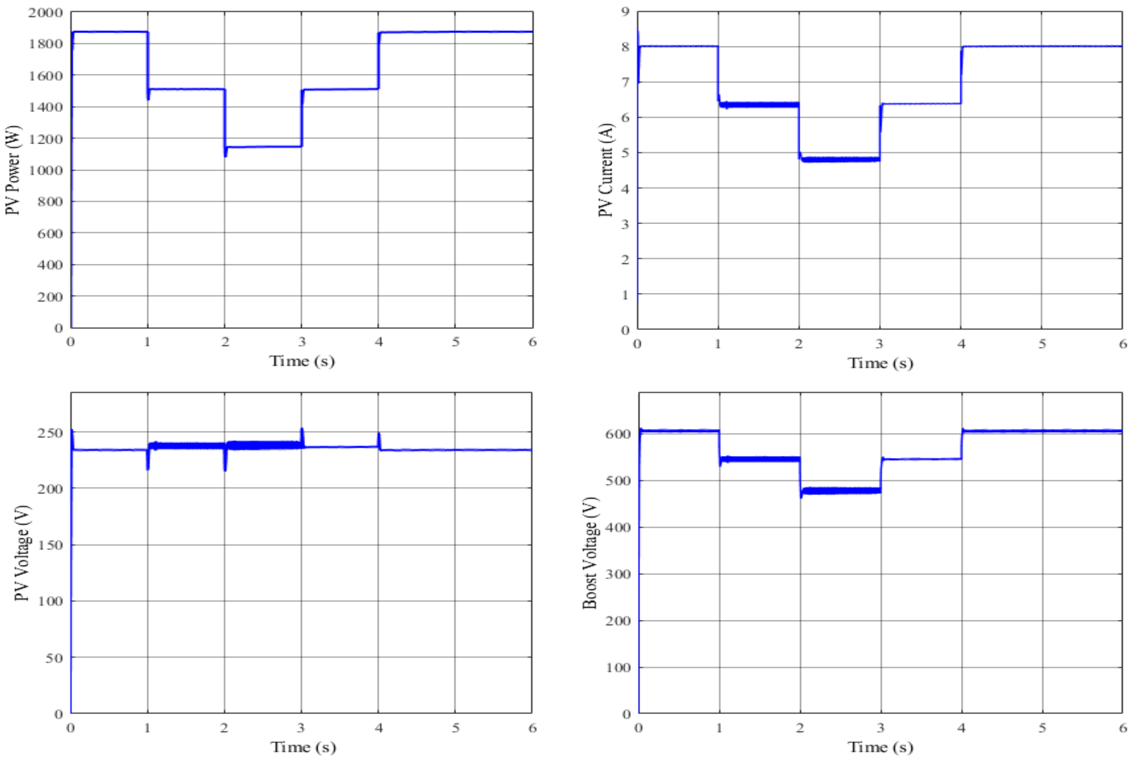

Fig IV.20: PV and Boost characteristics at variable Irradiance.

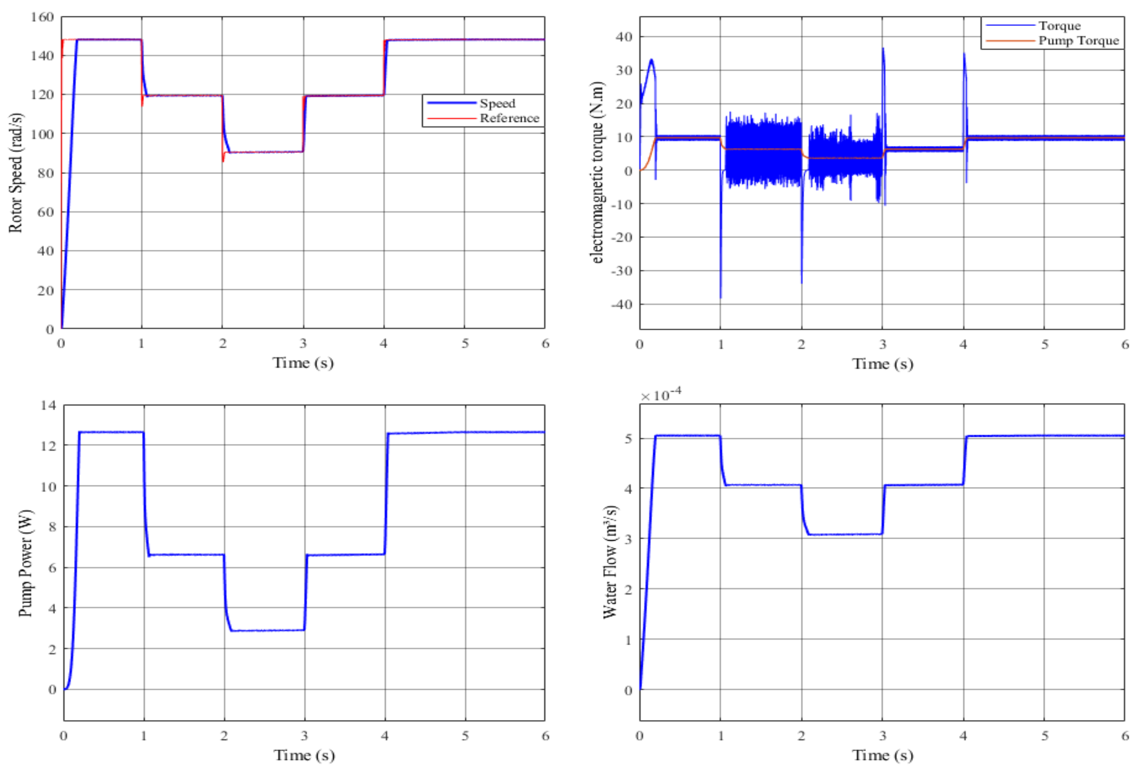

Fig IV.21: Motor-pump characteristics at variable Irradiance.

IV.11.5 Simulation results at variable temperatures

IV.11.5.2 P&O method

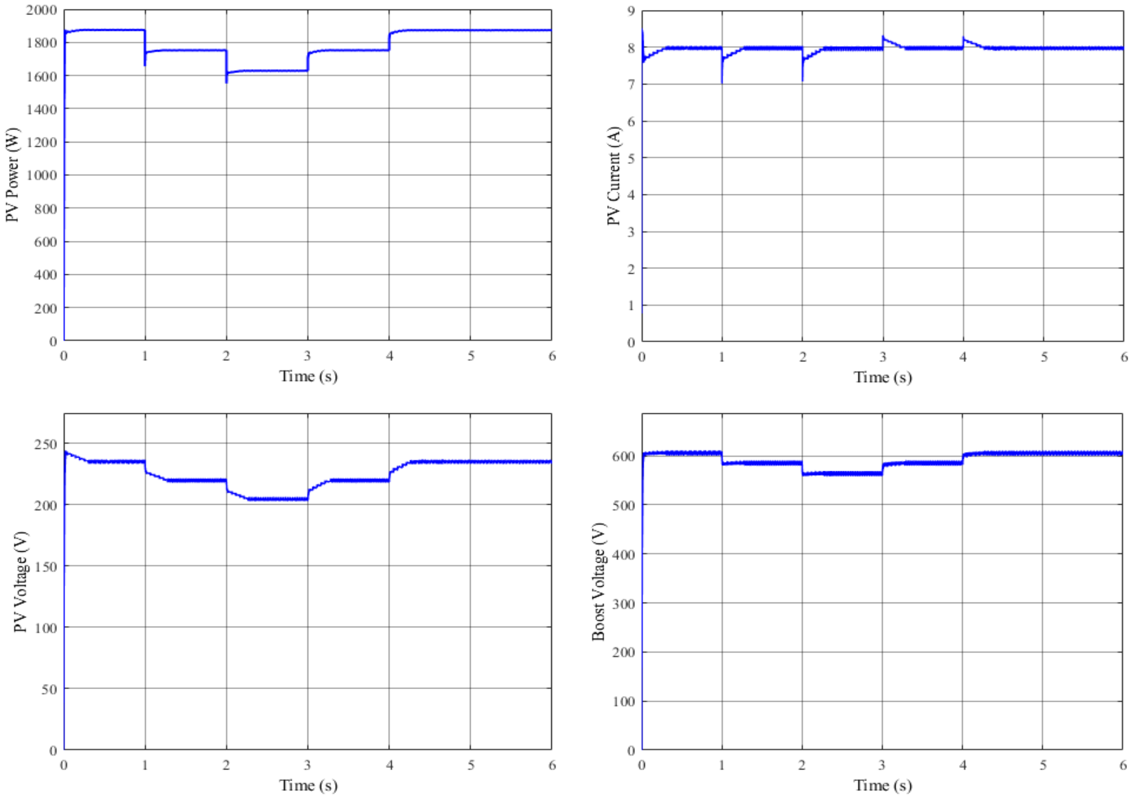

Fig IV.22: PV and Boost characteristics at variable temperatures.

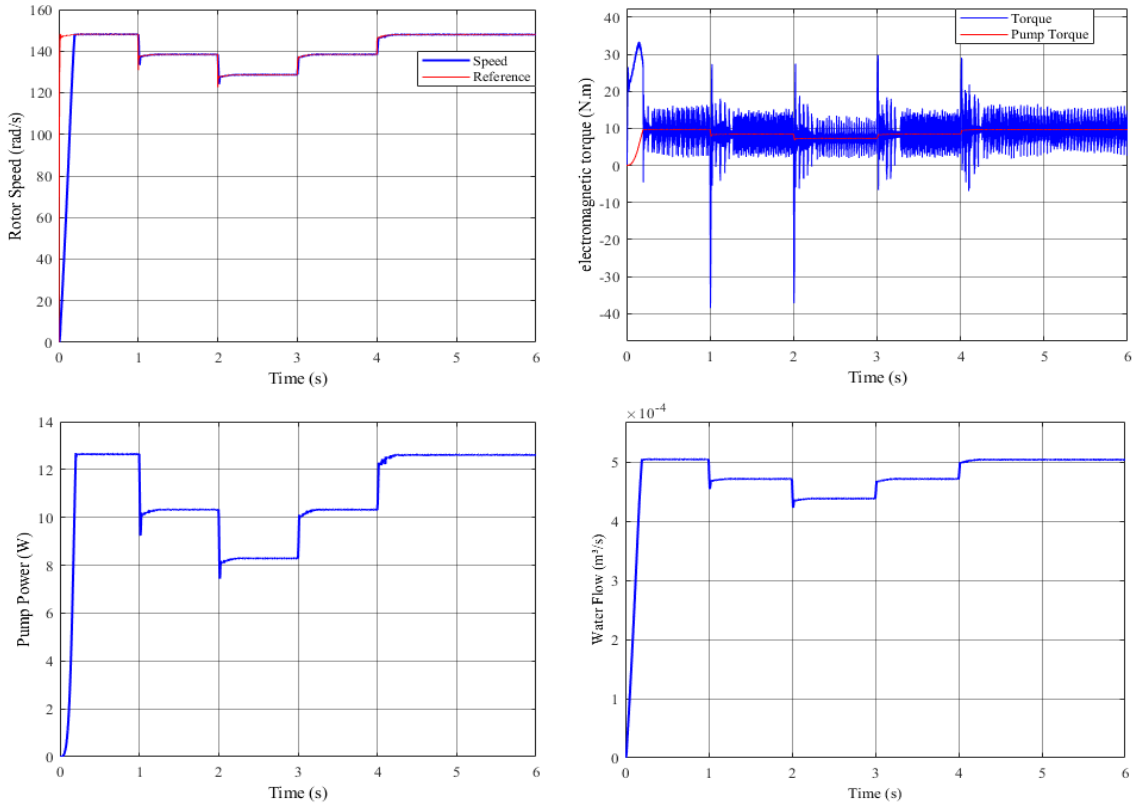

Fig IV.23: Motor-pump characteristics at variable temperatures.

IV.11.5.2 INC method

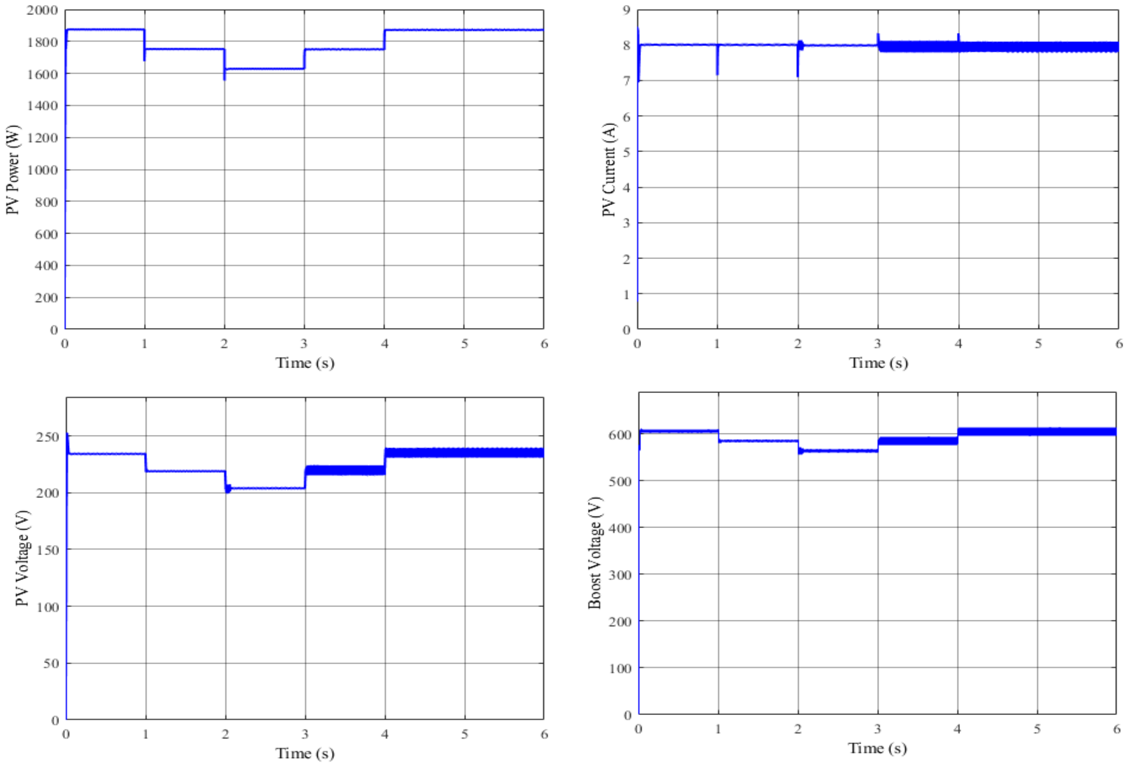

Fig IV.24: PV and Boost characteristics at variable temperatures.

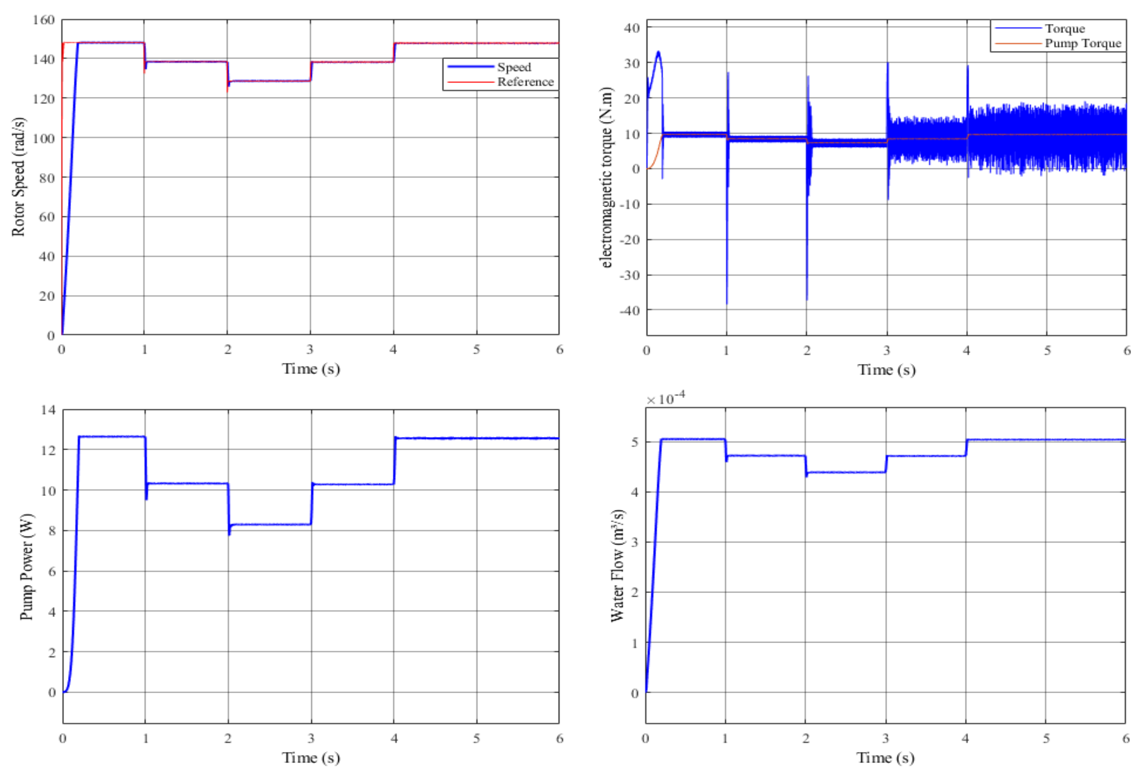

Fig IV.25: Motor-pump characteristics at variable temperatures.

IV.11.6 Comparison the impact of P&O and INC methods

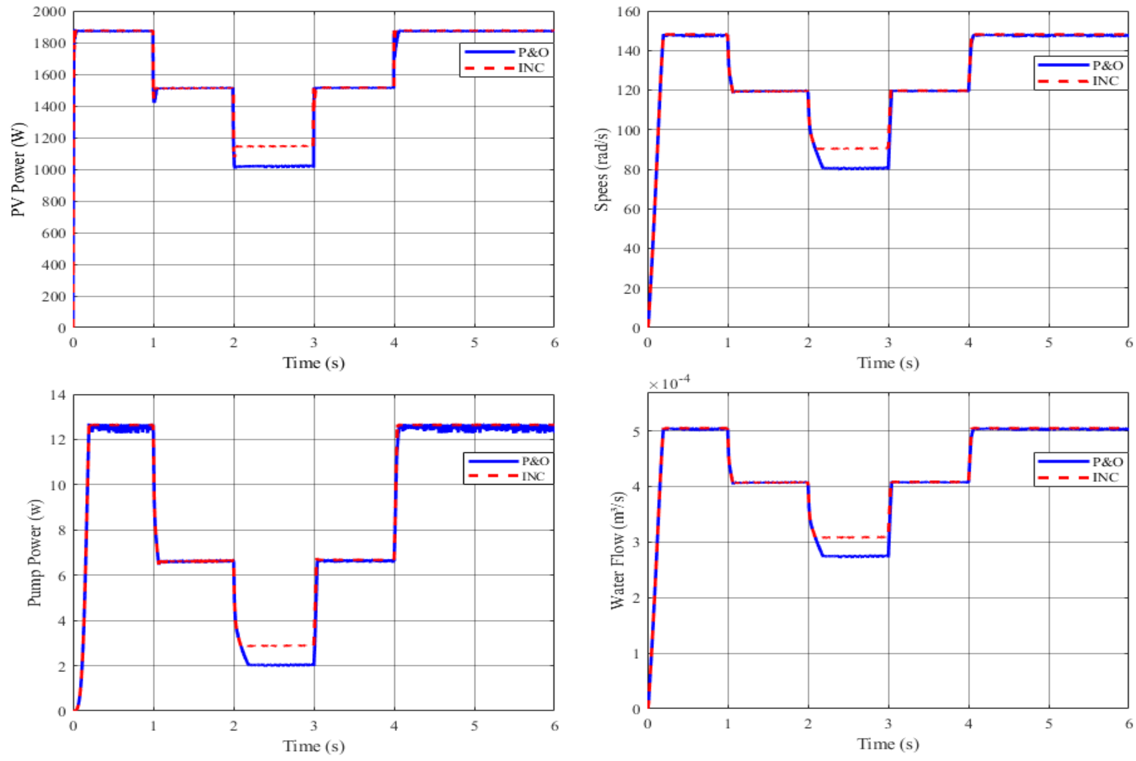

Fig IV.26: Comparison of the P&O and INC methods at variable irradiation.

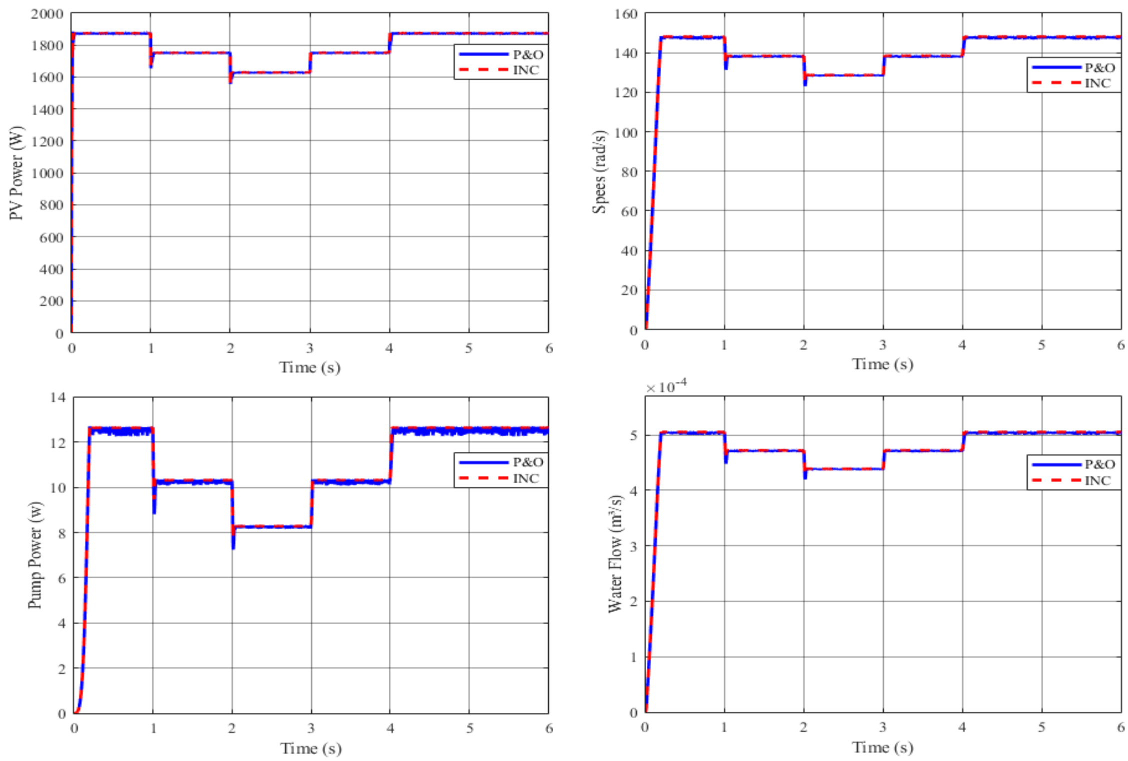

Fig IV.27: Comparison of the P&O and INC methods at variable temperatures.

IV.11.7 Interpretation of the results

- The figures (IV.14 to IV.17) shows the PV, Boost and The Motor-pump characteristics at (T=25°C and I=1000W/m^2). The result shows that the torque and the speed follow their references well with a very fast dynamics During the use of the (P&O) and the (INC) Method, and the latter presents a lower torque ripple than the P&O.
- The figures (IV.18 to IV.25) shows the PV, Boost and the Motor-pump characteristics at variable Irradiance and temperatures. It can be noticed that the speed of the motor presents a good fast response. While the torque has more ripples than the previous state (at T=25°C and I=1000W/m^2). Due to the presence of some drop in the PV power at the sudden change in the Irradiance or the temperature before its level stabilizes.
- On the pump side, it is noted that the water flow rate and the hydraulic power of the pump are always proportional to the speed of the induction motor.
- Figure (IV.26) and Fig (IV.27) shows the effect of the (P&O) method and the (INC) method on the performance of the system at variable irradiation and temperatures, It can be seen that the oscillation in P&O is higher than in INC. In addition, the figures shows that INC gives a better performance Especially when there is a significant drop in irradiation.

IV.12 Conclusion

In this chapter, the principles of direct torque control (DTC) were presented. Subsequently, simulation results demonstrated the application of DTC to an induction motor driving a photovoltaic water pumping system. These results suggest that DTC offers a viable solution to the robustness challenges encountered in conventional control techniques, particularly those arising from variations in solar irradiation or load torque. Notably, DTC excels due to its straightforward implementation and rapid dynamic response, improving system performance under variable operating conditions. Further research could investigate the optimization of DTC parameters for even better efficiency in photovoltaic pumping systems.

General Conclusion

General Conclusion

The work presented in this thesis focuses on the modeling and simulation of a photovoltaic water pumping system. This system facilitates water supply to isolated sites where no energy source is available. The chosen photovoltaic model was simulated using *MATLAB* under varying temperature and insolation conditions. The purpose of this simulation was to assess their impact on system performance, validate the efficiency of the motor drive (DTC), and evaluate its overall performance. Additionally, this study incorporated two MPPT control methods: P&O and INC combined with DTC for controlling the photovoltaic water pumping system.

Also, the objective of this study was to assess the resilience of direct torque control (DTC) in photovoltaic pumping system inverters. We conducted a series of experiments under varying radiation and temperature conditions to ensure system stability. Ultimately, our findings indicate that DTC delivers exceptional performance in typical motor pump operating conditions and maintains high durability even when faced with atmospheric fluctuations in radiation and temperature.

Appendix

A. Induction motor parameters :

IM	Values
Nominal power (P) [kW]	1.5
Rated speed(Ω) [rpm]	1420
Nominal frequency (f) [Hz]	50
Stator resistor (Rs) [Ω]	4.850
Rotor resistor (Rr) [Ω]	3.805
Stator inductor (Ls) [H]	0.274
Rotor inductor (Lr) [H]	0.274
Mutual inductor (M) [H]	0.258
Number of pole pairs (P)	2
Rated voltage [V]	220

B. Parameter values of the boost converter :

Boost converter parameters	Values
V_{dc}	600 V
C_1	1000 μF
C_2	500 μF
L	3 mH

C. PV Cell Parameters :

Parameters of the PV cell	Values
Maximum power (P_{mpp})[W]	235
Maximum current (I_{mpp})[A]	7.99
Maximum voltage (V_{mpp})[V]	29.42
Open circuit voltage (V_{oc})[V]	36.96
Short circuit current (I_{cc})[A]	8.48

References

[1] A.M. Al-Falahat, et al., *Energy performance and economics assessments of a photovoltaic-heat pump system*, Results Eng 13 (2022).

[2] I. Saady, et al., *Optimization for a photovoltaic pumping system using indirect field oriented control of induction motor*, Electronics, 10 (2021).

[3] D.M.N. Mahmood, I.M.A. Aljubury, *Experimental investigation of a hybrid photovoltaic evaporative cooling (PV/EC) system performance under arid conditions*, Results Eng, 15 (2022).

[4] Internet source : ae-solar.com.

[5] Internet source : US patent no. 2,402,662.

[6] A. FERRAI, *Dimensioning of Infrastructures Using Various Potential Renewable Energy Sources for the Electricity Supply of a Village*; Magister thesis, National Polytechnic School, Algiers, 2008.

[7] Aoun, N. and Bouchouicha, K. *Estimating daily global solar radiation by day of the year in Algeria*. The European Physical Journal Plus, 132(5), 216-228. (2017).

[8] A. Labouret and all, *Solar cells - the basics of photovoltaic energy*, 5th edition, Dunod, 2010.

[9] S. Astier. *Photovoltaic conversion: from solar radiation to the cell*, Engineering techniques, vol D3935, 2008.

[10] Santosh Das on electronicsandyou.com

[11] solardirect.com

[12] https://www.enerzytech.com/resources/articles/13-types-of-solar-pv-systems

[13] deegesolar.co.uk/different_types_of_solar_pv_systems/

[14] A. HADJ ARAB, M. BENGHANEM and A. GHARBI. *Dimensioning of Photovoltaic Pumping Systems. Review of Renewable Energies*. vol.8, pp (19 – 26), 2005.

[15] A, Oi. *Design And Simulation of Photovoltaic Water Pumping System*. these doctorate California Polytechnic. California: University San Luis Obispo, 2005.

[16] J, Royer and T, Djako. *Course Manual for Engineers and Technicians, Photovoltaic Pumping*. S.L.: University Of Ottawa, 2002.

[17] M. Benaissa, *Contribution to the study of energy transfer in photovoltaic systems*; Doctor a thesis, Djillali Liabes University Of Sidi-bel-Abbes, 2018.

[18] M. T. Boukadoum, A. Hamidat And N. Ourabia, *Photovoltaic Pumping*; Review of Renewable Energies. Arid Zones, pp (69-73),2002.

[19] https://www.us.lambda.tdk.com/resources/blogs/20200731.html

[20] L. Debbou and D. Maghribi, *Control of a hybrid (photovoltaic-wind) energy production system*; State engineer thesis. University of Bejaia, 2008

[21] A. BELHOCINE and S. ZAIDI. *Study and dimensioning of an autonomous photovoltaic pumping system.* Master's thesis 2. University of Bejaia, 2012.

[22] electricalvolt.com/difference-between-synchronous-asynchronous-motor/

[23] J. Royer, T. Djiako, E. Schiller, B. Sada Sy. *Photovoltaic Pumping*, Multi-world Editions,1998

[24] https://www.linkedin.com/pulse/differences-between-positive-displacement-centrifugal

[25] castlepumps.com/info-hub/positive-displacement-vs-centrifugal-pumps/

[26] M. Bessem Abdelghani, *Modeling and simulation of a photovoltaic pumping*; Master's Thesis, Badji Mokhtar University- Annaba.2018.

[27] V. Salas, E. Olias, A. Barrado, A. Lazaro. *Review of the maximum power point tracking algorithms for stand-alone photovoltaic systems*. Solar energy materials solar cells. vol 90, pp. 1555-1578, 2006;

[28] Bilel ben nasser, *study and modeling of the mppt command with matlab*, university of Quebec in rimouski, 2021.

[29] Aamar ouayache mohamed, *contribution to the optimization of a photovoltaic energy conversion chain*, doctor at of science in electrical engineering option, 2014.

[30] J. ferrieux, f. forest, *switching power supplies resonance converters: principles components modeling*. paris, france: Dunod, 1999.

[31] Salim arab-dalila toudert, *study of a photovoltaic system*, master's thesis, Mouloud Mammeri University of tizi-ouzou, 2017.

[32] K. H. Hussein, I. Muta, T. Hoshino, and M. Osakada, *Maximum photovoltaic power tracking: An algorithm for rapidly changing atmospheric conditions*, Proc. IEE—Generation, Transmission, Distribution, vol.142, no. 1, pp. 59–64, Jan. 1995.

[33] Hairul Nissah Zainudin, Saad Mekhilef, *Comparison Study of Maximum Power Point Tracker Techniques for PV Systems*, Proc. 14th international middle east power system conference (MMEPCON"10), Cairo University, Egypt, 2010, 750-755.

[34] Grellet G, Clerc G. Electric Actuators: Principles/Model/Controls, Collection Electrotechnique. Edition Eyrolles; 1997

[35] Lesenne J, Notel F. *Introduction to in-depth electrical engineering*, Technique et documentation. Paris, France; 1981

[36] A. Meroufel, *Decoupled control of an asynchronous machine without mechanical sensor*, Doctoral thesis, Djillali Liabes University Of Sidi-BelAbbès, 2004.

[37] S. Barkat . *Study of the voltage inverter-asynchronous motor association*. University of Mohamed Boudiaf M'sila. 2020.

[38] Takahashi, Noguchi T. A new quick-response and high-efficiency control strategy of an induction motor. IEEE Transactions on Industry Applications., Vol.22, No.5, pp.820–827, 1986.

[39] Depenbrock M. *Direct self control (DSC) of inverter fed induction machine*. IEEE Transactions on Power Electronics. 1988; 3(4):420-429.

[40] T. Bakhti and S. Bendaas, *DTC control of an asynchronous machine without speed sensor using an adaptive observer*, Engineering thesis, University of Batna, 2008.

[41] P. Vas, *Sensorless Vector and Direct Torque Control*, Oxford University Press, 1998.

[42] F. Bensmaine and N. Ameghchouche, *DTC control of an induction motor without speed sensor using an adaptive observer*, Engineering thesis, University of Batna, 2010.

[43] M. NEFSI, *Direct torque control of an asynchronous machine without mechanical sensor*, magister thesis, Djilali Liabes University Of Sidi Bel-Abbès, 2008.

[44] Ridha Kechida. *Use of direct control of the stator flow and the Kalman filter for direct torque control (DTC) of an asynchronous motor: Application to fault diagnosis*", Magister thesis, University of El-oued 2010.

[45] L. Bessouf, *Comparative study of the dynamic and stator performances of a JIB and a DTC of an induction machine*, Engineering thesis, University of Batna 2005.